TR-PL-13278

(2)

EXAMINATION OF CHEMICAL APPROACHES TO STABILIZING COMPOSITE PROPELLANT COMBUSTION

Merrill K. King
R. H. W. Waesche

ATLANTIC RESEARCH CORPORATION
Virginia Propulsion Division
5945 Wellington Road
Gainesville, VA 22065

FINAL REPORT
Contract F49620-90-C-0067

Air Force Office of Scientific Research
Building 410
Bolling AFB, DC 20332-6448

October 1991

Atlantic Research Corporation
a wholly owned subsidiary of Sequa Corporation

Virginia Propulsion Division
5945 Wellington Road
Gainesville, Virginia 22065-9187
703 754-5000

SEQUA

15 November 1991

Department of the Air Force
Air Force Office of Scientific Research
Bolling AFB, DC 20332-6448

Attn: Dr. Mitat Birkan
Code AFOSR/NA

Subj: Contract No. F49620-90-C-0067

Dear Dr. Birkan:

Atlantic Research Corporation is pleasd to submit six draft copies of the Final Technical Report for the subject contract.

Any questions regarding the content of this report should be directed to Dr. Woodward Waesche, Program Manager, at (703) 754-5369. We look forward to your comments.

Very truly yours,

ATLANTIC RESEARCH CORPORATION

Mark N. Director
Director of Technology

WHW:ces

Enclosures

TR-PL-13278

EXAMINATION OF CHEMICAL APPROACHES TO STABILIZING COMPOSITE PROPELLANT COMBUSTION

Merrill K. King
R. H. W. Waesche

ATLANTIC RESEARCH CORPORATION
Virginia Propulsion Division
5945 Wellington Road
Gainesville, VA 22065

FINAL REPORT
Contract F49620-90-C-0067

Air Force Office of Scientific Research
Building 410
Bolling AFB, DC 20332-6448

October 1991

UNCLASSIFIED
SECURITY CLASSIFICATION OF THIS PAGE

REPORT DOCUMENTATION PAGE

Form Approved
OMB No. 0704-0188

1a. REPORT SECURITY CLASSIFICATION: UNCLASSIFIED	1b. RESTRICTIVE MARKINGS: None
2a. SECURITY CLASSIFICATION AUTHORITY	3. DISTRIBUTION/AVAILABILITY OF REPORT: Unlimited
2b. DECLASSIFICATION/DOWNGRADING SCHEDULE	
4. PERFORMING ORGANIZATION REPORT NUMBER(S)	5. MONITORING ORGANIZATION REPORT NUMBER(S)
6a. NAME OF PERFORMING ORGANIZATION: Atlantic Research Corporation; 6b. OFFICE SYMBOL (If applicable):	7a. NAME OF MONITORING ORGANIZATION: Air Force Office of Scientific Research
6c. ADDRESS (City, State, and ZIP Code): 5945 Wellington Road, Gainesville, VA 22065	7b. ADDRESS (City, State, and ZIP Code): Building 410, Bolling AFB, DC 20332-6448
8a. NAME OF FUNDING/SPONSORING ORGANIZATION: AFOSR; 8b. OFFICE SYMBOL (If applicable): NA	9. PROCUREMENT INSTRUMENT IDENTIFICATION NUMBER: F49620-90-C-0067
8c. ADDRESS (City, State, and ZIP Code): Building 410, Bolling AFB, DC 20332-6448	10. SOURCE OF FUNDING NUMBERS: PROGRAM ELEMENT NO. 61102F; PROJECT NO. 2308; TASK NO. A1; WORK UNIT ACCESSION NO.

11. TITLE (Include Security Classification)
Examination of Chemical Approaches to Stabilizing Composite Propellant Combustion (U)

12. PERSONAL AUTHOR(S)
Dr. Merrill K. King and Dr. R. H. Woodward Waesche

13a. TYPE OF REPORT	13b. TIME COVERED	14. DATE OF REPORT (Year, Month, Day)	15. PAGE COUNT
Final	FROM 9/1/90 TO 8/31/91	1991, Oct, 15	

16. SUPPLEMENTARY NOTATION

17. COSATI CODES			18. SUBJECT TERMS (Continue on reverse if necessary and identify by block number)
FIELD	GROUP	SUB-GROUP	Composite Propellant, Solid Propellant, Combustion, Combustion Instability, Response Function

19. ABSTRACT (Continue on reverse if necessary and identify by block number)

Acoustic-mode combustion instability has long plagued the solid-propellant industry, and the increasingly frequent requirement for "reduced-smoke" propellants, with concommitant removal of metals from the propellant formulations (and, thus, removal of metal oxide particulate products, which have a major role in damping of acoustic oscillations) is expected to exacerbate this problem. One strategy for alleviating the problem involves identification and utilization of approaches to decreasing a major source of acoustic energy, namely, the transient burning rate response of the solid propellant to pressure and/or crossflow velocity oscillations. Previous preliminary modeling studies have indicated that it might be possible to decrease the pressure-coupled response functions of composite propellants by suitable modification of the relative activation energies of the fuel and oxidizer ablation processes. (Cont'd)

20. DISTRIBUTION/AVAILABILITY OF ABSTRACT	21. ABSTRACT SECURITY CLASSIFICATION
☒ UNCLASSIFIED/UNLIMITED ☐ SAME AS RPT ☒ DTIC USERS	UNCLASSIFIED
22a. NAME OF RESPONSIBLE INDIVIDUAL: Dr Merrill K. King	22b. TELEPHONE (Include Area Code): (202) 767-4938 / 22c. OFFICE SYMBOL: NA

DD Form 1473, JUN 86 — Previous editions are obsolete.

SECURITY CLASSIFICATION OF THIS PAGE
UNCLASSIFIED

TABLE OF CONTENTS

LIST OF ILLUSTRATIONS

LIST OF ILLUSTRATIONS (CONT'D)

LIST OF ILLUSTRATIONS (CONT'D)

LIST OF ILLUSTRATIONS (CONT'D)

LIST OF ILLUSTRATIONS (CONT'D)

LIST OF ILLUSTRATIONS (CONT'D)

LIST OF TABLES

1.0 ABSTRACT/SUMMARY

Acoustic-mode combustion instability has long plagued the solid-propellant industry, and the increasingly frequent requirement for "reduced-smoke" propellants, with concommitant removal of metals from the propellant formulations (and, thus, removal of metal oxide particulate products, which have a major role in damping of acoustic oscillations) is expected to exacerbate this problem. One strategy for alleviating the problem involves identification and utilization of approaches to decreasing a major source of acoustic energy, namely, the transient burning rate response of the solid propellant to pressure and/or crossflow velocity oscillations. Previous preliminary modeling studies have indicated that it might be possible to decrease the pressure-coupled response functions of composite propellants by suitable modification of the relative activation energies of the fuel and oxidizer ablation processes.

However, the modeling utilized in arrival at this preliminary conclusion was very oversimplified; accordingly, the purpose of the current study was to examine this concept further using a much more sophisticated composite propellant combustion model (steady- and unsteady-state). During the course of this work, such a model was developed and exercised parametrically to define potential effects of varying either oxidizer or fuel ablation energy on the all-important real part of the pressure-coupled response function. Results of this study indicate that additional factors not included in the previous simplified modeling greatly diminish the hoped-for beneficial effects of increasing the activation energy of the fuel ablation process at a constant value of oxidizer ablation activation energy. With respect to variation of the activation energy of oxidizer ablation at a fixed value of the fuel ablation activation energy, the previously-calculated beneficial effects of reducing oxidizer ablation activation energy are strongly reversed; in addition, increasing the activation energy from the baseline value associated with unmodified ammonium perchlorate has only a miniscule beneficial effect. Accordingly, the initial conclusion of this study is that the originally postulated approach to decreasing pressure-coupled response functions of composite propellants via suitable modification of the oxidizer and/or fuel ablation activation energies actually holds little promise.

2.0 INTRODUCTION/BACKGROUND

Over the years, the appearance of combustion instabilities in solid rocket motors, in developmental stages, and even in operational systems (as the propellants age, with changes in burning characteristics) has cost hundreds of millions of dollars in developmental and refurbishment costs as well as leading to performance compromises associates with "fixes" to these instabilities. (Such acoustic instabilities, occurring over a wide range of frequencies, are generally intolerable in that they can lead to unacceptable interactions with control systems, structure, and/or payload and, in some cases, to catastrophic motor failure.) Before approximately 1960, instabilities occurred quite frequently in solid motors, particularly tactical motors where natural resonant frequencies are typically in the 1 Khz and higher regime. A fortuitous "fix" to many (though not all) of these instabilities was found to be addition of large amounts of metal additives to the propellant formulations, with the resulting condensed-phase products producing large amounts of damping of oscillations due to velocity lags dissipating large amounts of acoustic energy. (In fact, large amounts of metal were first added to propellants just for this effect, before it was found that such metal addition also provided significant performance gains.)

However, increasingly stringent mission requirements (with increased energy density) have led to increased incidence of instabilities in modern rocket motors, even with large amounts of metal additive. In addition (and probably most important), there is a major recent shift to a requirement for "reduced smoke" propellants for tactical missiles to improve survivability (by reducing detectability) of the missiles and their launch platforms, e.g., aircraft. This requirement precludes inclusion of more than very minor amounts of metal particles in propellant formulations, leading to a considerable increase in the occurrence of instability problems due to removal of a major acoustic energy sink (damping term) associated with the condensed-phase products. Accordingly, it is important that an alternative approach to alleviating instability problems, namely reduction of driving (acoustic energy source) terms be addressed. One major source term (generally the most important source) is associated with interaction of an acoustic wave with the solid propellant combustion processes. Both pressure and flow oscillations

associated with an acoustic wave can cause solid propellant burning rate (energy release rate) oscillations which, in turn, can feed energy into the acoustic wave.

The relationship between burning rate oscillations and pressure oscillations is referred to as the pressure-coupled response function (a complex variable) of the propellant, while that between burning rate oscillations and velocity oscillations is referred to as the velocity-coupled response function (although the latter is generally agreed not to be an intrinsic propellant property, depending strongly on the structure of the local mean flowfield). Attention here will be restricted, at least for the time being, to the pressure-coupled response function; it is easily shown that the real part of this complex response function is the important quantity as regards driving of acoustic waves, with relationships between the growth constant for oscillations and the pressure-coupled response function being presented and discussed in numerous references, most notably CPIA Publication 290, "Combustion Instability in Solid Rocket Motors."[1] For typical scenarios, it is found that the pressure-coupled response is a major contributor (driver) in the acoustic energy balance.

Accordingly, development of means of reducing the amplitudes of the pressure-coupled response functions of a wide range of solid propellants, leading to significant reduction of the driving terms in acoustic energy balances for motors, should lead to major reduction or elimination of instability problems in motors utilizing such propellants. Thus, it is apparent that development of a systematic approach (principle) to reduction of the magnitude of composite propellant pressure-coupled response functions would be of tremendous potential importance to the solid rocket field.

For many years, analysts have attempted to estimate pressure-coupled response functions for composite propellants using theoretical approaches (in general, equivalent to the well-known ZN approach)[2] which are strictly applicable (at best) to homogeneous propellants. As shown by King[3-5] in the early 1980's (utilizing very simplified composite propellant combustion models to demonstrate the point clearly), composite propellants provide an additional potential destabilizing mechanism beyond those treated by the ZN-type

approaches. This mechanism involves production of oscillations in the oxidizer/fuel ratio of "packets" of propellant gases leaving the surface of the propellant (and, thus, oscillations in the gas-phase heat release) accompanying oscillations in surface temperature due to different activation energies for the fuel and oxidizer ablation processes. A brief outline of how this comes about follows.

The oxidizer/fuel ratio of each "packet" of gas leaving the composite propellant surface may be calculated as:

$$OF_{packet} = \frac{A_1 \exp(-E_{ox}/RT_s)\ S_{ox}}{A_2 \exp(-E_{fuel}/RT_s)\ S_f} \tag{1}$$

where S_{ox} and S_f are the nondimensional surface areas associated with oxidizer and fuel respectively. At steady-state, overall continuity forces these surface areas to adjust such that OF is equal to the overall propellant oxidizer/fuel ratio, independent of the mean surface temperature, $\bar{T}_s$. Thus,

$$\frac{\bar{S}_{ox}}{\bar{S}_f} = OF_{prop} \frac{A_2 \exp(-E_{fuel}/R\bar{T}_s)}{A_1 \exp(-E_{ox}/R\bar{T}_s)} \tag{2}$$

Now if under oscillatory conditions the frequency is sufficiently high that S_{ox} and S_f cannot adjust significantly away from their steady-state values, it may easily be shown through combining of Equations 1 and 2 (linearizing around $\bar{T}_s$) that:

$$OF_{packet} = OF_{prop} \exp[(E_{ox} - E_{fuel})(T_s - \bar{T}_s)/R\bar{T}_s^{\,2}] \tag{3}$$

(It is, of course, recognized that in actuality there will be oscillations in surface structure at least partially compensating for the differential temperature sensitivities of fuel and oxidizer ablation, with the degree of compensation increasing with decreasing oscillation frequency until total compensation occurs as the frequency approaches zero; this is treated in the current modeling activity as discussed in later sections of this report.) For

a typical AP/HTPB composite propellant, the available chemical enthalpy is related to the oxidizer/fuel ratio approximately (again linearizing) by:

$$H_{packet} = 800 + 180(OF_{packet} - 3.87) \tag{4}$$

leading to:

$$H_{packet} = 800 + 180(OF_{prop}\exp[(E_{ox}-E_{fuel})(T_s-\bar{T}_s)/R\bar{T}_s^2) - 3.87] \tag{5}$$

Based on the current literature, it appears that the ablation of ammonium perchlorate has a somewhat higher activation energy than the ablation of typical HTPB binders (by approximately 5 kcal/mole). Thus, upward perturbations in surface temperature will be accompanied by similar perturbations in oxidizer/fuel ratio of "packets" of gas leaving the propellant surface; since AP/HTPB formulations are generally fuel-rich, this will in turn lead to increases in gas-phase heat release (following from Equation 5) accompanying increases in surface temperature, a destabilizing mechanism as discussed further in the next paragraph.

In the work described in Reference 5, the above equation for H_{packet} as a function of instantaneous surface temperature, T_s, was combined with simplified gas-phase combustion model, a "full-up" perturbation analysis of the entire equation set describing surface and gas-phase processes, and a Fourier analysis of the subsurface region for development of expressions relating the real part of the pressure-coupled response function $[R_{pc}^{(real)} \equiv (m_s'/\bar{m})/(P'/\bar{P})]$ to the dimensionless angular frequency of oscillations (standard presentation format) at several values of $E_{ox}-E_{fuel}$. As may be seen from Figure 1, the differential dependence of oxidizer and fuel ablation rates was predicted to have significant effects on the real part of the pressure-coupled response function, the predicted $R_{pc}^{(r)}$ peak increasing dramatically with increasing values of that difference. Thus, a potential destabilizing mechanism in AP-composite propellant combustion which is not present with homogeneous propellants (and which is not properly handled by the classical Zeldovich analysis) is suggested. Most important, this reasoning suggests a possible significant fundamental approach to development of a class

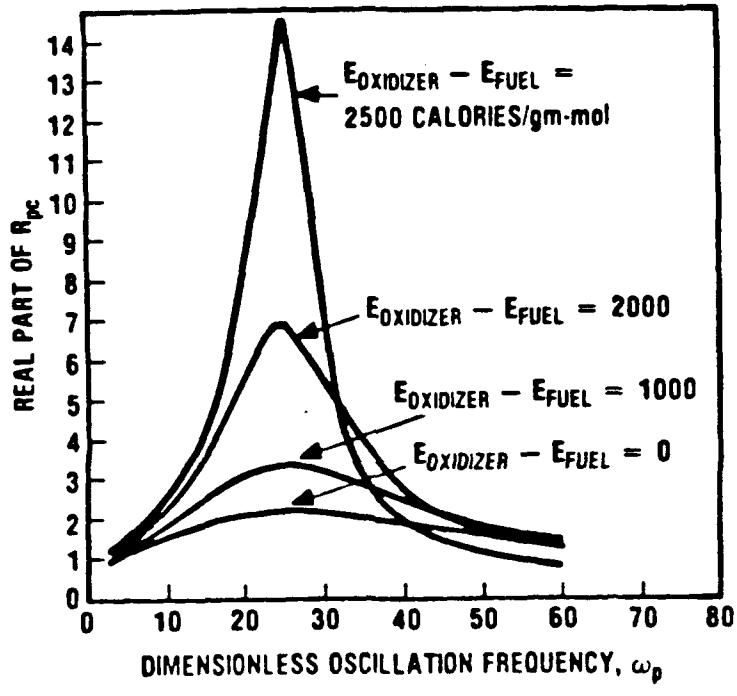

Figure 1. Effect of Allowance for Dependence of Oxidizer/Fuel Ratio of Gases Leaving the Surface on Surface Temperature.

1091-AFSOR

of AP-composite propellants which will burn stably over a much wider range of motor conditions than do current formulations; this approach is centered around development of means of increasing the temperature sensitivity of fuel ablation or decreasing that of oxidizer ablation resulting in decrease (or perhaps even reversal) of the effect of the gas-phase heat release oscillations relative to the surface temperature oscillations.

The current program was accordingly directed at further examination of this approach to reduction of pressure-coupled response functions of AP-composite propellants, to be carried out in three steps:

1. Detailed modeling involving perturbation studies using a complex composite propellant combustion model which has been verified against data, to quantitate potential effects of alteration of oxidizer or fuel ablation activation energies.
2. Development of means of tailoring (changing) these ablation activation energies. At this time, it appears that the most promising approaches to modifying the oxidizer ablation characteristics would involve occlusion of possible catalysts in the oxidizer crystals or co-crystallization of mixed oxidizers (such as ammonium perchlorate or hydroxyl ammonium perchlorate, for example). With respect to modifying the temperature sensitivity of fuel ablation, various approaches including the use of catalysts, substitution of various moieties on the basic polymer chains, and variation of crosslinker type and level are available. In this phase of the work, techniques for simultaneously measuring ablation rate and surface temperature of the ingredients (ablating alone under the influence of an external radiation flux) will be utilized, probably in collaboration with Prof. Tom Brill of the University of Delaware.
3. T-burner and pulsed motor testing with formulations containing these modified ingredients to confirm the approach.

3.0 STEADY-STATE MODEL UTILIZED

A complex steady-state model for combustion of composite solid propellants developed by King[6-9] in the late 1970's and used quite successfully in predicting effects of various formulation parameters and pressure on AP/HTPB composite propellant burning rates was selected as a starting point for this analysis. This model, based on the same general principles as the classic Beckstead-Derr-Price (BDP) model[10], but containing several major modifications, was first further modified to eliminate a discrepancy present in most (if not all) of the BDP-type models. [In these models, the relative surface areas of the oxidizer and fuel are calculated via geometrical considerations, with the ratio of the surface area of the fuel to the planar oxidizer surface area being assumed to be equal to the volumetric ratio of fuel to oxidizer in the formulation; as a result, since the volumetric ablation rates of the fuel and oxidizer are in general different, mass is not conserved in most cases. That is, the mass ratio of oxidizer and fuel ablation is not in general equal to the mass ratio of these ingredients in the propellant.] This deficiency has been corrected in the modified steady-state model used as a basis for this study in which an iterative approach regarding calculation of the fuel surface area associated with a given oxidizer particle planar surface area is utilized to ensure that the ratio of the products of areas and mass fluxes of oxidizer and fuel <u>is</u> equal to the mass ratio of these ingredients in the propellant.

The basic model is centered around an energy balance, the product of burning mass flux and energy requirements to raise ingredients from ambient to surface temperature (related to burning rate by an Arrhenius function) and to vaporize that fraction not consumed in subsurface reactions being equated to the sum of heat release rates from subsurface reactions and from two gas flame zones (Figure 2). Thus, burning rate is controlled by three heat release zones: (1) a thin subsurface zone immediately adjacent to the surface; (2) a gas-phase AP decomposition product monopropellant flame; and (3) an extended diffusion flame in which AP products and binder pyrolysis products are mixed and burned. Subsurface heat release is calculated using an estimated subsurface temperature profile substituted into a rate expression representing subsurface heat release data measured by Waesche and Wenograd[11]. This

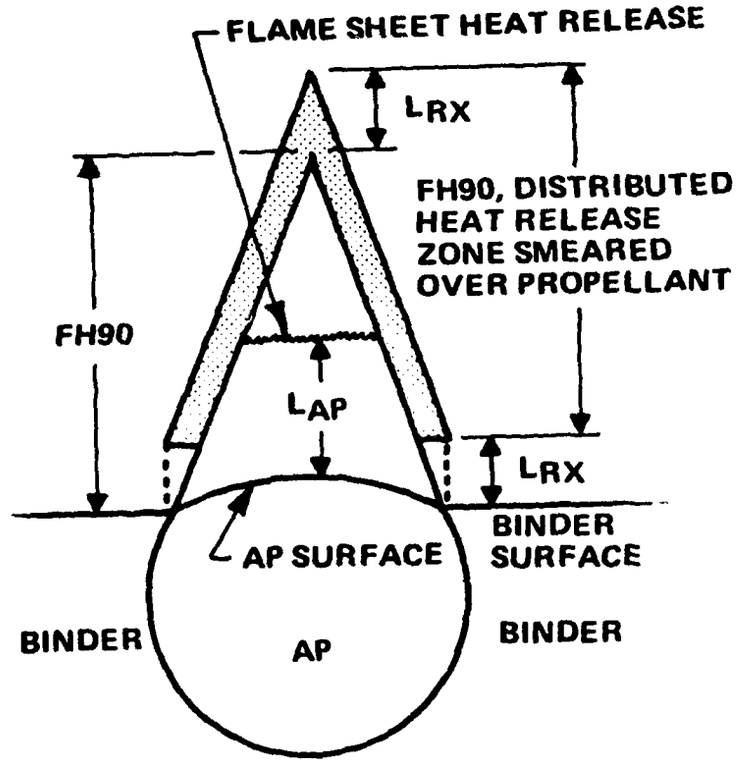

Figure 2. Multiple Flame Structure Model Schematic for AP/HTPB Composite Propellants.

1091-AFSOR

expression is integrated from the surface to a depth where the temperature equals the AP melting point to obtain total subsurface heat release. (This procedure differs somewhat from the BDP model, in which subsurface heat release per unit mass of propellant is assumed to be constant, independent of burning rate.)

For the gas-phase, a two-flame approach was chosen (in contrast to the three-flame approach of BDP), the flames being an AP monopropellant flame (infinitesimally thin flame sheet parallel to the propellant surface) and a columnar diffusion (Burke-Schumann[12]) flame. Three distances (FH90, L_{AP}, and L_{RX} in Figure 2) are important in determining heat feedback from these flames. FH90 is a distance associated with 90% mixing of the fuel and oxidizer gases from the propellant surface, while L_{RX} and L_{AP} are reaction distances (products of gas velocity away from the surface and reaction times) associated with the diffusion and monopropellant flames respectively. AP monopropellant heat release is assumed to occur at one plane, while the diffusion flame releases heat in a distributed fashion (as defined by a Burke-Schumann analysis described in some detail in Reference 6) between distances L_{RX} and L_{RX} + FH90 from the propellant surface. (Details of the calculational procedure for obtaining the heat flux from these flames back to the propellant surface are also discussed in Reference 6.)

Details of the equation development for this model appear in References 6 and 7. Included in the model are three "free" constants (pre-exponentials associated with the subsurface rate expression and the two rate expressions used to calculate the gas-phase reaction times). Optimized values for these constants are chosen using burning rate versus pressure data for four unimodal oxidizer AP/HTPB formulations and subsequently used for all other calculations for noncatalyzed AP/HTPB formulations. Extension of the model to treat multimodal-oxidizer formulations and metalized AP/HTPB formulations are discussed in References 7 through 9.

A brief description of the steady-state burning rate calculation procedure for unimodal oxidizer propellants follows. Again, the reader is referred to References 6-9 for more details (including treatment of effects of steady-state crossflow, which are not considered in this study).

1. Guess surface temperature, T_s.
2. Calculate mass burning fluxes and linear burning rates of oxidizer and fuel using:

$$m_{ox,s} = A_{OX} e^{-E_{ox}/RT_s} \tag{6}$$

$$m_{fu} = A_{FU} e^{-E_{fu}/RT_s} \tag{7}$$

$$r_{ox,s} = m_{ox,s}/\rho_{ox} \tag{8}$$

$$r_{fu} = m_{fu}/\rho_{fu} \tag{9}$$

3. Utilize geometrical arguments in combination with r_{ox} to calculate the effective cured oxidizer surface area (see Reference 7), ASOX, of a single oxidizer particle.
4. Calculate fuel surface area associated with a single oxidizer particle. In the first loop of a trial-and-error procedure, calculate this value by equating the ratio of fuel surface area to oxidizer planar-projection surface area to the volumetric ratio of these ingredients in the formulation. In subsequent loops, calculate the ratio of [oxidizer mass flux times oxidizer surface area divided by fuel mass flux times fuel area] to overall oxidizer/fuel ratio - if this ratio is greater than unity, raise the value of fuel area, if less than unity, lower the value. Continue this procedure until the ratio causes unity and then use a Newton-Raphson procedure to final convergence.
5. Calculate the final flame temperature, T_f, from the input oxidizer/fuel ratio and a table of flame temperature versus O/F ratio.
6. Calculate energy transport and release rates associated with various processes in order to perform an energy balance at the propellant surface:
   a) Heat rate associated with heating binder from the propellant conditioning temperature to the surface temperature at a rate equal to its ablation flux.

$$\dot{q}_1 = m_{fu} A_{fuel} [C_{P,fuel}(T_s - T_o) + Q_{melt,f}] \quad (10)$$

b) Heat rate associated with ablating binder not consumed in surface/subsurface reactions

$$\dot{q}_3 = m_{fu} A_{fuel} Q_{fuel,vap} (1-\beta) \quad (11)$$

β = Fraction of fuel consumed in surface/subsurface reactions (discussed below)

c) Heat rate associated with heating oxidizer from the propellant conditioning temperature to the surface temperature at a rate equal to its ablation flux

$$\dot{q}_2 = m_{ox} A_{s,ox} [C_{pox}(T_s - T_o) + Q_{melt,ox}] \quad (12)$$

d) Heat rate associated with ablating oxidizer not consumed in surface/subsurface reactions

$$\dot{q}_4 = m_{ox} A_{s,ox} Q_{subl} (1-\alpha) \quad (13)$$

α = Fraction of oxidizer consumed in surface/subsurface reactions

e) Heat release rate associated with surface/subsurface reactions

$$\dot{q}_5 = m_{ox} A_{s,ox} Q_{EXO} \alpha \quad (14)$$

Q_{EXO} = Heat release per gram of AP consumed in surface/subsurface reactions

The quantity α is calculated assuming that surface/subsurface reactions occur only in a region where temperature exceeds the melting point of AP and that a reaction rate expression:

$$R_\alpha = B_{sub} e^{-E_{sub}/RT} \tag{15}$$

is superimposed on an unperturbed (unchanged by the heat release) subsurface temperature profile given by:

$$T = (T_s - T_o) \exp (r_{ox,s} \rho_{ox} C_{pox} x/\lambda_{ox}) + T_o \tag{16}$$

with α then being calculated as:

$$\alpha = \int_{X=0}^{X=X_{AP,melt}} R_\alpha dx/r_{ox,s} \tag{17}$$

(Details are given in References 6 and 7). The quantity β is then calculated from α assuming a stoichiometric reaction.

7. Calculate the net heat release per unit mass of propellant associated with <u>all</u> surface/subsurface processes as:

$$\Delta Q_{surf} = \frac{(-\dot{q}_3 - \dot{q}_4 + \dot{q}_5)\ (\text{Wt Fraction Oxidizer})}{(\text{Oxidizer Mass Flux})\ (\text{Oxidizer Surface Area})} \tag{18}$$

8. Calculate rate of heat transfer back to surface from the AP and O/F flames depicted in Figure 2 using an analysis detailed in References 6 and 7.

$$\dot{q}_{fdbk} = f\ (L_{RX}, L_{AP}, FH90, m, T_f, T_s) \tag{19}$$

In this analysis, the oxidizer/fuel heat release is assumed to be a distributed release between L_{RX} and L_{RX} + FH90, while the AP flame heat release is a sheet flame (planar) heat release at distance L_{AP} from the surface. Three different calculational procedures are used depending on whether $L_{AP} < L_{RX} + FH90$, $L_{RX} < L_{AP} < L_{RX} + FH90$, or $L_{AP} > L_{RX} + FH90$. In these calculations, L_{RX} and L_{AP} are calculated as the products of gas velocity off

the propellant surface and reaction times:

$$L_{RX} = \frac{K_{OF} V_{gas,surf} (1+\phi)^2 T_f^2 \exp(E_{ACT,OF}/RT_F)}{p^{(n-1)}\phi} \tag{20}$$

$$L_{AP} = \frac{K_{AP} V_{gas,surf}}{p^{(n-1)}} \tag{21}$$

while tables generated from calculations performed using Burke-Schumann theory are used for calculation of FH90 as a function of such parameters as diffusivity, gas velocity off the surface, flame stoichiometry parameters, and oxidizer and fuel dimensions.

9. Compare the sum of $\dot{q}_1$-$\dot{q}_4$ with $\dot{q}_5$ plus $\dot{q}_{fdbk}$; if they are not equal, guess a new value of surface temperature and return to Step 1. Repeat to convergence.

10. After convergence, calculate propellant mass flux and burning rate from:

$$m_{propellant} = \frac{m_{ox,s} A_{ox,s}}{(\text{wt Fraction Oxidizer})} \frac{1}{A_{ox,p} + A_{fu}} \tag{22}$$

$$r_{propellant} = m_{propellant}/\rho_{propellant} \tag{23}$$

4.0 COMPARISON OF STEADY-STATE MODEL PREDICTIONS WITH DATA

As mentioned earlier, there are three "free" constants, B_{sub} in Equation 15, and K_{OF} and K_{AP} in Equations 20 and 21, included in the model described above; optimized values for these constants were chosen by calibration against burning rate versus pressure data for few unimodal-oxidizer-size AP/HTPB formulations (three 73-weight-percent AP formulations with oxidizer diameters of 5, 20, and 200 microns and one 77-weight-percent AP formulation with 20 micron diameter particles). Burning rate data and predictions made using the optimized values of these constants over a pressure range of 10 to 150 atmospheres are presented in Figure 3. As may be seen, predictions and data agree quite well except for the 200-micron AP formulation, where predicted values range from 5 percent high at 10 atmospheres to approximately 40 percent high at 150 atmospheres. Similar predicted and experimental burning rates versus pressure for five 82-weight-percent AP multimodal particle size formulations (four bimodals and one trimodal), with the same values of the constants being used for the predictions, are presented in Figure 4. Agreement between predictions and experimental data was seen to be excellent for all formulations except the fifty-fifty 20/200-micron bimodal AP formulation, where the predictions are approximately 10% high over the entire pressure range. Thus, it appears that this steady-state model, used as a basis for the unsteady-state burning rate studies described in the remainder of this report, is a good representation of AP/HTPB composite propellant combustion.

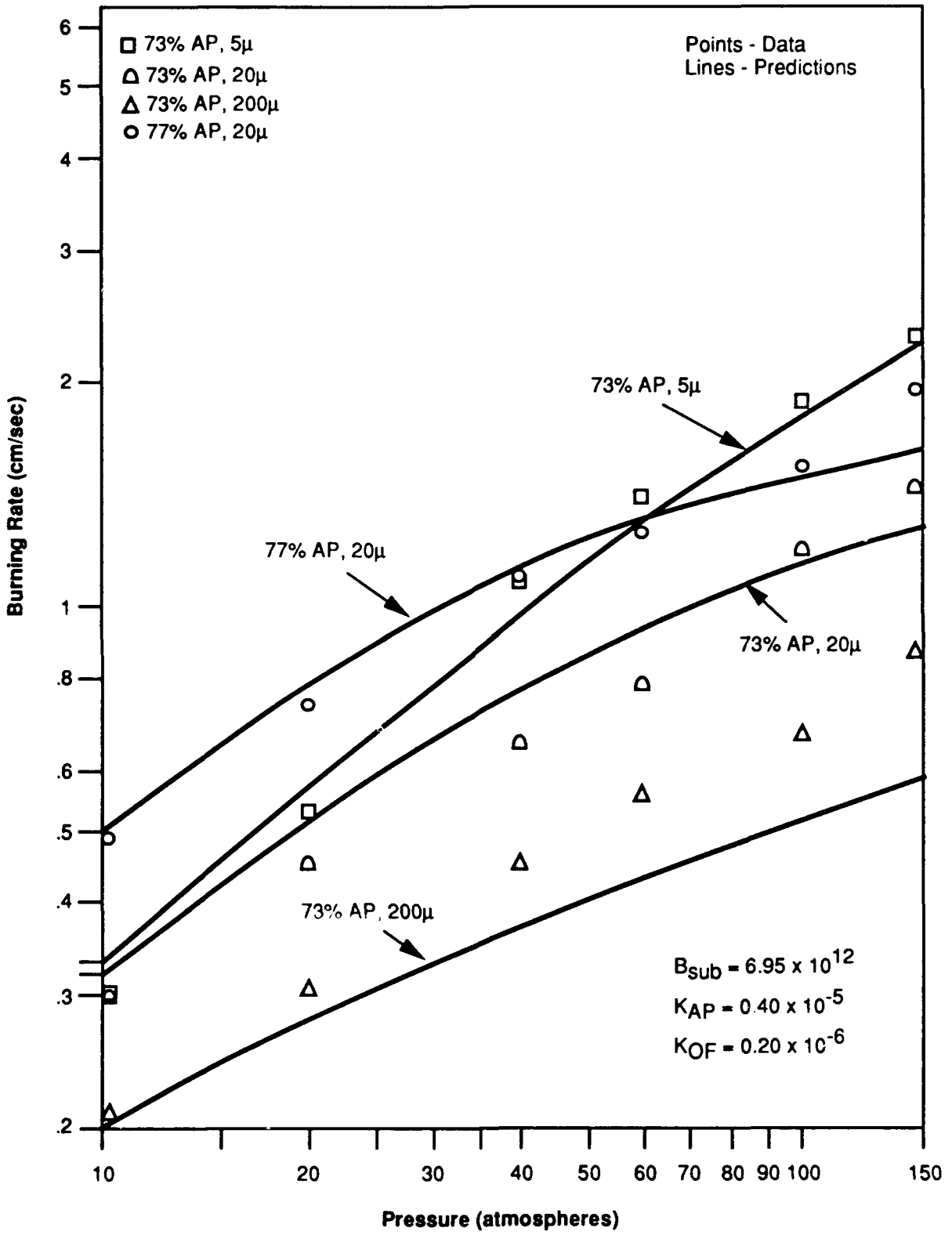

Figure 3. Predicted and Experimental Burning Rate as a Function of Pressure for Four Unimodal Oxidizer Formulations

1091-AFSOR

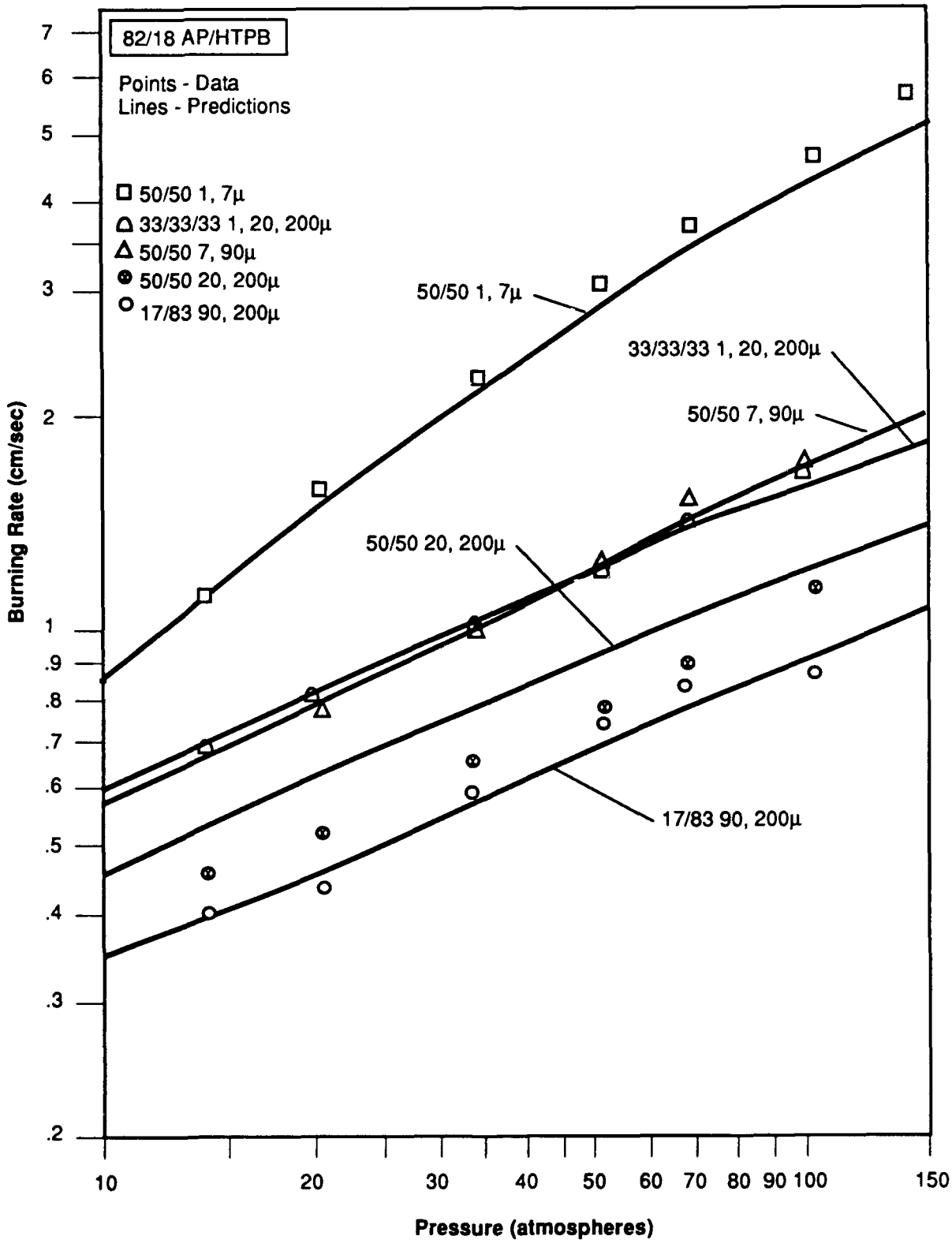

Figure 4. Predicted and Experimental Burning Rate as a Function of Pressure for Five Multimodal Oxidizer Formulations

1091-AFSOR

5.0 UNSTEADY-STATE MODELING

In this section, a description of a perturbation analysis of the steady-state model described in previous sections, consisting of a Fourier analysis of the solid propellant subsurface region plus a quasi-steady-state analysis of the surface and gas-phase processes and including allowance for perturbations in gas-phase oxidizer (fuel ratio), is presented. As a critical part of this analysis, the effects of partial adjustments of the relative oxidizer and fuel surface areas to oscillations in ablation fluxes of these ingredients were treated on a parametric basis. (For very rapid oscillations, there is no time for any surface area adjustment, while for slow oscillations approaching zero frequency in the limit, area adjustments, required for satisfaction of mass balances on oxidizer and fuel, are total.) Estimates of the degree of response of relative surface areas (between these two limits) to mass flux oscillations were made based on the ratio of the oscillation period to the time required for burning of a propellant thickness equal to the oxidizer diameter.

The analysis of the response of the subsurface regions to oscillations in heat feedback flux is a fairly standard one, used previously by this author (and many others) and described in detail in Reference 3. This analysis results in the following relationship between the perturbation values of the temperature gradient just below the surface, the surface temperature, and the burning rate:

$$K_s \frac{\partial T'}{\partial X}\bigg|_{s^-} = \rho_p \bar{r} C_{PS} \left[\lambda T_s' + \frac{(\bar{T}_s - T_\infty)}{\lambda} \frac{r'}{\bar{r}}\right] \tag{24}$$

where λ is a complex function of the oscillation frequency, given by:

$$\lambda^2 - \lambda - \frac{j\omega_p}{4} = 0 \tag{25}$$

$$W_p = \frac{4 K_s \rho_p \omega}{\bar{m}^2 C_{PS}} \tag{26}$$

ω_p = Dimensionless angular frequency of oscillations

K_s = Solid propellant thermal conductivity

ρ_p = Solid propellant density

C_{PS} = Solid propellant specific heat

$\bar{r}$ = Steady-state (mean) burning rate

$\bar{m}$ = Steady-state (mean) burning mass flux

ω = Angular frequency of oscillations ($2\pi f$)

X = Axial distance (from surface) into propellant

T' = Perturbation value of temperature

r' = Perturbation value of burning rate

Solution of Equation 25, with proper application of boundary conditions yields the following expressions for the real and imaginary parts of λ as functions of frequency:

$$\lambda_{real} = \frac{1}{2}\left\{1 + \frac{1}{\sqrt{2}}\left[(1 + \omega_p^2)^{1/2} + 1\right]^{1/2}\right\} \tag{27a}$$

$$\lambda_{imaginary} = \frac{1}{2\sqrt{2}}\left[(1 + \omega_p^2)^{1/2} - 1\right]^{1/2} \tag{27b}$$

Application of a surface energy balance at any instant of time yields a relationship between the instantaneous rate of heat transfer into the solid and the instantaneous rate of heat feedback from the gas phase above the propellant surface (S^+ represents a plane just above the surface, while S^- represents a plane just below it):

$$K_g \left.\frac{\partial T}{\partial X}\right|_{s^+} = K_s \left.\frac{\partial T}{\partial X}\right|_{s^-} - m_s Q_{surf} \tag{28}$$

where Q_{surf} is the sum of all heats of melting, vaporization, and surface/subsurface reactions (sign convention chosen to be positive for net exothermic process) per unit mass of propellant. (It should be noted here that an important approximation has been made in assignment of all these heat release/absorption processes to an infinitesimally thin region at the surface rather than treatment of processes occurring over a finite thickness of the

subsurface region.) Expansion of Equation 28 into mean and perturbation quantities yields:

$$K_g \frac{\partial T'}{\partial X}\bigg|_{s+} = K_s \frac{\partial T'}{\partial X}_{s-} - m'_s \bar{Q}_{surf} - \bar{m} Q'_{surf} \tag{29}$$

where the perturbation value of surface heat release per unit mass of propellant is expressed as:

$$Q'_{surf} = \frac{dQ_{surf}}{dT_s} T'_s \tag{30}$$

under an assumption that this heat release is a function of instantaneous surface temperature alone.

Since, as discussed earlier, a critical part of the current study involves allowance for differential perturbations in oxidizer and fuel ablation rates with oscillating surface temperature (due to different activation energies for the fuel and oxidizer ablation processes), considerable care must be taken in the calculation of m'_s and Q'_{surf} as functions of T'_s. Two limiting cases were analyzed in this study. In one it is assumed that surface area adjustments accompanying mass flux oscillations are negligible (high-oscillation-frequency limit); while in the other, it is assumed that there is time for adjustments in fuel and oxidizer surface areas to totally compensate for the differential variations in oxidizer and fuel mass flux oscillations such that the O/F ratio of material leaving the surface is constant at the overall propellant O/F ratio (low-oscillation-frequency limit). (As will be discussed later, parametric studies as regards frequencies between these two limiting cases were carried out as part of this study via linear combinations of the limiting case expressions.) The first limiting case (no surface-area adjustment) will be referred to as Scenario A in the remainder of the model description, while the second limiting case will be referred to as Scenario B. In the model developed in this study, $m'_s - T'_s$ and $Q'_{surf} - T'_s$ relationships are calculated numerically via calculation (using the steady-state model equations presented earlier) of m and Q_{surf} at the mean surface temperature value and at slightly higher values, both with forbidden (A) and allowed (B) surface area adjustments. With this procedure, values of f_{1A}, f_{1B} (where f_1 is defined as $(m'/\bar{m})/T'_s$ and dQ_{surf}/dT_s under Scenarios A and B are calculated.

Combination of Equations 28-30 with $m_s'/\bar{m}_s = f_1 T_s'$, with consideration subsequent mathematical manipulation yields an expression relating perturbation values of heat feedback flux (from the gas phase) and surface temperature:

$$q'_{fdbk} = \bar{m}\, C_{PS} \bar{T}_s \left[\lambda + \frac{A}{\lambda} + AB - \frac{1}{C_{ps}} \frac{dQ_{surf}}{d\bar{T}s} \frac{T_s'}{\bar{T}_s} \right] \tag{31}$$

where:

$$\left.\begin{aligned} A &= f_1 (\bar{T}_s - T_\infty) \\ \beta &= - \frac{\bar{Q}_{surf}}{C_{ps} (\bar{T}_s - T_\infty)} \end{aligned}\right\} A\beta = \frac{f_1 \bar{Q}_{surf}}{C_{PS}}$$

Further manipulation, utilizing a steady-state (mean) energy balance at the surface and $m_s'/\bar{m}_s = f_1 T_s'$ finally yields a desired relationship between perturbation mass burning flux and perturbation gas-phase heat feedback flux:

$$\frac{m_s'/\bar{m}_s}{q'_{fdbk}/\bar{q}_{fdbk}} = \frac{A(1+\beta)}{\lambda + \frac{A}{\lambda} + A\beta - \frac{1}{C_{PS}} \frac{d\, Q_{surf}}{d\bar{T}_s}} \tag{32}$$

Next, the gas-phase processes must be analyzed for development of an additional equation relating q'_{fdbk}, m_s', and P': this equation is then combined with Equation 32 for elimination of q'_{fdbk}, yielding an expression for the ratio of $(m_s'/\bar{m}_s)$ to $(P'/\bar{P})$, defined as the pressure-coupled response function.

With the gas-phase analysis employed in this model (described in the steady-state modeling section), there are basically only three independent parameters influencing the instantaneous heat feedback flux to the propellant surface; these are the instantaneous surface temperature (T_s), the instantaneous flame temperature (T_f), and the instantaneous pressure (P). [Of course, T_s affects many other parameters which in turn influence the heat feedback flux (e.g., fuel surface area, oxidizer surface area, fuel mass flux,

oxidizer mass flux, fractions of oxidizer and fuel consumed in surface/subsurface reactions.)] As indicated earlier, the gas phase processes are assumed to be quasi-steady-state. Accordingly, the basic procedure employed in this analysis involves calculation of partial derivatives relating perturbations in heat feedback flux to perturbations in surface temperature, flame temperature, and pressure.

First, the surface temperature is set equal to the mean surface temperature value (calculated from the steady-state analysis described earlier) and the quasi-steady-state gas phase analysis (same as described earlier) is used to calculate the gas-phase heat feedback flux at the mean (steady-state) pressure and flame temperature values. Next, the surface temperature is perturbed slightly (approximately 1 degree Kelvin) upward, with pressure and flame temperature being held at their mean values, and new values of heat feedback flux are calculated under two scenarios. (In Scenario A, the fuel and oxidizer surface areas are held at their steady-state values, while under Scenario B, they are adjusted to cause the ratio of oxidizer to fuel gases entering the gas combustion zones to be equal to the overall oxidizer/fuel ratio of the propellant.) From these three calculated heat feedback fluxes, the partial derivative of heat feedback flux with respect to surface temperature at constant pressure and flame temperature is calculated for each scenario from:

$$L = \left.\frac{\partial \dot{q}_{fdbk}}{\partial \bar{T}_s}\right|_{T_f,P} = \frac{\dot{q}_{fdbk,\ \bar{T}_s + \Delta T_s,\ \bar{T}_f,\ \bar{P}} - \dot{q}_{fdbk,\ \bar{T}_s,\ \bar{T}_f,\ \bar{P}}}{\Delta \bar{T}_s} \qquad (33)$$

Next, surface temperature and flame temperature are held at their mean (steady-state) values, and pressure is perturbed slightly upward for calculation of a fourth heat feedback flux value; the partial derivative of heat feedback flux with respect to pressure at constant surface temperature and flame temperature is then calculated as:

$$N = \left.\frac{\partial \dot{q}_{fdbk}}{\partial \bar{P}}\right|_{T_s,T_f} = \frac{\dot{q}_{fdbk,\ \bar{T}_s,\ \bar{T}_f,\ \bar{P} + \Delta P} - \dot{q}_{fdbk,\ \bar{T}_s,\ \bar{T}_f,\ \bar{P}}}{\Delta P} \qquad (34)$$

Finally, surface temperature and pressure are held at their mean (steady-state) values, and flame temperature is perturbed slightly upward for calculation of a fifth value of heat feedback flux; the partial derivative of heat feedback flux with respect to flame temperature at constant pressure and surface temperature is then calculated as:

$$M \equiv \left.\frac{\partial \dot{q}_{fdbk}}{\partial \bar{T}_f}\right|_{T_s,P} = \frac{\dot{q}_{fdbk,\ \bar{T}_s,\ \bar{T}_f + \Delta T_f,\ \bar{P}} - \dot{q}_{fdbk,\ \bar{T}_s,\ \bar{T}_f,\ \bar{P}}}{\Delta T_f} \qquad (35)$$

Using linear superposition principles (this is a linearized analysis), perturbations in heat feedback flux are then related to perturbations in surface temperature, flame temperature, and pressure by:

$$q'_{fdbk} = LT'_s + MT'_f + Np' \qquad (36)$$

At this point, we have four equations (Equations 30, 32, 36, and $m'_s/\bar{m}_s = f_1 T'_s$) in six perturbation quantities (T'_s, T'_f, P', m'_s, Q'_{surf}, and q'_{fdbk}). One more equation is required to permit the desired calculation of m'_s as a function of P' (the true independent parameter in this study). This final closure equation is derived from perturbation analysis of the gas-phase energy balance, which may be written as:

$$m_s Q_{gas} = m_s C_{pg} (T_f - T_s) + \dot{q}_{fdbk} \qquad (37)$$

$$Q_{gas} = \Delta H_{TOT} - Q_{surf} = \left[f \frac{m_{ox,s} ASOX}{m_{ox,s} ASOX + m_{fu} AFU} \right] - Q_{surf} \qquad (38)$$

Q_{gas} = Gas-phase heat release (cal/gm)

Q_{surf} = Heat release in surface processes (cal/gm)

ΔH_{TOT} = Total available energy associated with a "slug" of oxidizer and fuel leaving the surface at a given instant of time (cal/gm)

ΔH_{TOT} is, of course, dependent on the relative mass flow rates (mass flux-surface area products) of oxidizer and fuel leaving the surface at any time. (ASOX is the instantaneous surface area of oxidizer, while AFU is the corresponding instantaneous surface area of fuel.) A series of calculations of this available energy as a function of oxidizer/fuel ratio over a range of interest covering practical AP-composite propellant compositions results in:

$$\Delta H_{TOT} = -2050 + 3600 \left[\frac{m_{ox,s} ASOX}{m_{ox,s} ASOX + m_{fu} AFU} \right] \tag{39}$$

The quantity inside the brackets, in turn, is a function of the surface temperature; the functionality obviously differs under the Scenario A (no surface area adjustment during oscillations) and Scenario B (adjustment of surface areas to maintain constant O/F ratio gas "slugs" leaving the propellant surface) assumptions. Again with use of linearized analysis and definition of the constant relating perturbations in the bracketed term to perturbations in surface temperature as:

$$f_3 \equiv [\quad]' / T_s' \tag{40}$$

it is easily shown that under Scenario B, $f_3 = 0$, while under Scenario A,

$$f_3 = \frac{\dfrac{A_{ox} \exp\left[-E_{ox}/R\,(\bar{T}_s + T_s')\right] \overline{ASOX}}{A_{ox} \exp\left[-E_{ox}/R\,(\bar{T}_s - T_s')\right] \overline{ASOX} + A_{fu} \exp\left[-E_{fu}/R\,(\bar{T}_s + T_s')\right] \overline{AFU}} - WFO}{T_s'} \tag{41}$$

where WFO is the weight fraction of oxidizer in the propellant. Perturbation of Equation 39, with substitution of Equation 40 then yields:

$$\Delta H_{TOT}' = 3600\, f_3 T_s' \tag{42}$$

with subsequent perturbation of Equation 38 then yielding:

$$Q'_{gas} = 3600\, f_3 T'_s - \frac{dQ_{surf}}{dT_s} T'_s = f_4 T'_s \tag{43}$$

where $f_4 = 3600\, f_3 - dQ_{surf}/dT_s$.

Expansion of Equation 22 into steady-state and perturbation quantities next yields (after considerable algebraic manipulation):

$$q'_{fdbk} = \frac{m'_s \bar{q}_{fdbk}}{\bar{m}_s} + \bar{m}_s Q'_{gas} - \bar{m}_s C_{pg} (T'_f - T'_s) \tag{44}$$

which, in conjunction with Equation 43, provides the final equation needed for closure of this analysis. At this point, we have six equations (Equations 30, 32, 36, 43, 44, and $m'_s/\bar{m}_s = f_1 T'_s$) in seven unknown perturbation quantities (q'_{fdbk}, T'_s, T'_f, P', m'_s, Q'_{surf}, Q'_{gas}); these can be worked into the desired expression for $R_{PC} = (m'_s/\bar{m}_s)/(P'/\bar{P})$ with sufficient effort. In the interest of space, the required manipulation will not be presented here; the final expression for the pressure-coupled response function is:

$$R_{pc} = \frac{m'_s/\bar{m}_s}{P'/\bar{P}} = \frac{N}{\left\{\left(\frac{M}{\bar{m}_s C_{pg}} + 1\right)\left(\frac{\lambda + A/\lambda + A\beta - \frac{1}{C_{ps}}\frac{dQ_{surf}}{dT_s}\dot{\bar{q}}_{fdbk}}{A(1+\beta)\bar{P}}\right) - \left(\frac{\bar{m}\,\dot{\bar{q}}_{fdbk}}{\bar{m}_s C_{pg}\bar{P}} - \left(\frac{f_4}{C_{pg} f_1} + \frac{L}{f_1 M} + \frac{1}{f_1}\frac{M}{\bar{P}}\right)\right)\right\}} \tag{45}$$

where procedures for calculation of A, B, L, M, N, dQ_{surf}/dT_s, f_1, and f_4 under either limiting scenario as regards surface topology adjustment during

oscillations have been previously discussed, and $\bar{q}_{fdbk}$ and $\bar{m}_s$ are available from the steady-state model. Given values for all of these parameters, the real part of the pressure-coupled response is calculated for various frequencies using the following procedure.

First, the frequency is substituted into Equation 26 for calculation of the dimensionless angular frequency. Equations 27a and 27b are then used to calculate the real and imaginary parts of λ. These are then substituted into Equation 45 for calculation of the real and imaginary parts of R_{PC}. From calculations of various frequencies, a map of the real part of the pressure-coupled response versus frequency is generated for each case examined.

As indicated earlier, two limiting case scenarios as regards surface topology adjustments during pressure oscillations were treated in the equation development for f_1 (appearing in the constant, A), f_4, dQ_{surf}/dT_s, and L; in the parameter studies described in the remainder of this report, allowance was made for partial surface area adjustments (intermediate between the two limiting cases of zero adjustment at very high oscillation frequency to full adjustment, for maintenance of constant O/F ratio of gas "slugs" leaving the propellant surface, at very low oscillation frequency). A quantity, ZFRACT, defining the fractional location of actual operation between the two limiting cases (ZFRACT = 0 for Scenario A, ZFRACT = 1.0 for Scenario B) was utilized in these calculations, with the values of each of the quantities which are scenario-dependent being calculated as:

$$X_j = (1\text{-ZFRACT})\ X_{j,\text{Scenario A}} + \text{ZFRACT}\ X_{j,\text{Scenario B}} \qquad (46)$$

In the first phase of the numerical studies, ZFRACT was treated simply as a model input, with effects on calculated response function versus frequency curves being examined parametrically. In the second phase of the study, an expression relating the value of ZFRACT to the ratio of the characteristic oscillation time (inversely proportional to the oscillation frequency) and the time required to burn through a thickness of propellant equal to one oxidizer diameter was utilized. This time ratio, TIMRAT, was calculated as:

$$TIMRAT = \frac{\bar{m}}{f\ \rho_{prop} D_{ox}} \tag{47}$$

$\bar{m}$ = Propellant burning mass flux (mean)
f = Oscillation frequency
ρ_{prop} = Propellant density
D_{ox} = Average oxidizer particle diameter

Included in the user inputs to the computer code in this study phase were a value of TIMRAT above which ZFRACT = 1.0 (TRATMX) and a value of TIMRAT below which ZFRACT = 0.0 (TRATMN); between these limits, it was assumed that ZFRACT could be related to TIMRAT by an expression of the form:

$$ZFRACT = K_1 + K_2 \ln (TIMRAT) \tag{48}$$

where K_1 and K_2 were calculated using ZFRACT = 1.0 at TIMRAT = TRATMX and ZFRACT = 0.0 at TIMRAT = TRATMN, leading to:

$$K_2 = \frac{1.0}{\ln (TRATMX) - \ln (TRATMN)} \tag{49}$$

$$K_1 = -K_2 \ln (TRATMN) \tag{50}$$

6.0 RESULTS OF PARAMETRIC STUDIES

As indicated earlier, there were two major phases in the numerical studies performed utilizing a computer code based on the analyses, described in the previous section, for calculation of the real part of the pressure-coupled response functions of AP-composite propellants versus oscillation frequency. In the first part of the study, ZFRACT, a parameter characterizing the fractional distance from zero-surface-topology-adjustment toward full adjustment for maintenance of constant oxidizer/fuel ratio in the gas phase was treated parametrically, with results being calculated for various user-input values of this parameter (held constant over the frequency range studied); in this case, closed-form expressions for the real part of the pressure-coupled response function in the form:

$$R_{pc}^{(real)} = \frac{TERM4}{\lambda + A/\lambda + TERM5} \tag{51}$$

where TERM4, TERM5, and A are constant over the entire frequency range for a given propellant and mean pressure, could be obtained. In the second phase of the study, where ZFRACT is calculated as a function of the ratio of oscillation time to time required for burning of one oxidizer diameter thickness of propellant, ZFRACT is obviously a function of the oscillation frequency; in this case, such a closed-form expression cannot be obtained.

6.1 Variant I - Input Values of ZFRACT

Calculations in this phase of the study were first made with baseline values of the oxidizer and fuel ablation activation energies for definition of the effects of the ZFRACT parameter on pressure-coupled response functions of propellant in which these activation energies have not been modified by chemical alterations of the ingredients. Subsequently, the effects of different values of these activation energies on predicted response of burning rate oscillations to imposed pressure oscillations were examined.

6.1.1 Calculations Using Baseline Ablation Activation Energies

Typical plots of predicted values of the real part of the pressure-coupled response versus frequency are presented in Figures 5-8; ZFRACT values of 0, 0.2, 0.4, 0.6, 0.8, and 1.0 were used in these calculations. As may be seen, the predicted magnitudes of the real parts of the response function decrease significantly with increasing values of ZFRACT; that is, allowance for surface area variations partially or totally compensating for the differential sensitivity of oxidizer and fuel ablation fluxes to surface temperature variations results in considerable stabilization of the burning processes. Another way of viewing the result is that it demonstrates the strong destabilizing contribution of variations in the oxidizer/fuel ratio of "slugs" of propellant leaving the surface (accompanying surface temeprature oscillations) in the absence of such surface area variation compensating effects.

Values of TERM4, TERM5, and A (Equation 51), along with maximum values of the real part of the pressure-coupled response function are tabulated in Table I for 82/18 AP/HTPB formulations for various values of ZFRACT, pressure, and ammonium perchlorate particle size. (Similar tables were generated for 77/23 AP/HTPB and 73/27 AP/HTPB formulations, but are not presented here since they add little additional information.) Again, it is seen that the maximum value of the real part of the pressure-coupled response function decreases significantly as more and more surface area adjustment is allowed (increased values of ZFRACT). Careful examination of the results reveals that the maximum value of the real part of the pressure-coupled response function, normalized by the steady-state burning rate exponent, n, correlates quite well with TERM5 values, this normalized maximum value decreasing as TERM5 increases. (See Figure 9.) This behavior is also exhibited for the 77/23 and 73/27 AP/HTPB cases. It is of interest to examine the components of TERM5 further to see what factors lead to increased values and thus to decreased real part of the pressure-coupled response function.

Comparison of Equations 45 and 51 permits derivation of an expression for TERM5 as a function of various parameters:

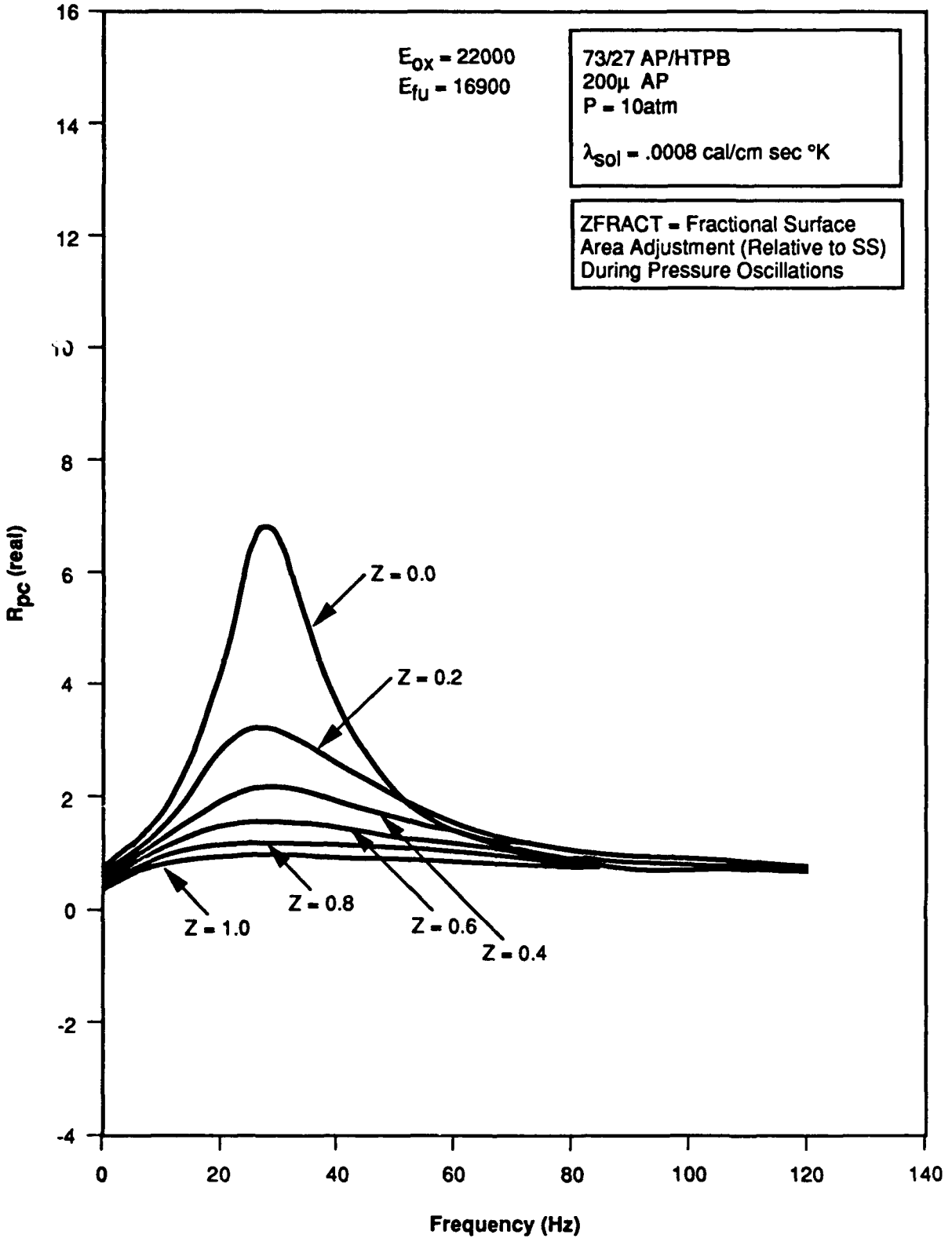

Figure 5. Predicted R_{pc} (real) vs. Frequency Curves for Various Values of ZFRACT.

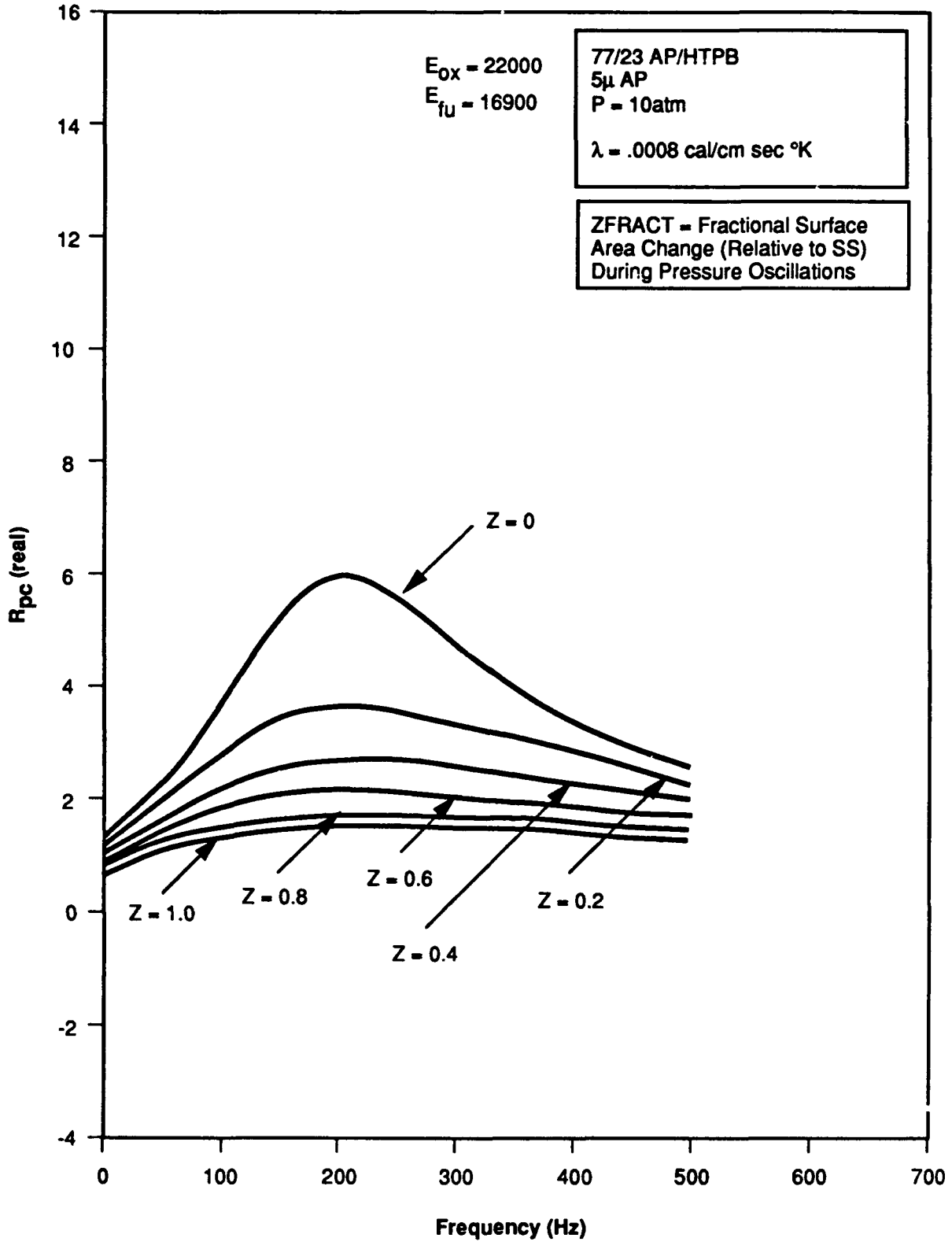

Figure 6. Predicted R_{pc} (real) vs. Frequency Curves for Various Values of ZFRACT.

1091-AFSOR

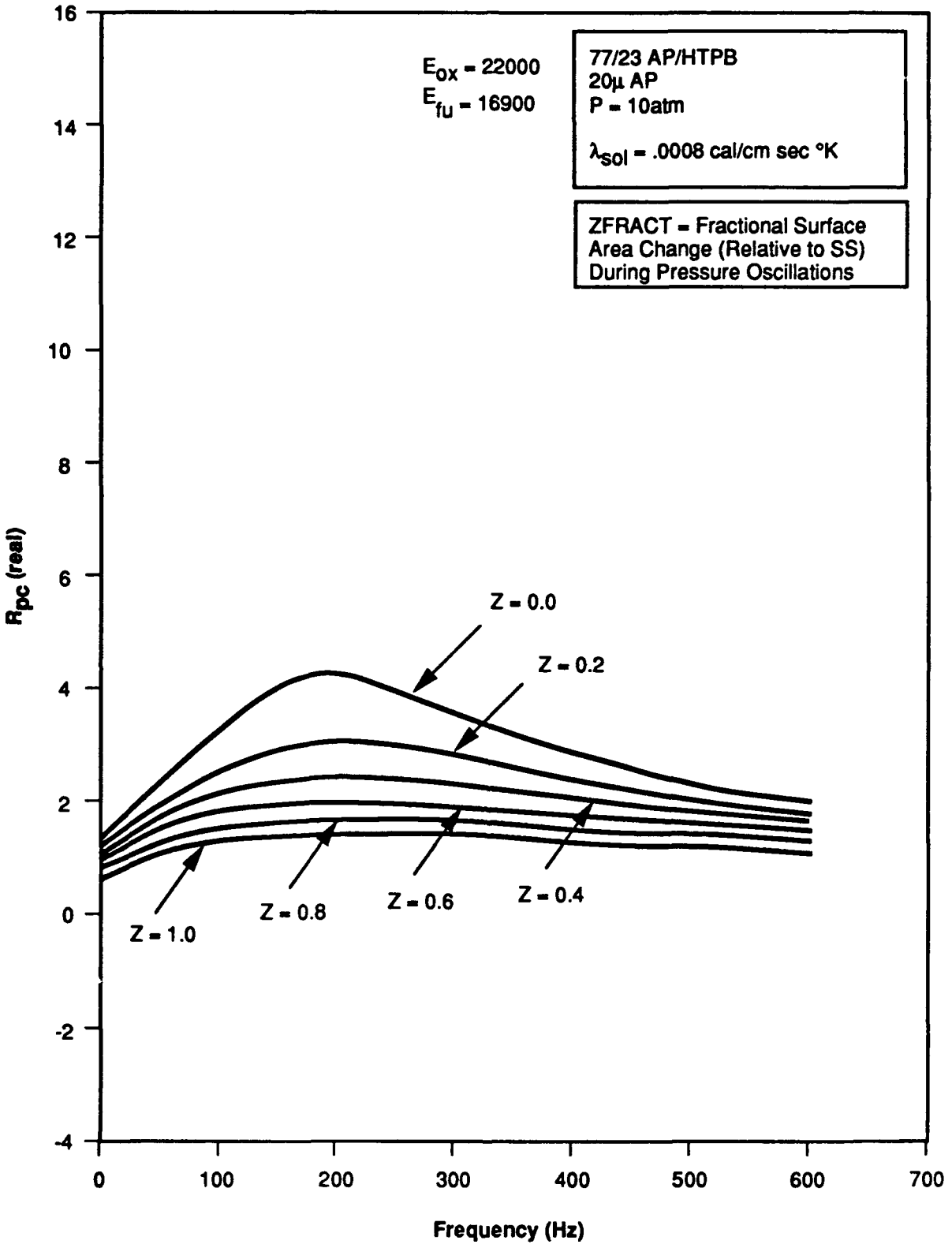

Figure 7. Predicted R_{pc} (real) vs. Frequency Curves for Various Values of ZFRACT.

1091-AFSOR

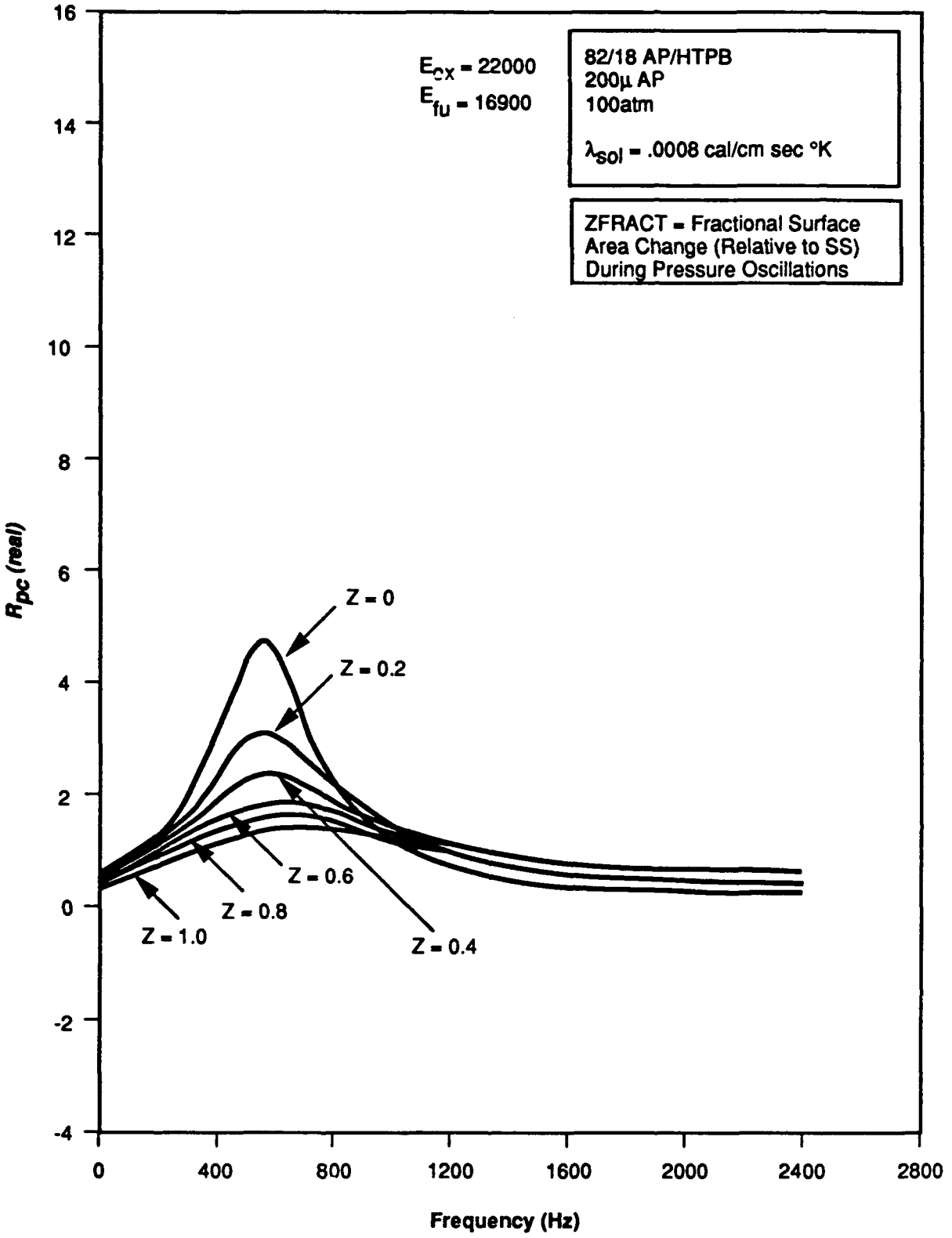

Figure 8. Predicted R_{pc} (real) vs. Frequency Curves for Various Values of ZFRACT.

1091-AFSOR

Table I. TERM4, TERM5, A, and Maximum Value of $R_{pc}^{(real)}$ for Various Values of AP Size, Pressure, and ZFRACT.

82/18 AP/HTPB E_{ox} = 22000 E_{fu} = 16900 K_{solid} = 0.0008 cal/cm-sec°K

AP Diameter (μ)	Pressure (atm)	ZFRACT	TERM4*	A*	TERM5*	Max $R_{pc}^{(real)}$
1.0	10	1.0	11.131	8.3933	+3.6953	1.22
1.0	10	0.8	10.933	8.2435	+3.0251	1.32
1.0	10	0.6	10.734	8.0937	+2.3550	1.43
1.0	10	0.4	10.535	7.9439	+1.6848	1.62
1.0	10	0.2	10.337	7.7941	+1.0146	1.84
1.0	10	0	10.138	7.6443	+0.3445	2.13
1.0	40	1.0	8.6270	7.0454	+2.4818	1.28
1.0	40	0.8	8.6679	7.0789	+1.9318	1.37
1.0	40	0.6	8.7089	7.1124	+1.3816	1.53
1.0	40	0.4	8.7499	7.1458	+0.8316	1.71
1.0	40	0.2	8.7908	7.1793	+0.2815	1.90
1.0	40	0	8.8318	7.2127	-0.2686	2.18
1.0	100	1.0	7.5366	6.7556	+1.6248	1.30
1.0	100	0.8	7.5641	6.7803	+1.1354	1.43
1.0	100	0.6	7.5916	6.8050	+0.6461	1.58
1.0	100	0.4	7.6192	6.8297	+0.1567	1.71
1.0	100	0.2	7.6467	6.8544	-0.3326	1.95
1.0	100	0	7.6743	6.8791	-0.8220	2.25
7.0	10	1.0	10.747	8.3677	+3.8099	1.20
7.0	10	0.8	10.563	8.2243	+3.1498	1.27
7.0	10	0.6	10.379	8.0810	+2.4897	1.37
7.0	10	0.4	10.195	7.9376	+1.8296	1.54
7.0	10	0.2	10.011	7.7943	+1.1696	1.72
7.0	10	0	9.8265	7.6510	+0.5095	1.99
7.0	40	1.0	6.8037	7.1141	+3.5080	0.83
7.0	40	0.8	6.8360	7.1479	+3.0135	0.88
7.0	40	0.6	6.8684	7.1817	+2.5191	0.98
7.0	40	0.4	6.9007	7.2155	+2.0246	1.08
7.0	40	0.2	6.9330	7.2493	+1.5301	1.19
7.0	40	0	6.9654	7.2831	+1.0356	1.30
7.0	100	1.0	4.0828	6.9305	+3.4805	0.53
7.0	100	0.8	4.1027	6.9642	+3.0798	0.55
7.0	100	0.6	4.1226	6.9980	+2.6792	0.57
7.0	100	0.4	4.1424	7.0317	+2.2786	0.59
7.0	100	0.2	4.1623	7.0654	+1.8780	0.64
7.0	100	0	4.1821	7.0991	+1.4774	0.73

*$R_{pc}^{(real)}$ = TERM4/(λ + A/λ + TERM5)

Table I. TERM4, TERM5, A, and Maximum Value of $R_{pc}^{(real)}$ for Various Values of AP Size, Pressure, and ZFRACT (Cont'd).

82/18 AP/HTPB E_{ox} = 22000 E_{fu} = 16900 K_{solid} = 0.0008 cal/cm-sec°K

AP Diameter (μ)	Pressure (atm)	ZFRACT	TERM4*	A*	TERM5*	Max $R_{pc}^{(real)}$
20.0	10	1.0	9.0925	8.3116	+4.3698	0.97
20.0	10	0.8	8.9549	8.1858	+3.7508	1.01
20.0	10	0.6	8.8174	8.0601	+3.1319	1.08
20.0	10	0.4	8.6798	7.9344	+2.5129	1.17
20.0	10	0.2	8.5423	7.8086	+1.8940	1.30
20.0	10	0	8.4047	7.6829	+1.2750	1.47
20.0	40	1.0	4.1385	7.2869	+4.0268	0.50
20.0	40	0.8	4.1573	7.3201	+3.6296	0.52
20.0	40	0.6	4.1762	7.3532	+3.2323	0.56
20.0	40	0.4	4.1950	7.3864	+2.8350	0.60
20.0	40	0.2	4.2137	7.4195	+2.4378	0.63
20.0	40	0	4.2326	7.4527	+2.0405	0.66
20.0	100	1.0	2.8102	7.1923	+2.8546	0.40
20.0	100	0.8	2.8221	7.2228	+2.5211	0.42
20.0	100	0.6	2.8340	7.2532	+2.1875	0.44
20.0	100	0.4	2.8459	7.2837	+1.8539	0.46
20.0	100	0.2	2.8578	7.3142	+1.5203	0.49
20.0	100	0	2.8697	7.3446	+1.1867	0.52
90.0	10	1.0	4.2907	7.8660	+3.4874	0.54
90.0	10	0.8	4.2889	7.8627	+3.0963	0.56
90.0	10	0.6	4.2871	7.8594	+2.7051	0.59
90.0	10	0.4	4.2854	7.8561	+2.3140	0.63
90.0	10	0.2	4.2835	7.8529	+1.9229	0.67
90.0	10	0	4.2818	7.8496	+1.5317	0.71
90.0	40	1.0	3.5945	8.2683	+1.4943	0.59
90.0	40	0.8	3.5448	8.1539	+1.1589	0.61
90.0	40	0.6	3.4951	8.0396	+0.8240	0.65
90.0	40	0.4	3.4453	7.9252	+0.4879	0.69
90.0	40	0.2	3.3956	7.8108	+0.1524	0.74
90.0	40	0	3.3459	7.6964	-0.1830	0.79
90.0	100	1.0	2.9627	8.5188	-0.9098	0.80
90.0	100	0.8	2.8980	8.3329	-1.2234	0.89
90.0	100	0.6	2.8334	8.1470	-1.5370	0.98
90.0	100	0.4	2.7687	7.9612	-1.8506	1.09
90.0	100	0.2	2.7041	7.7753	-2.1641	1.20
90.0	100	0	2.6394	7.5894	-2.4777	1.36

*$R_{pc}^{(real)}$ = TERM4/(λ + A/λ + TERM5)

Table I. TERM4, TERM5, A, and Maximum Value of $R_{pc}^{(real)}$ for Various Values of AP Size, Pressure, and ZFRACT (Cont'd).

82/18 AP/HTPB E_{ox} = 22000 E_{fu} = 16900 K_{solid} = 0.0008 cal/cm-sec°K

AP Diameter (μ)	Pressure (atm)	ZFRACT	TERM4*	A*	TERM5*	Max $R_{pc}^{(real)}$
200.0	10	1.0	3.6739	7.5769	+1.7430	0.60
200.0	10	0.8	3.7118	7.6549	+1.4477	0.62
200.0	10	0.6	3.7497	7.7330	+1.1523	0.65
200.0	10	0.4	3.7875	7.8111	+0.8569	0.69
200.0	10	0.2	3.8254	7.8892	+0.5615	0.74
200.0	10	0	3.8633	7.9673	+0.2662	0.81
200.0	40	1.0	3.5252	8.0509	-0.8644	0.96
200.0	40	0.8	3.5013	7.9965	-1.1385	1.02
200.0	40	0.6	3.4775	7.9420	-1.4125	1.10
200.0	40	0.4	3.4536	7.8875	-1.6866	1.21
200.0	40	0.2	3.4298	7.8331	-1.9607	1.36
200.0	40	0	3.4059	7.7786	-2.2347	1.53
200.0	100	1.0	2.9379	8.4323	-2.5698	1.40
200.0	100	0.8	2.8828	8.2741	-2.8299	1.56
200.0	100	0.6	2.8277	8.1158	-3.0899	1.89
200.0	100	0.4	2.7725	7.9576	-3.3501	2.32
200.0	100	0.2	2.7174	7.7993	-3.6102	3.09
200.0	100	0	2.6622	7.6410	-3.8703	4.76

*$R_{pc}^{(real)}$ = TERM4/(λ + A/λ + TERM5)

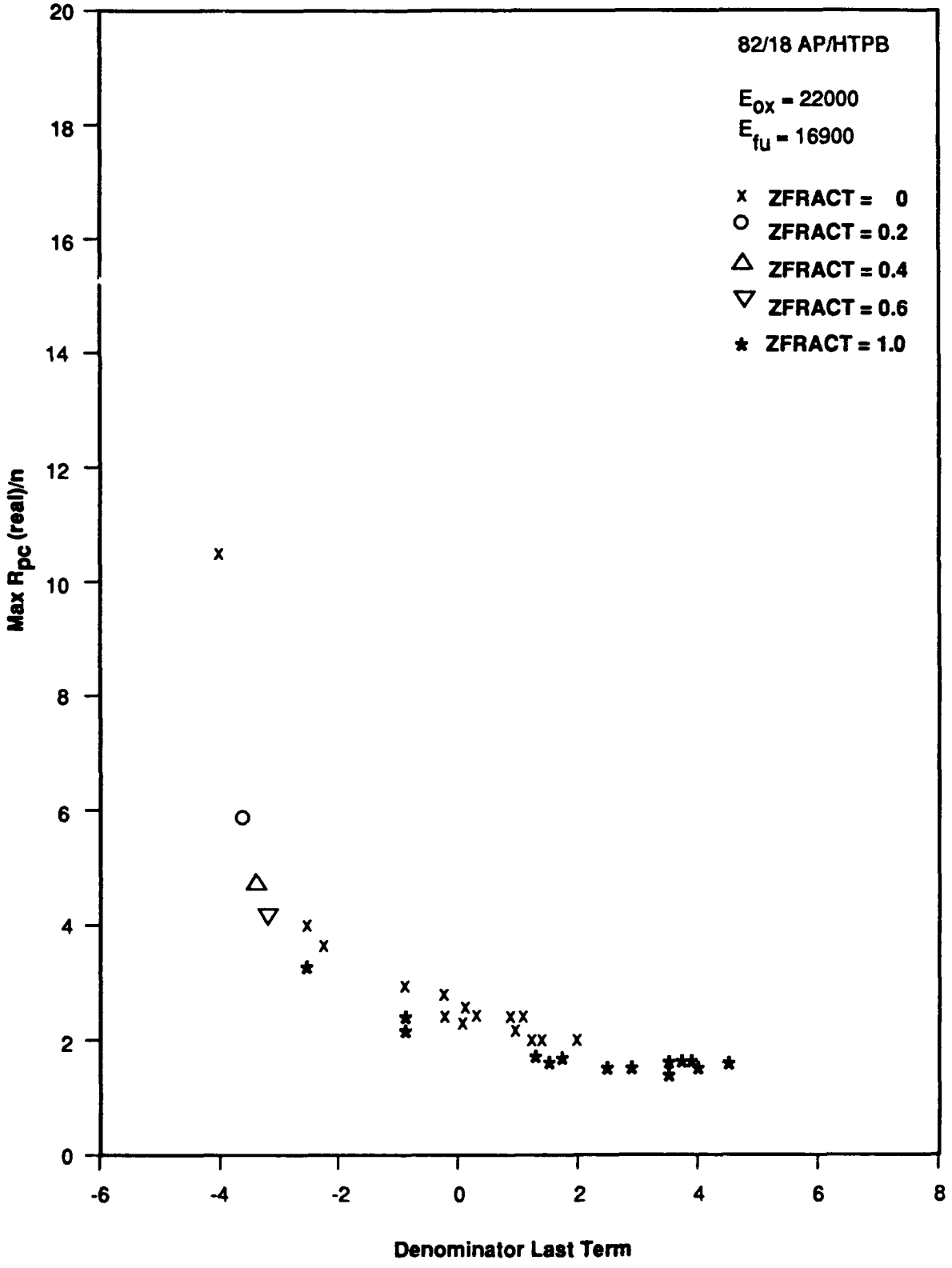

Figure 9. Variation of Maximum Value of Real Part of Pressure-Coupled Response Function (Normalized by Burning Rate Exponent) with TERM5 (Eqn 51).

$$\text{TERM5} = -\frac{A\bar{Q}_{surf}}{C_p\,(\bar{T}_s - T_0)} - \frac{1}{C_{p_s}}\frac{dQ_{surf}}{d\bar{T}_s}$$

$$- M\,(\bar{T}_s - T_0)\left(\frac{\bar{q}_{fdbk}\,f_1}{\bar{m}_s\,C_{p_{gas}}} + \frac{f_4}{C_{p_{gas}}} + \frac{L}{M} + 1.0\right) \qquad (52)$$

$$\left(\frac{M}{\bar{m}_s\,C_{p_{gas}}} + 1.0\right)\bar{q}_{fdbk}\left(1 - \frac{\bar{Q}_{surf}}{C_{p_s}\,(\bar{T}_s - T_0)}\right)$$

As may be seen from this equation, decreases in dQ_{surf}/dT_s (more negative values), f_4 (less positive values), and L (less positive or more negative values) all lead to increases in TERM5 and thus to decreases in the maximum value of $R_{pc}^{(real)}/n$; examination of detailed intermediate ouputs of the computer code indicate that such decreases in these these parameters accompany increases in ZFRACT (representing greater degree of surface area adjustment during pressure oscillations). Changes in L and dQ_{surf}/dT_s with ZFRACT are roughly equal in their contribution to increases in TERM5, while changes in f_4 are dominant for small AP particle size cases but considerably less important for large AP cases. Noting that $f_4 = dQ_{gas}/dT_s$ and $L = \partial\dot{q}_{fdbk}/\partial T_s$ (at constant flame temperature and pressure), we can see that increases in ZFRACT lead to decreases in maximum $R_{pc}^{(real)}/n$ values (accompanying increases in TERM5) by causing decreases in the partial derivative of heat feedback flux with respect to surface temperature (at constant T_{flame} and pressure) and decreases in the derivative of gas-phase plus surface heat release with respect to surface temperature (which, in turn, leads to decreases in the derivative of flame temperature with respect to surface temperature, also leading to lower increases in heat feedback flux accompanying a given increase in surface temperature.

6.1.2 Effects of Changes in Activation Energies of Fuel and Oxidizer Ablation Processes

In this phase of the study, R_{pc} expressions were calculated and $R_{pc}^{(real)}$ versus frequency curves developed for ZFRACT = 0 (no surface area adjustment) and ZFRACT = 1 (total surface area adjustment needed for constancy of O/F ratio of gas "slugs" leaving the propellant surface) cases; results for 82/18 AP/HTPB formulations with 1, 7, 20, 90, and 200 micron diameter AP at various pressures are presented and discussed here. In one set of calculations (for each pressure - AP size combination), the activation energy of the oxidizer ablation process was held at its baseline value of 22000 calories/mole with the activation energy of the fuel being varied; in a second set of calculations, the fuel ablation activation energy was held at its baseline value of 16900 calories/mole, while the oxidizer ablation activation energy was varied. In all cases, for either ingredient, the pre-exponential in the ablation rate expression was varied along with the activation energy so as to keep the steady-state burning rate at the prescribed pressure constant as the activation energy varied. (Obviously, other scenarios, such as holding the pre-exponential constant, could have been examined, but these would have made analysis of the results considerably more difficult/confusing. Further studies with different treatments of the pre-exponential factors are, of course, possible.) Results, in the form of R_{pc} expressions and maximum $R_{pc}^{(real)}$ values versus binder ablation activation energy at E_{ox} = 22000 and versus oxidizer activation energy at E_{fuel} = 16900 are presented in Appendix A for various AP sizes and pressures for ZFRACT = 0 and ZFRACT = 1.

Plots of the maximum value of the real part of the pressure-coupled response are plotted against the activation energy of the binder ablation process at a fixed value of oxidizer ablation activation energy (baseline value of 22000 calories/mole) for various pressure-particle size combinations for ZFRACT = 0 and ZFRACT = 1 (the two limiting cases as regards surface area adjustments during oscillations) in Figures 10-16. Similar plots of maximum $R_{pc}^{(real)}$ values versus oxidizer ablation activation energy for the baseline fuel ablation activation energy of 16900 calories/mole are presented as Figures 17-23. [As mentioned earlier, the previous simplified analysis of References 3-5 indicated that the real part of the pressure-coupled response

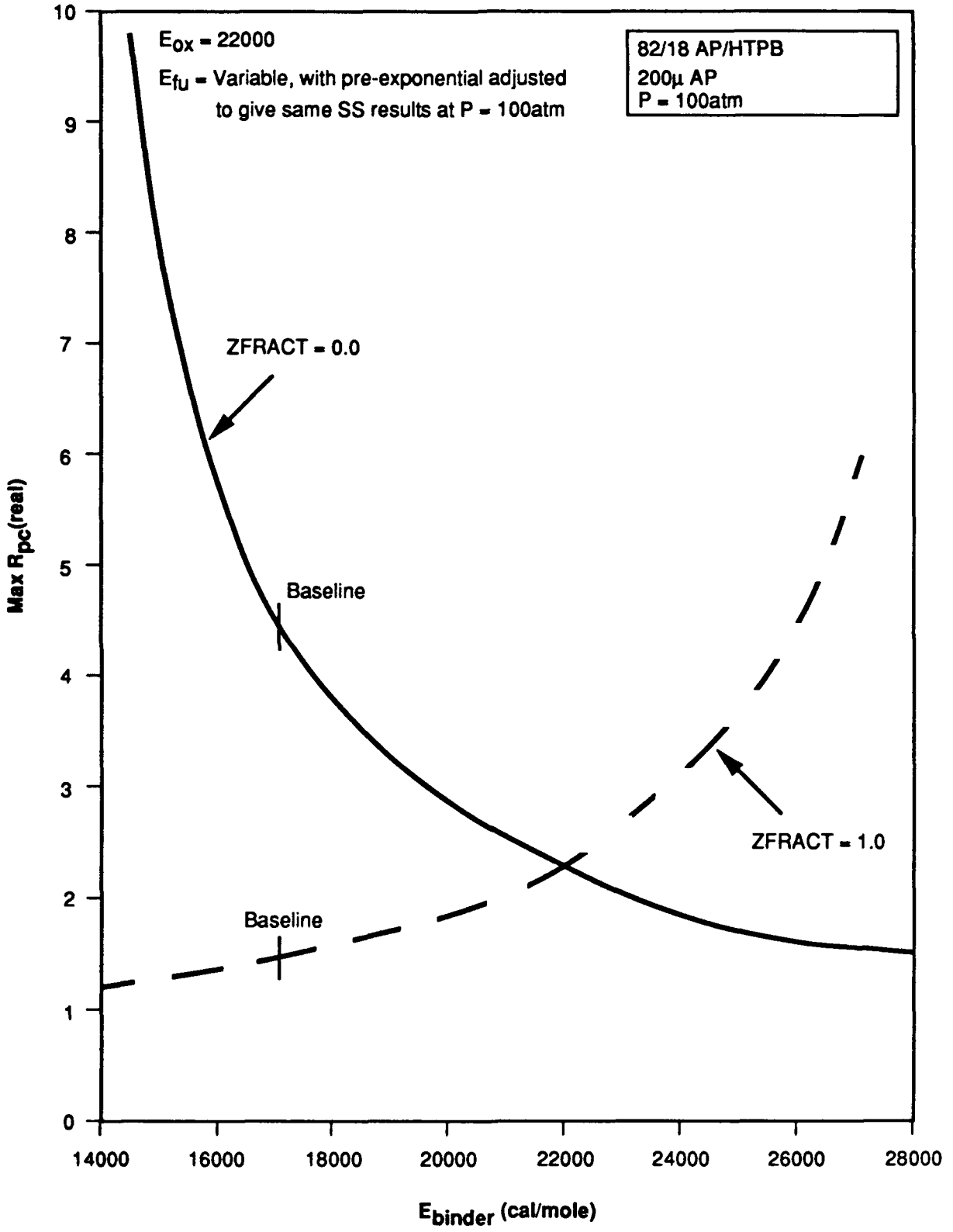

Figure 10. Dependence of Maximum Value of Real Part of Pressure-Coupled Response on Binder Ablation Activation Energy

1091-AFSOR

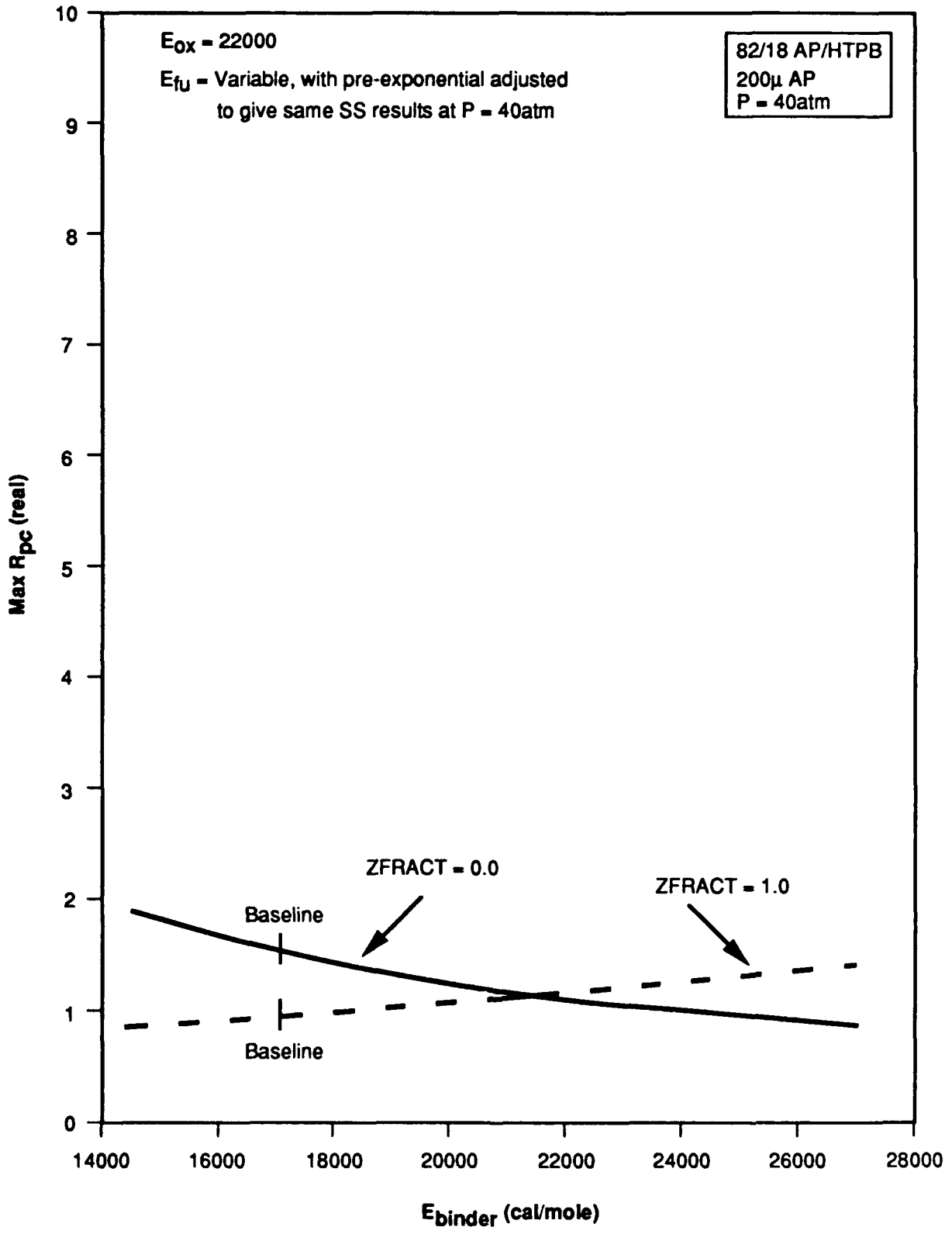

Figure 11. Dependence of Maximum Value of Real Part of Pressure-Coupled Response on Binder Ablation Activation Energy

1091-AFSOR

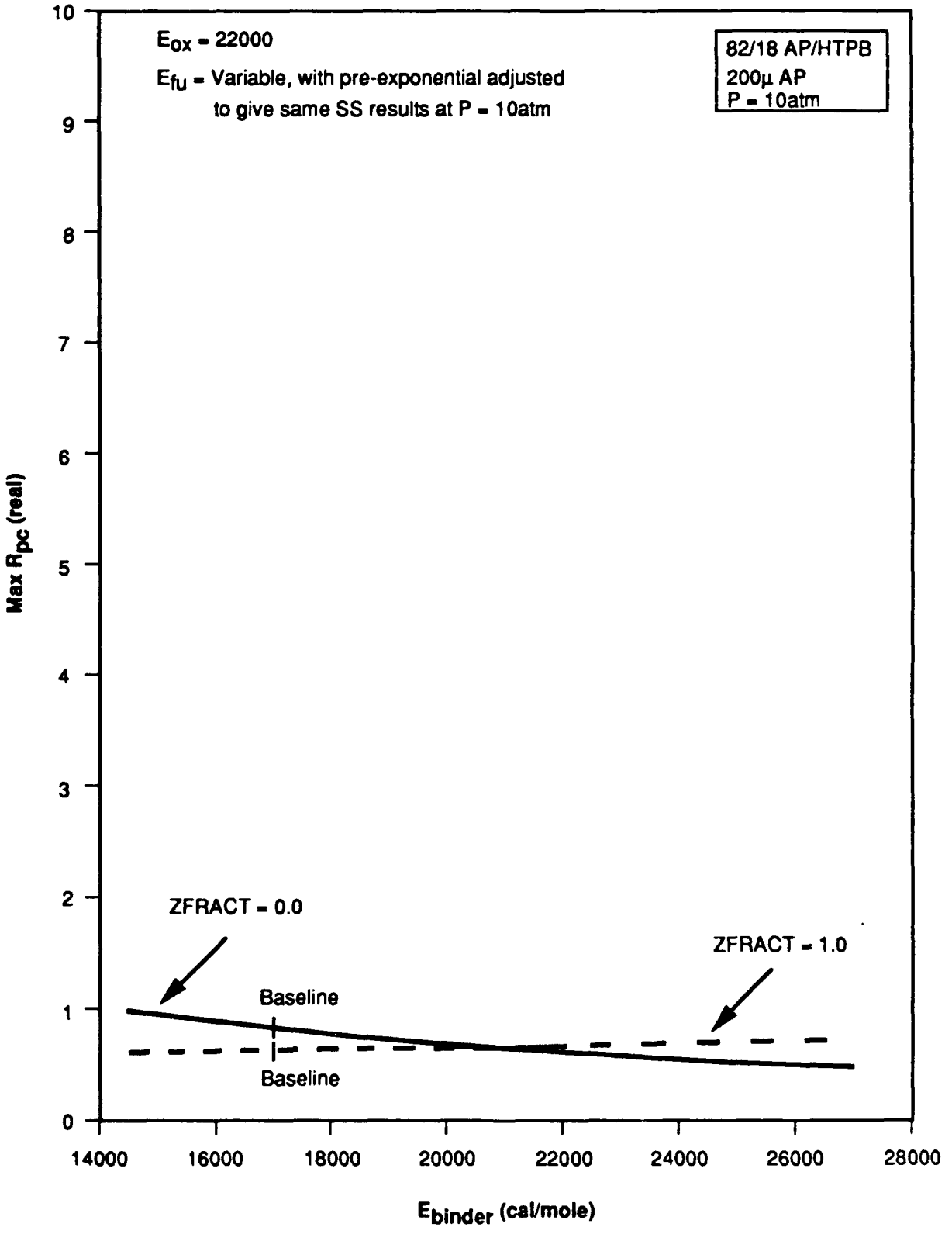

Figure 12. Dependence of Maximum Value of Real Part of Pressure-Coupled Response on Binder Ablation Activation Energy

1091-AFSOR

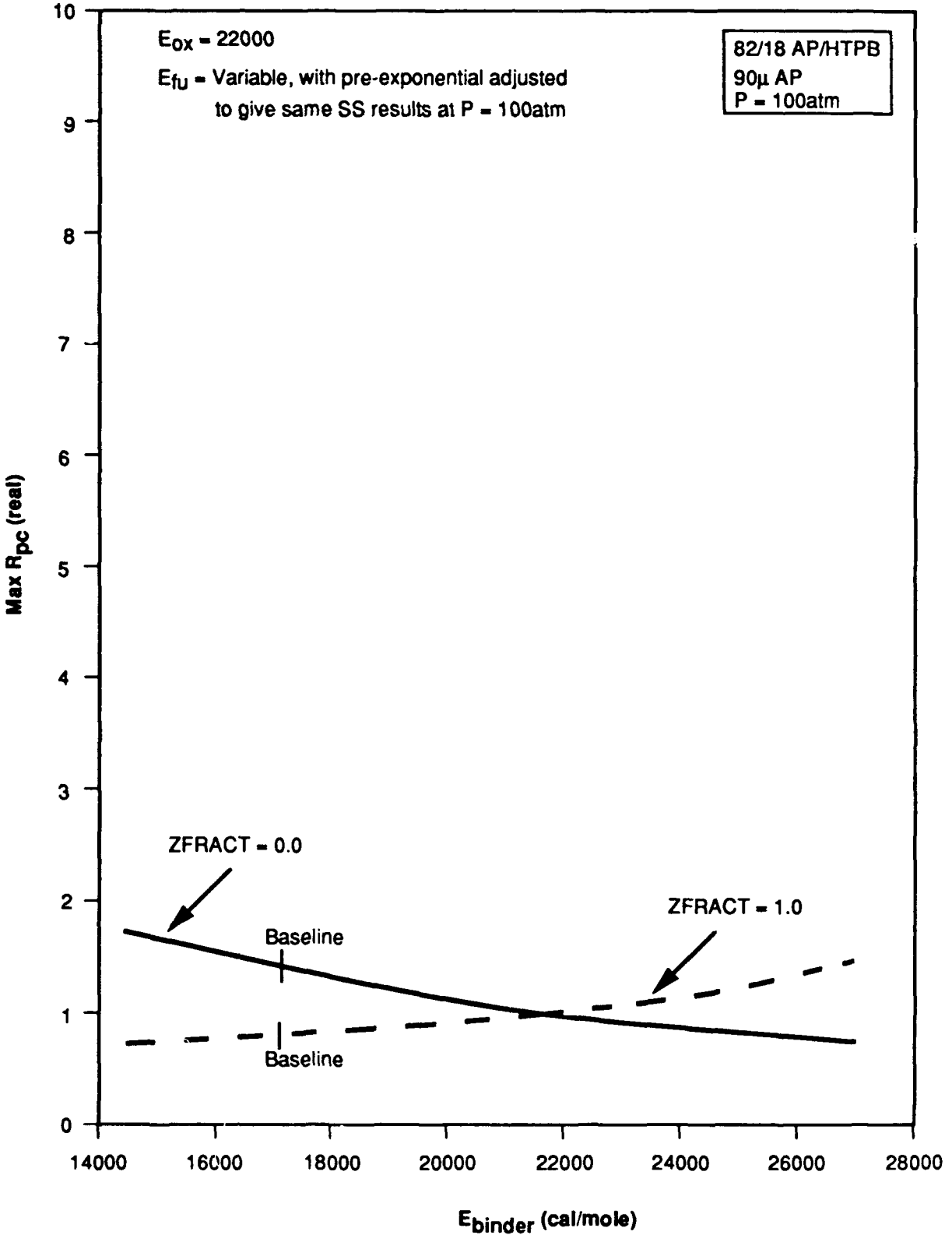

Figure 13. Dependence of Maximum Value of Real Part of Pressure-Coupled Response on Binder Ablation Activation Energy

1091-AFSOR

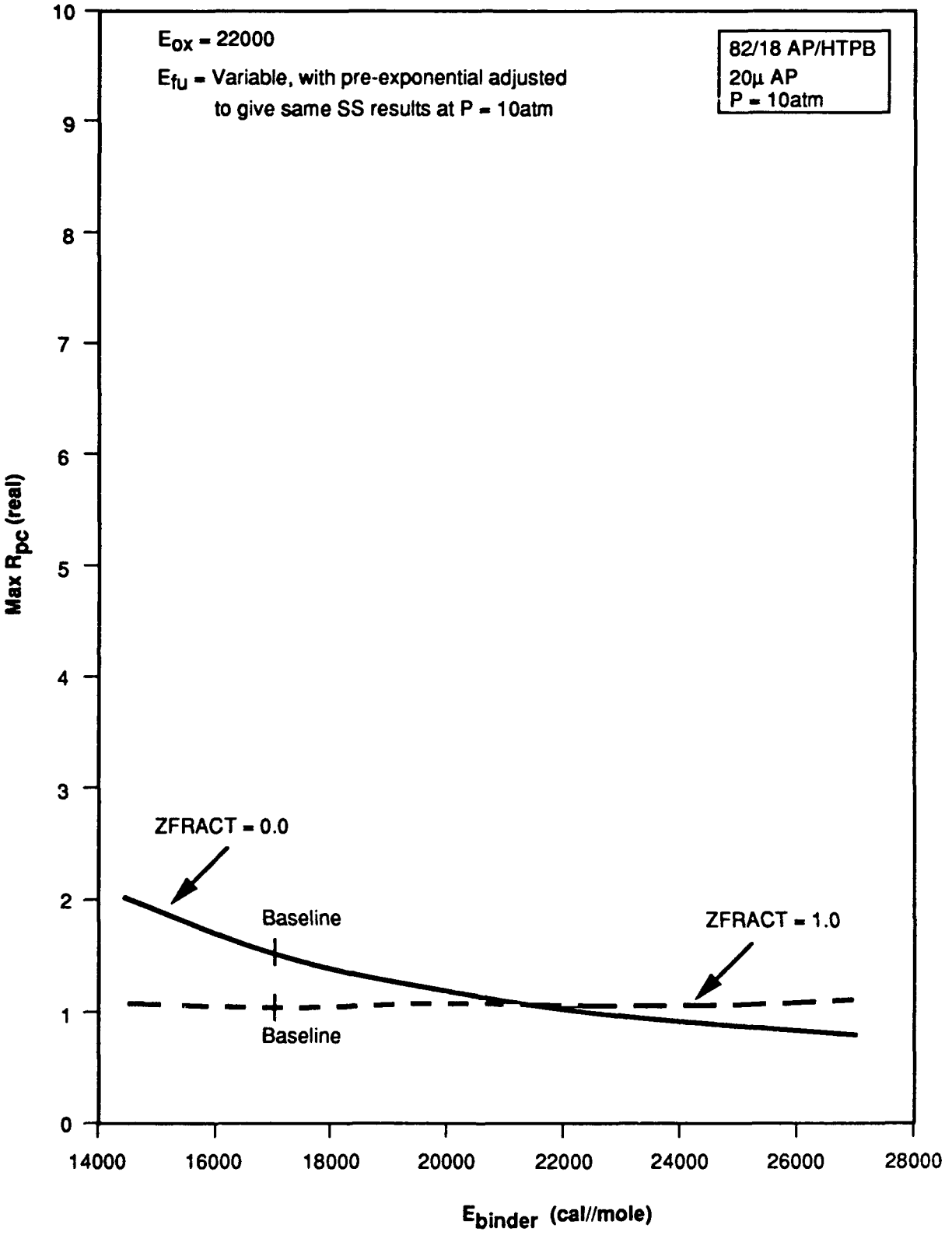

Figure 14. Dependence of Maximum Value of Real Part of Pressure-Coupled Response on Binder Ablation Activation Energy

1091-AFSOR

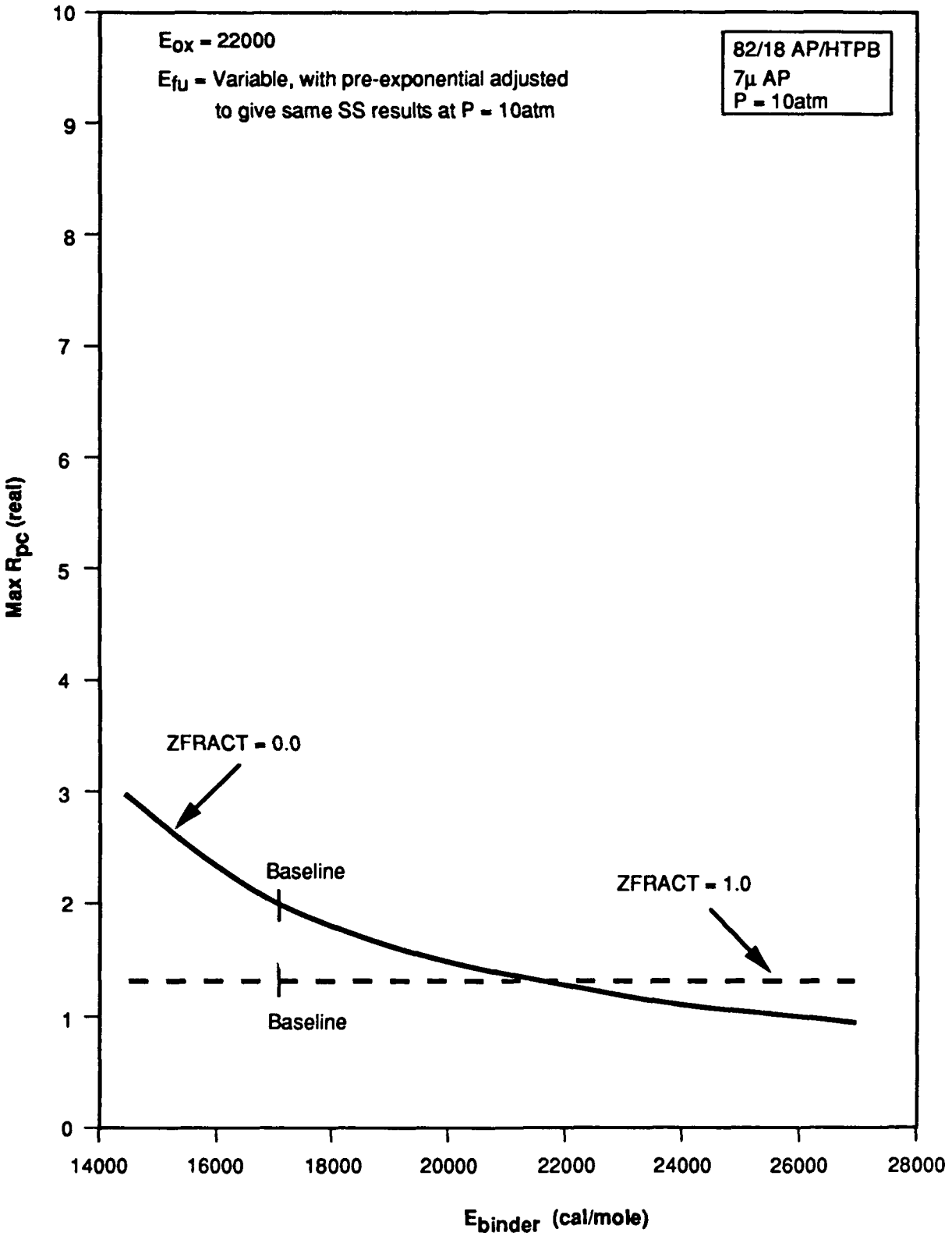

Figure 15. Dependence of Maximum Value of Real Part of Pressure-Coupled Response on Binder Ablation Activation Energy

1091-AFSOR

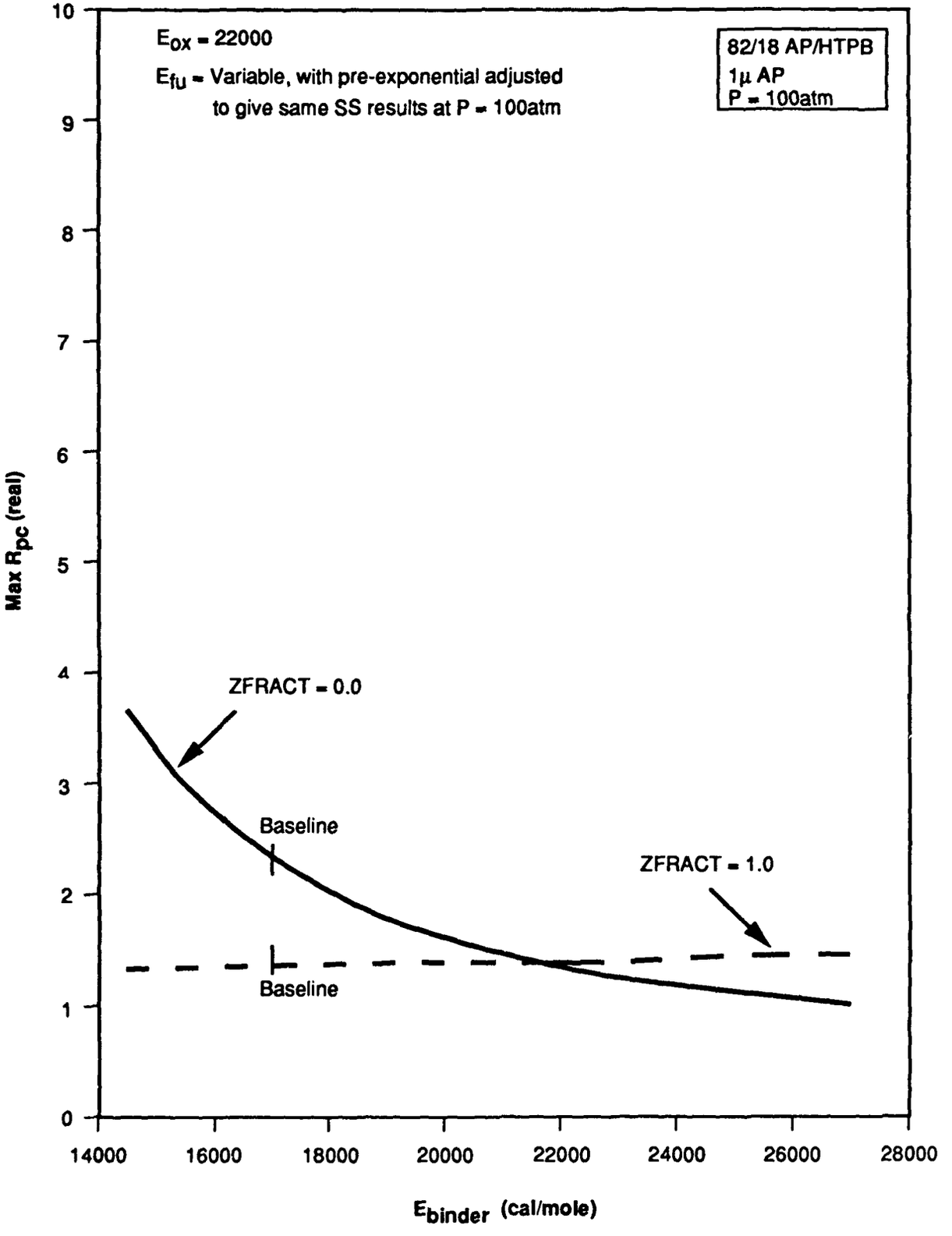

Figure 16. Dependence of Maximum Value of Real Part of Pressure-Coupled Response on Binder Ablation Activation Energy

1091-AFSOR

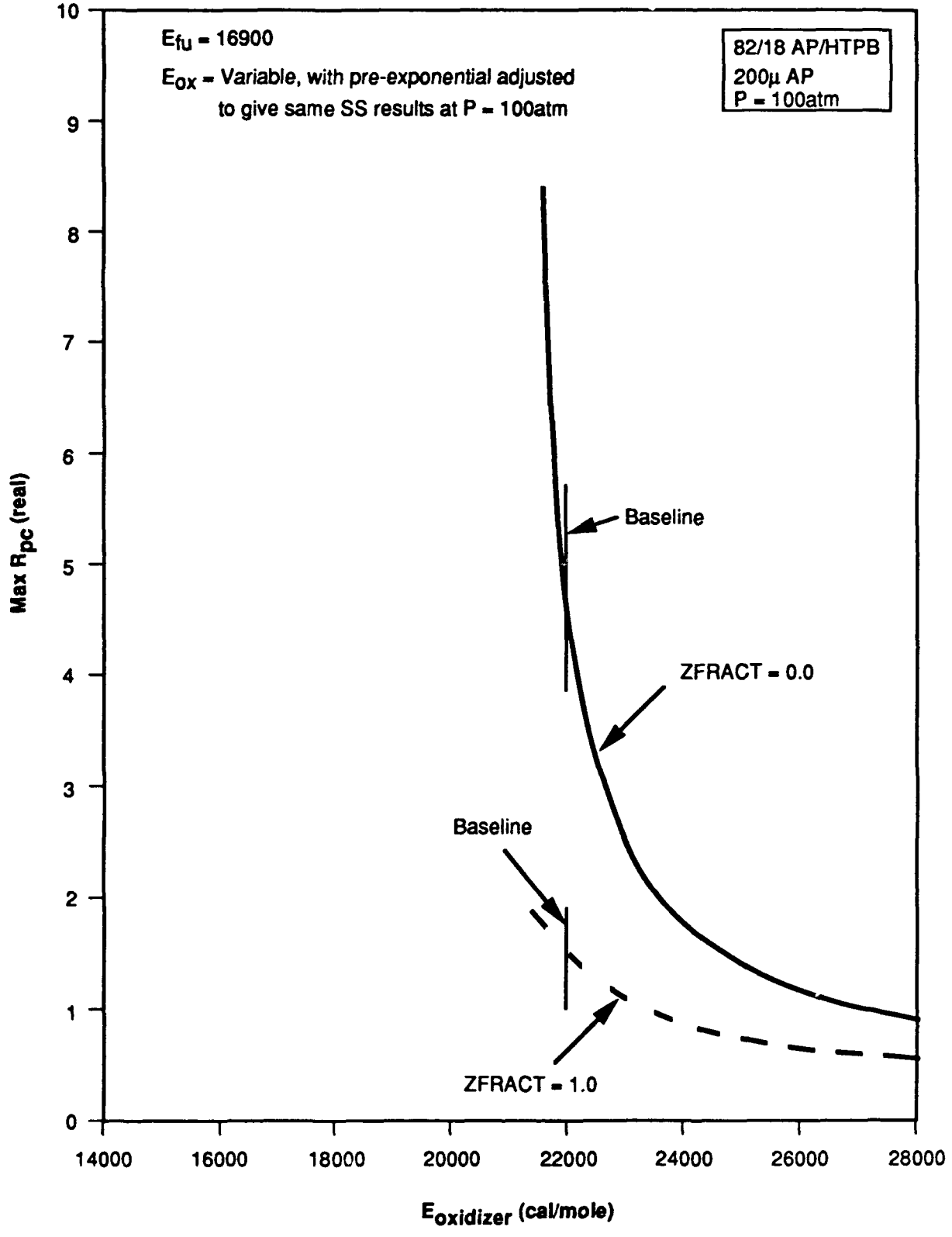

Figure 17. Dependence of Maximum Value of Real Part of Pressure-Coupled Response on Oxidizer Ablation Activation Energy

1091-AFSOR

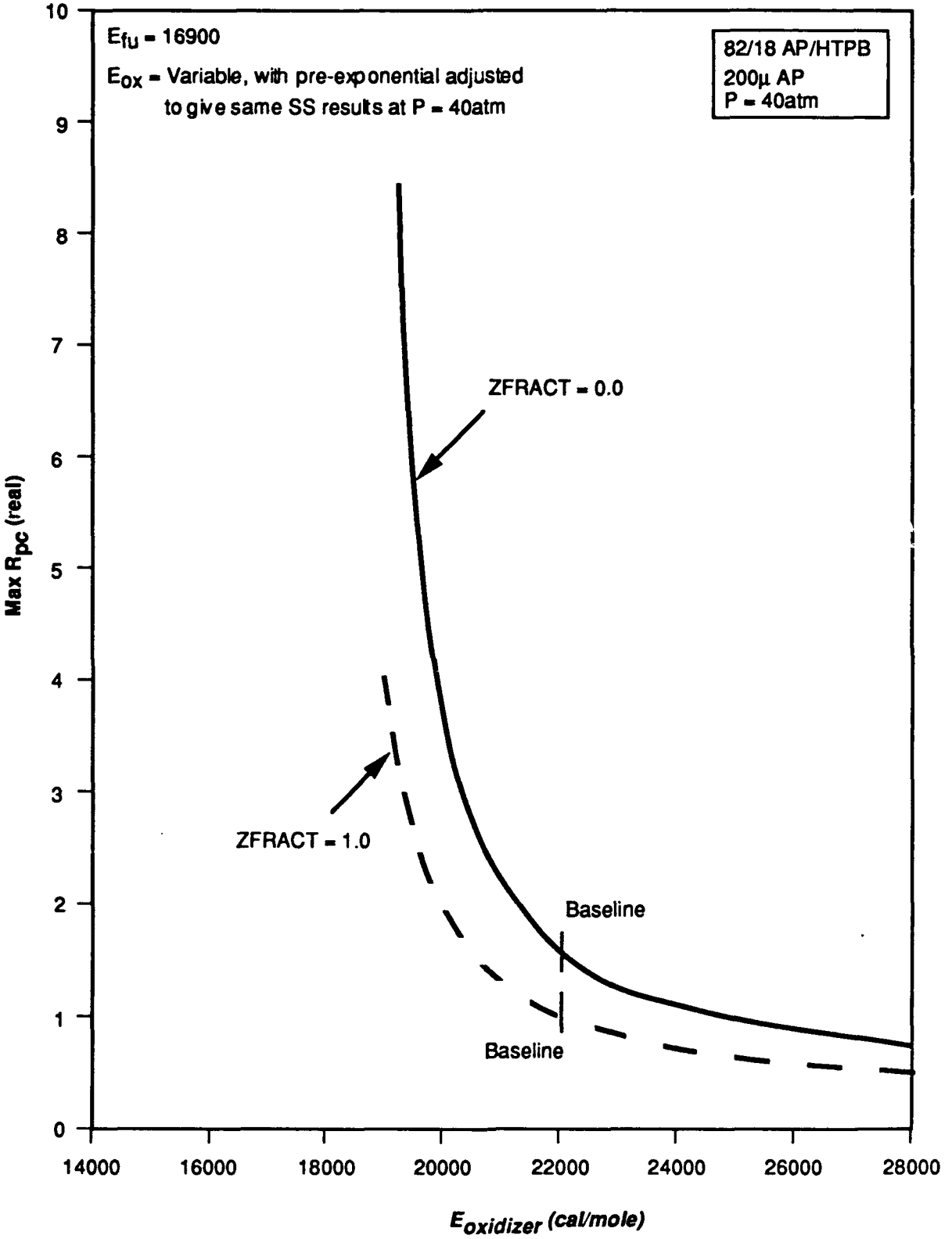

Figure 18. Dependence of Maximum Value of Real Part of Pressure-Coupled Response on Oxidizer Ablation Activation Energy

1091-AFSOR

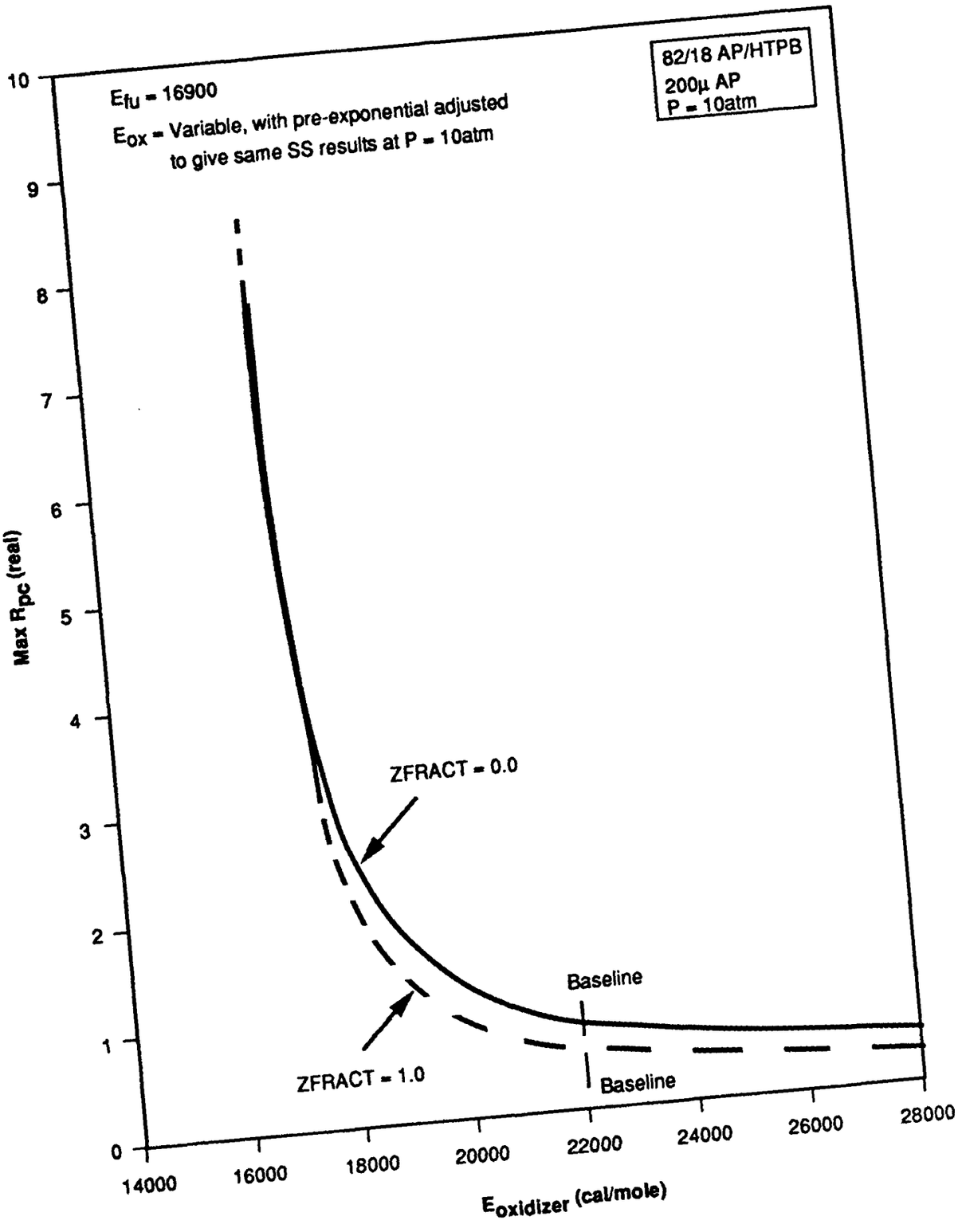

1091-AFSOR

Figure 19. Dependence of Maximum Value of Real Part of Pressure-Coupled Response on Oxidizer Ablation Activation Energy

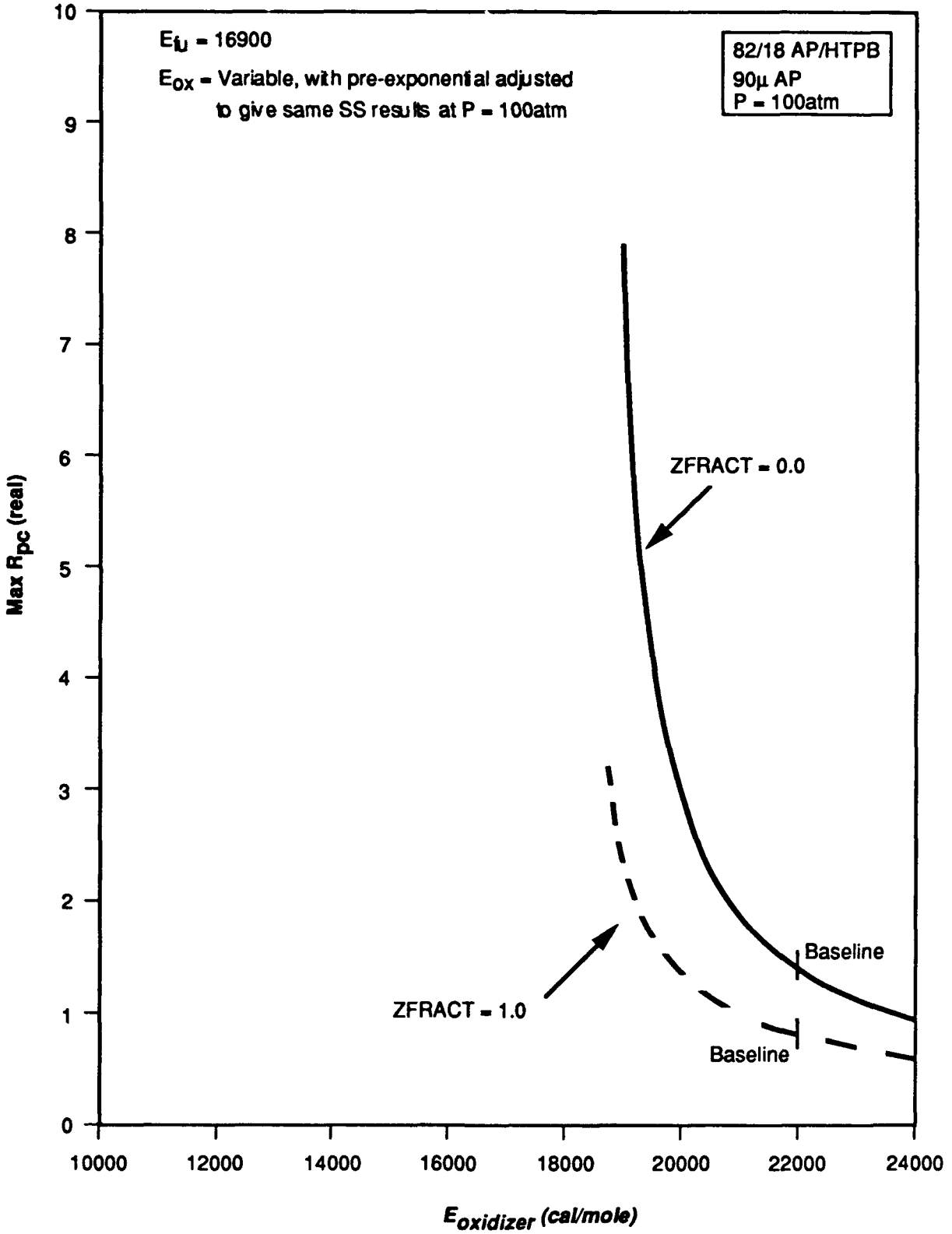

Figure 20. Dependence of Maximum Value of Real Part of Pressure-Coupled Response on Oxidizer Ablation Activation Energy

1091-AFSOR

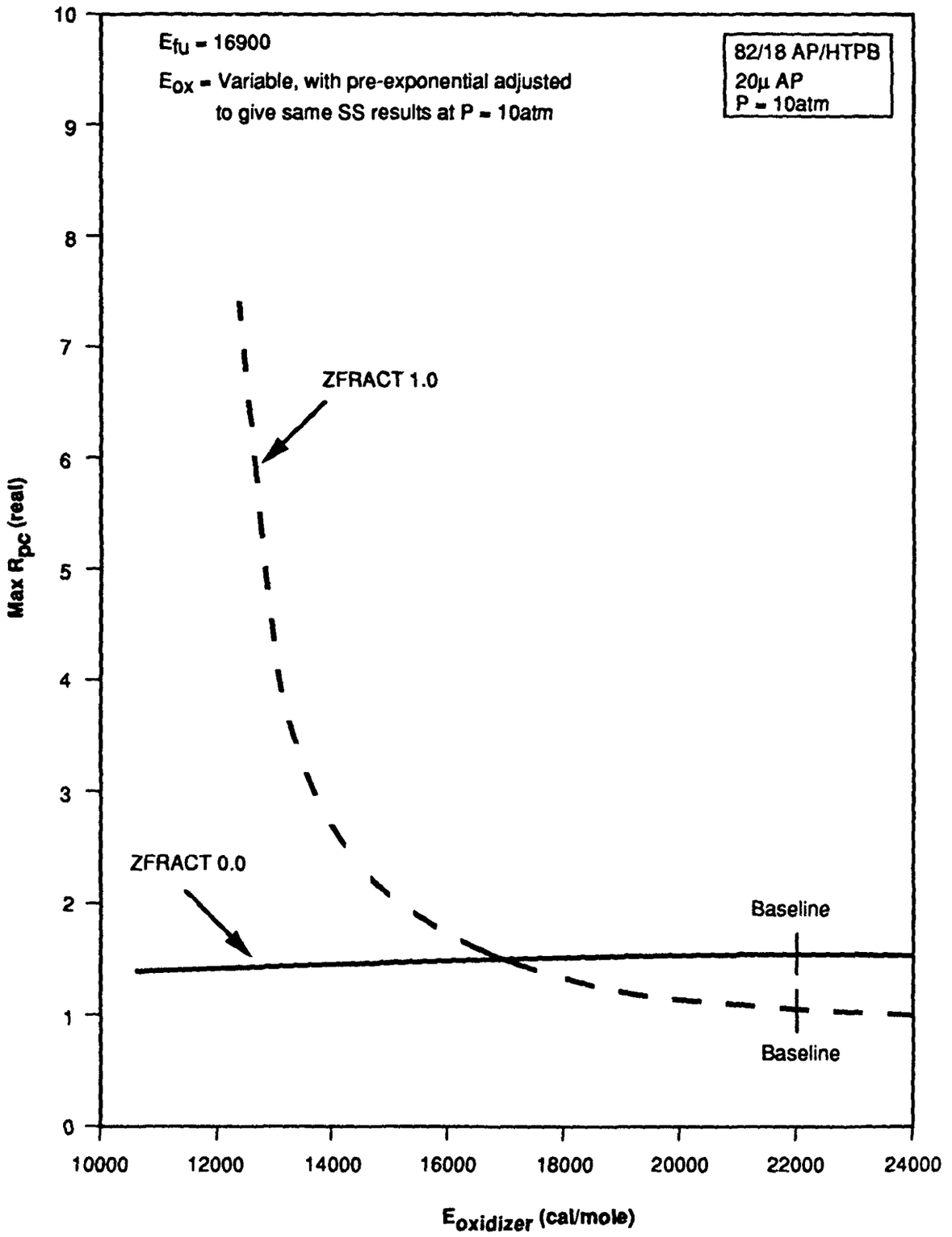

Figure 21. Dependence of Maximum Value of Real Part of Pressure-Coupled Response on Oxidizer Ablation Activation Energy

1091-AFSOR

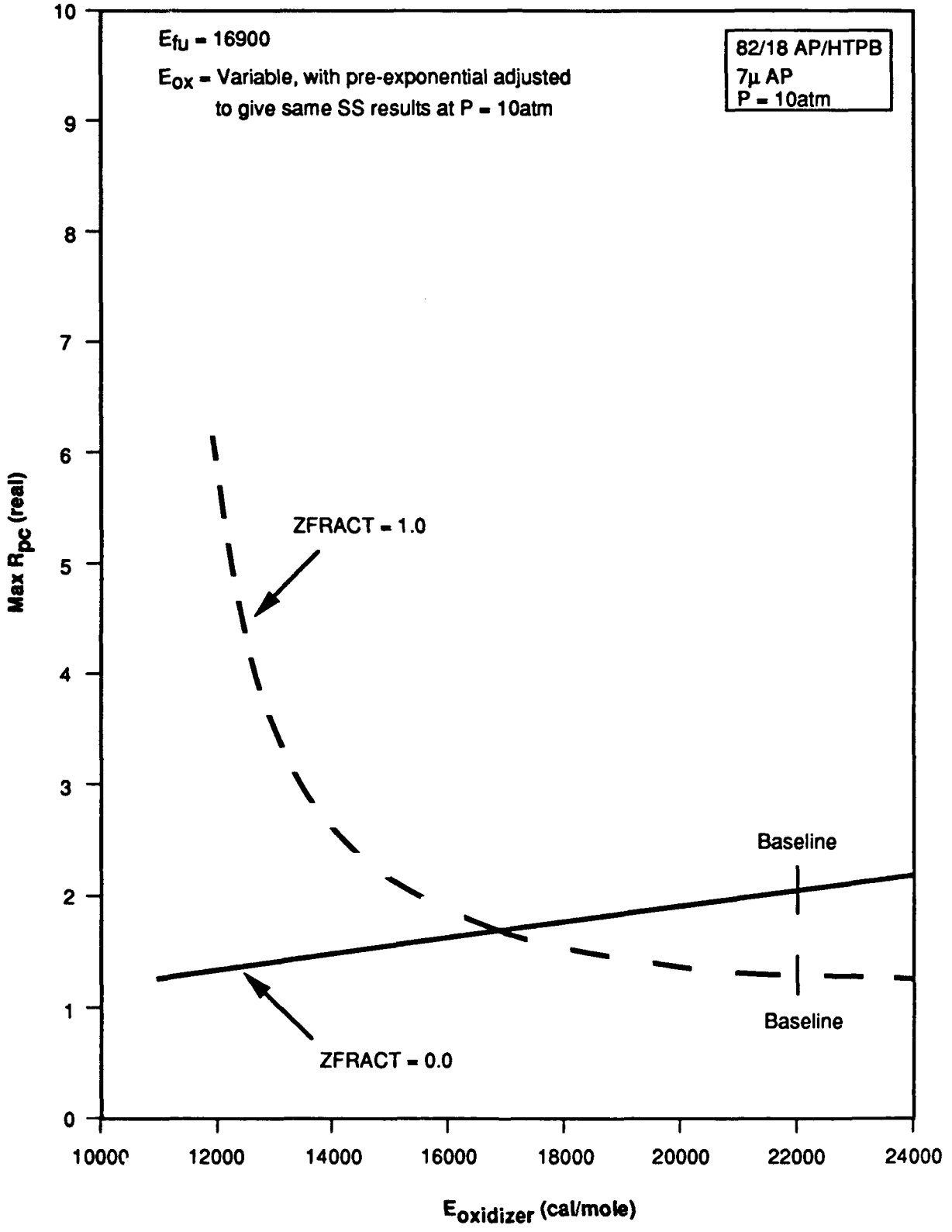

Figure 22. Dependence of Maximum Value of Real Part of Pressure-Coupled Response on Oxidizer Ablation Activation Energy

1091-AFSOR

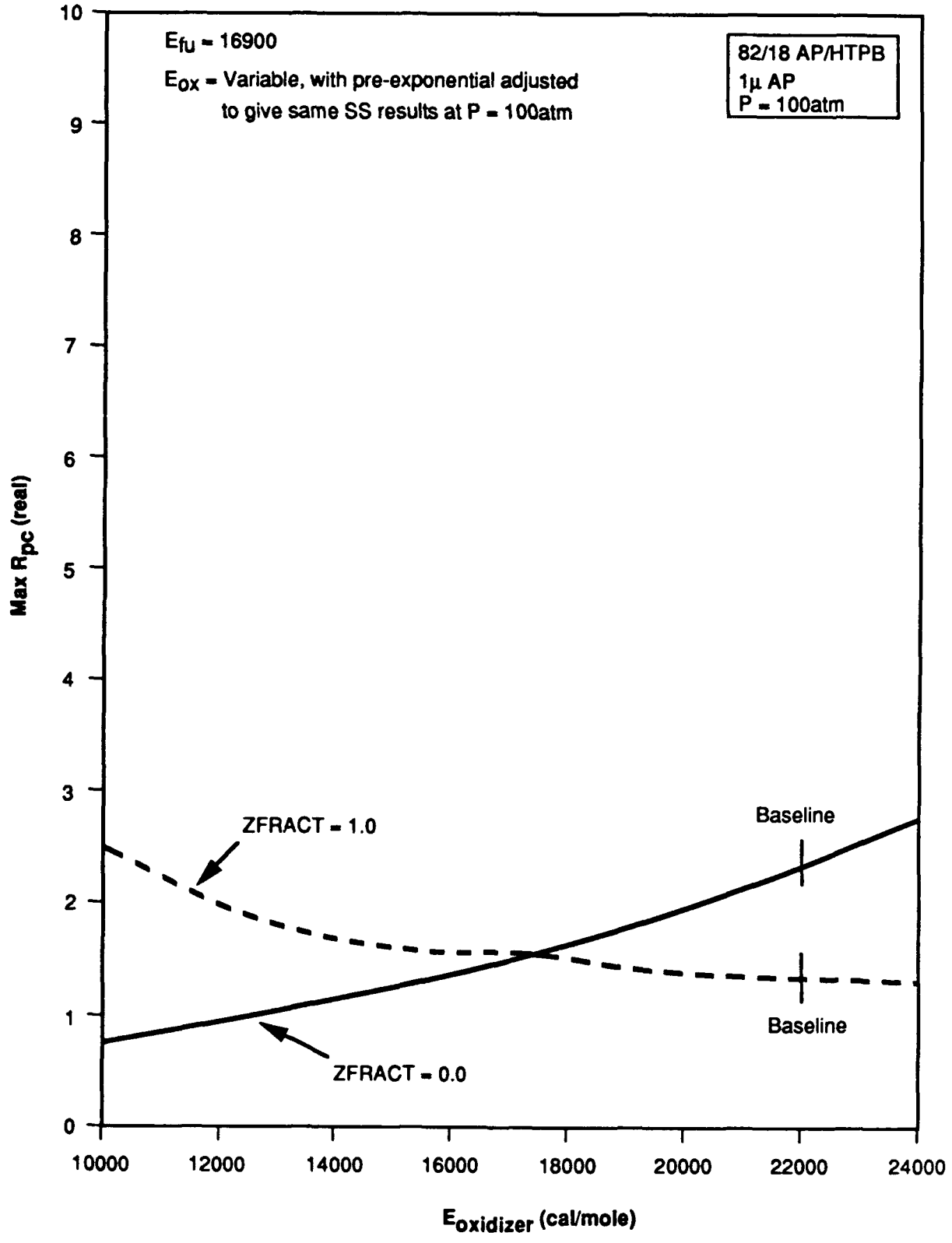

Figure 23. Dependence of Maximum Value of Real Part of Pressure-Coupled Response on Oxidizer Ablation Activation Energy

1091-AFSOR

decreased monotonically with decreases in $E_{OXIDIZER} - E_{BINDER}$ (also designated as ΔE); this corresponds to monotonic decreases of maximum $R_{pc}^{(real)}$ with <u>increasing</u> E_{BINDER} at fixed $E_{OXIDIZER}$ and with <u>decreasing</u> $E_{OXIDIZER}$ at fixed E_{BINDER}.] As may be seen from Figures 10-16, for ZFRACT = 0 (no surface area adjustment, as in the earlier simplified analysis), the maximum $R_{pc}^{(real)}$ values decrease monotonically with increasing E_{BINDER} (decreasing $E_{OXIDIZER}-E_{BINDER}$) as in that earlier study. However, even for the no-surface-topology-adjustment cases, the predicted effects of varying $E_{OXIDIZER}$ at constant E_{BINDER} (Figures 17-23) are not as simple; for 1-micron and 7-micron AP cases, the maximum $R_{pc}^{(real)}$ values decrease with decreasing $E_{OXIDIZER}$ (decreasing $E_{OXIDIZER} - E_{BINDER}$) as in the earlier study, but for 20-micron AP, these values are essentially invariant with changes in $E_{OXIDIZER}$, while for 90-micron and 200-micron AP, the maximum $R_{pc}^{(real)}$ values increase strongly with decreasing $E_{OXIDIZER}$ (decreasing $E_{OXIDIZER} - E_{BINDER}$) in direct contradiction to the previous results. With complete surface area adjustment during oscillations (ZFRACT = 1), giving constant O/F ratio for gases leaving the propellant surface, the maximum value of the real part of the pressure-coupled response either increases or remains constant (depending on oxidizer size and pressure) with increasing binder ablation activation energy (decreasing $E_{OXIDIZER} - E_{BINDER}$) for fixed oxidizer ablation activation energy, while it decreases with increasing oxidizer ablation activation energy (increasing $E_{OXIDIZER} - E_{BINDER}$) at constant fuel ablation activation energy (opposite of predictions from the old study). For most cases, there seems to be little improvement (decrease) in pressure-coupled response relative to baseline values (marked on the figures) available from modification of either binder or oxidizer ablation activation energies.

The maximum values of the real part of the pressure-coupled response (maximum in the $R_{pc}^{(real)}$ versus frequency curves) were found to correlate quite well with TERM5 in the response function equation (Equation 51) over the entire range of activation energies and ZFRACT values examined for each pressure-particle size combination (Figures 24-30), with these maximum values decreasing with increasing values of TERM5. Normalization of these maximum values by the burning rate exponents yields similarly good correlation with TERM5; a summary of these results is presented in Figure 31.

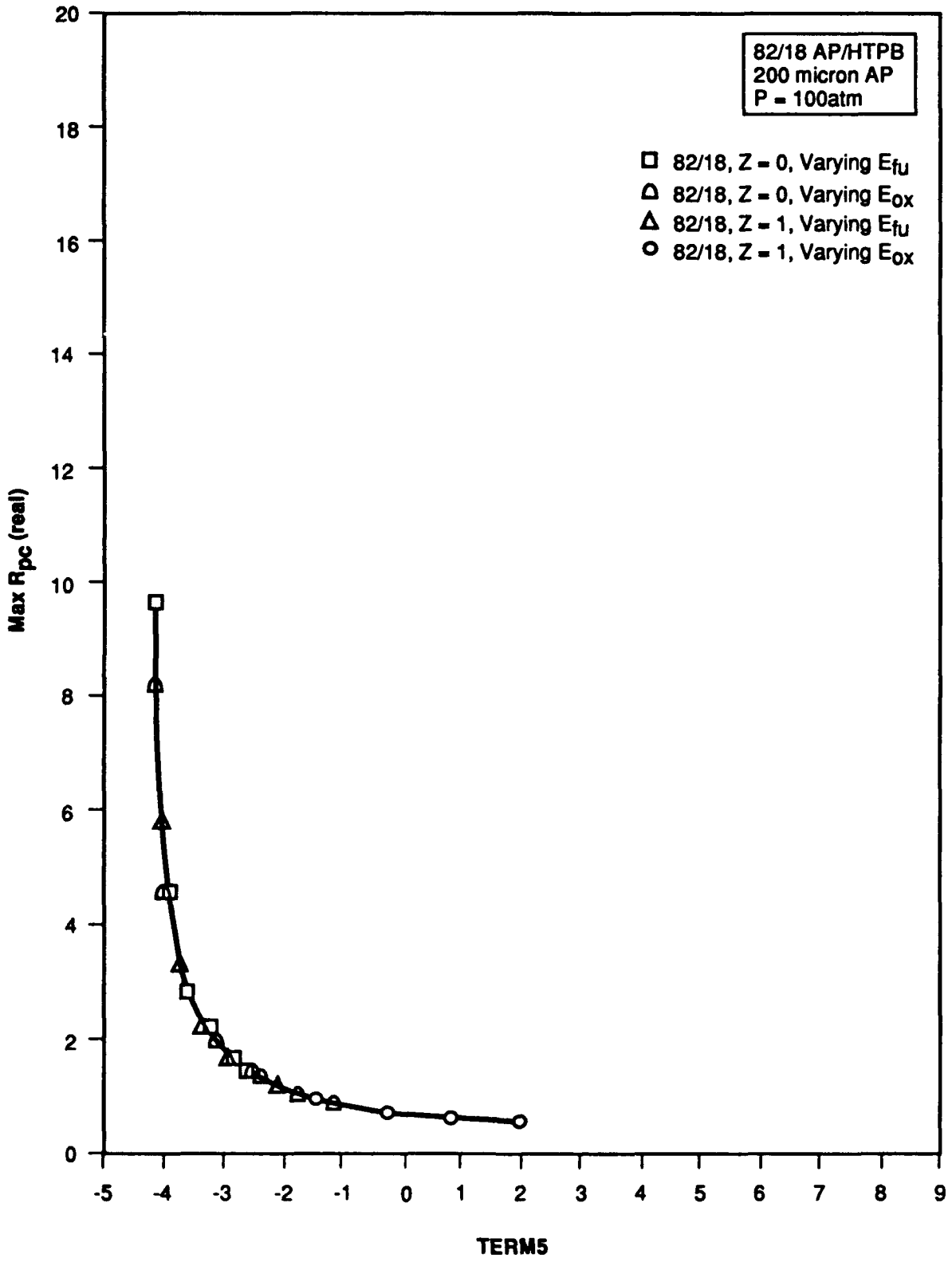

Figure 24. Maximum Value of Real Part of Pressure-Coupled Response vs. TERM5

1091-AFSOR

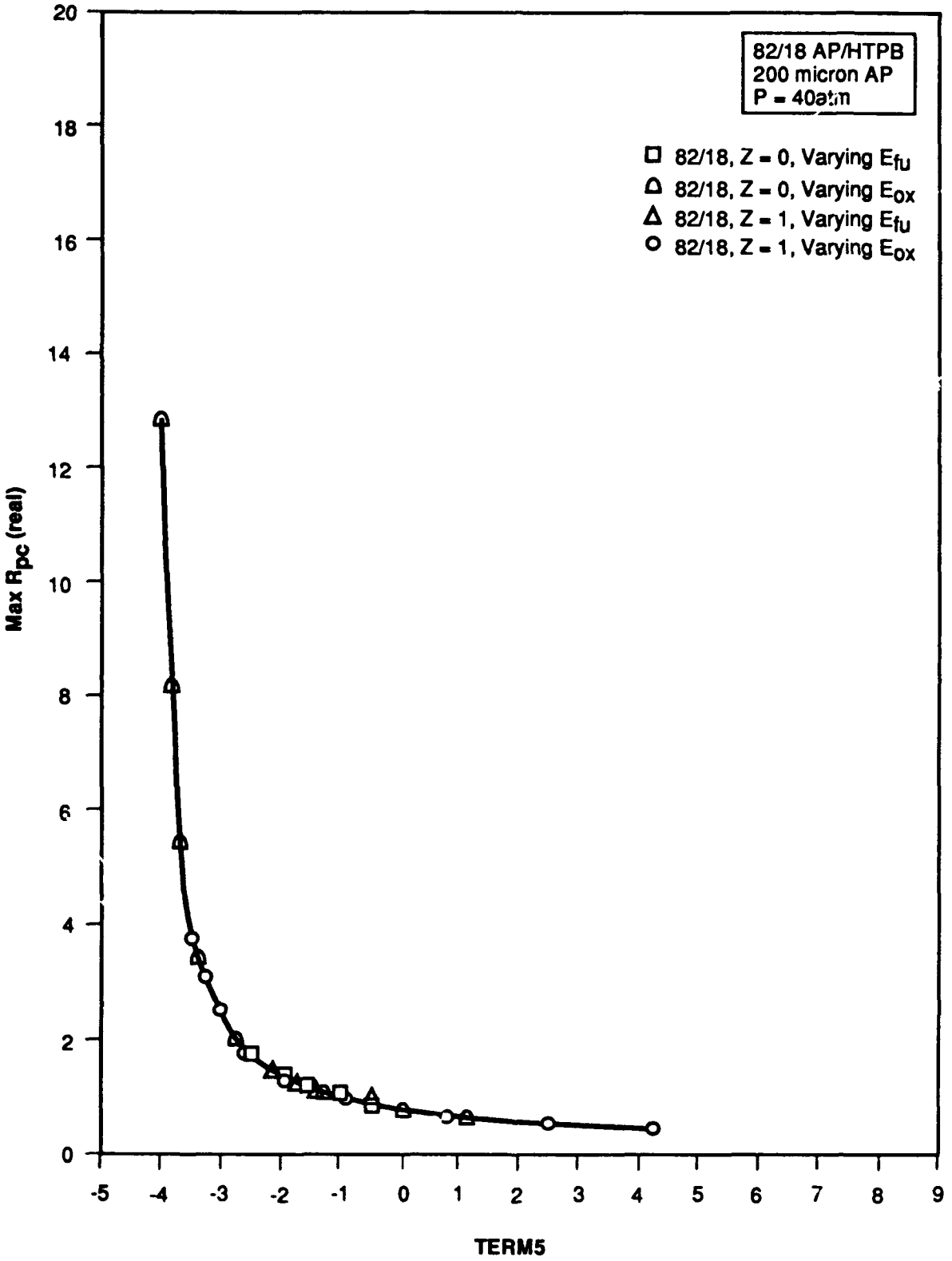

Figure 25. Maximum Value of Real Part of Pressure-Coupled Response vs. TERM5

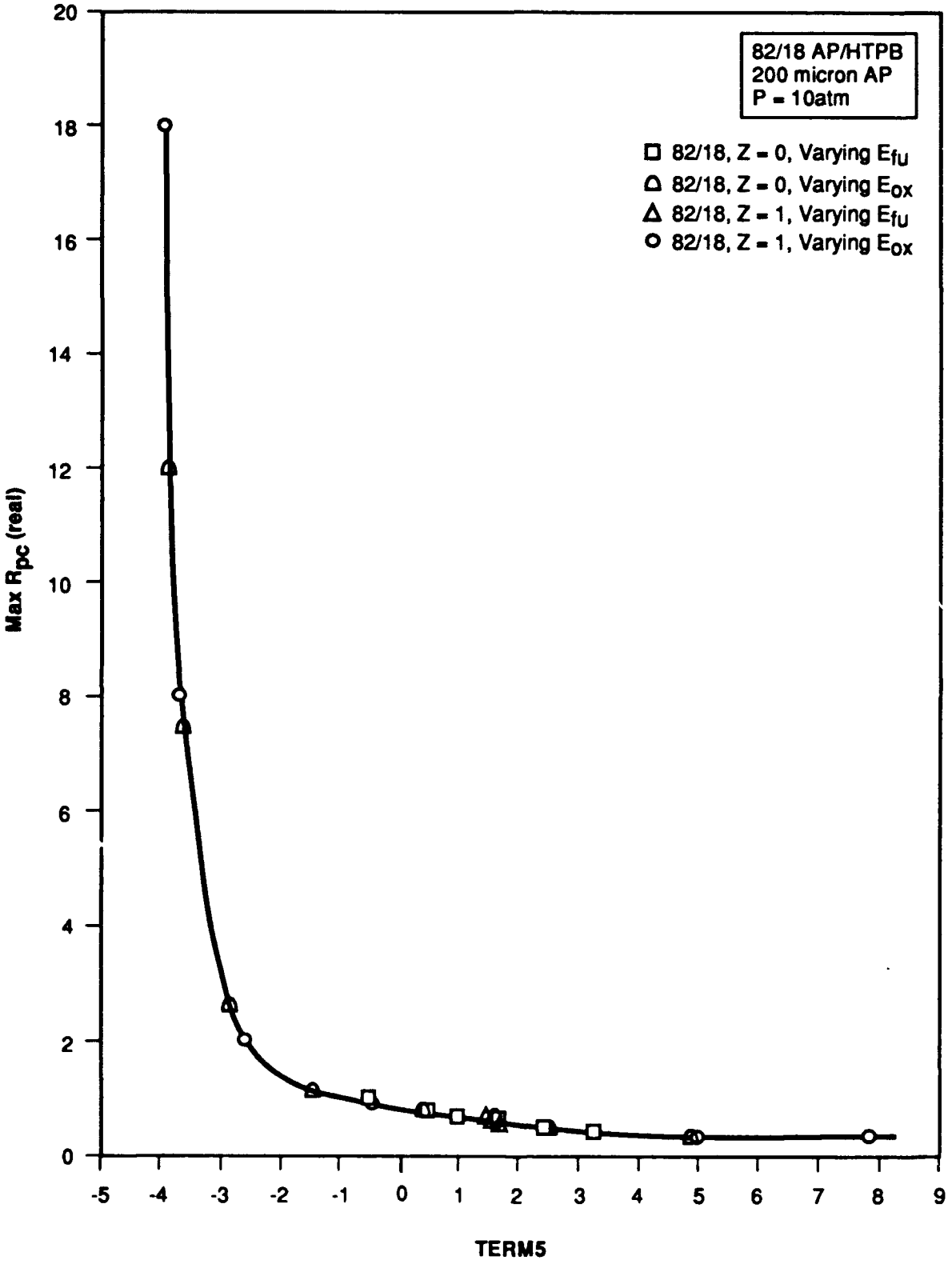

Figure 26. Maximum Value of Real Part of Pressure-Coupled Response vs. TERM5

1091-AFSOR

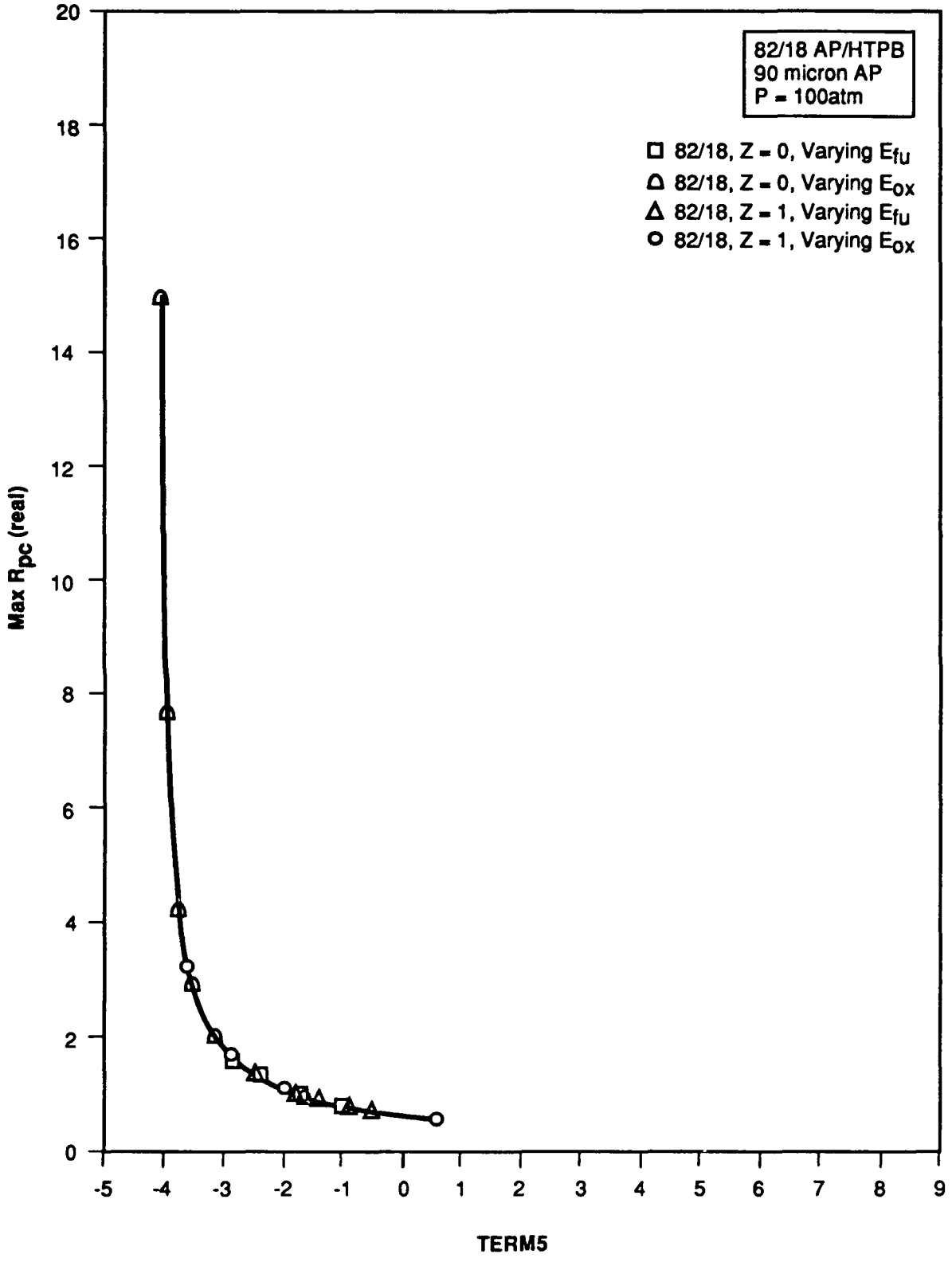

Figure 27. Maximum Value of Real Part of Pressure-Coupled Response vs. TERM5

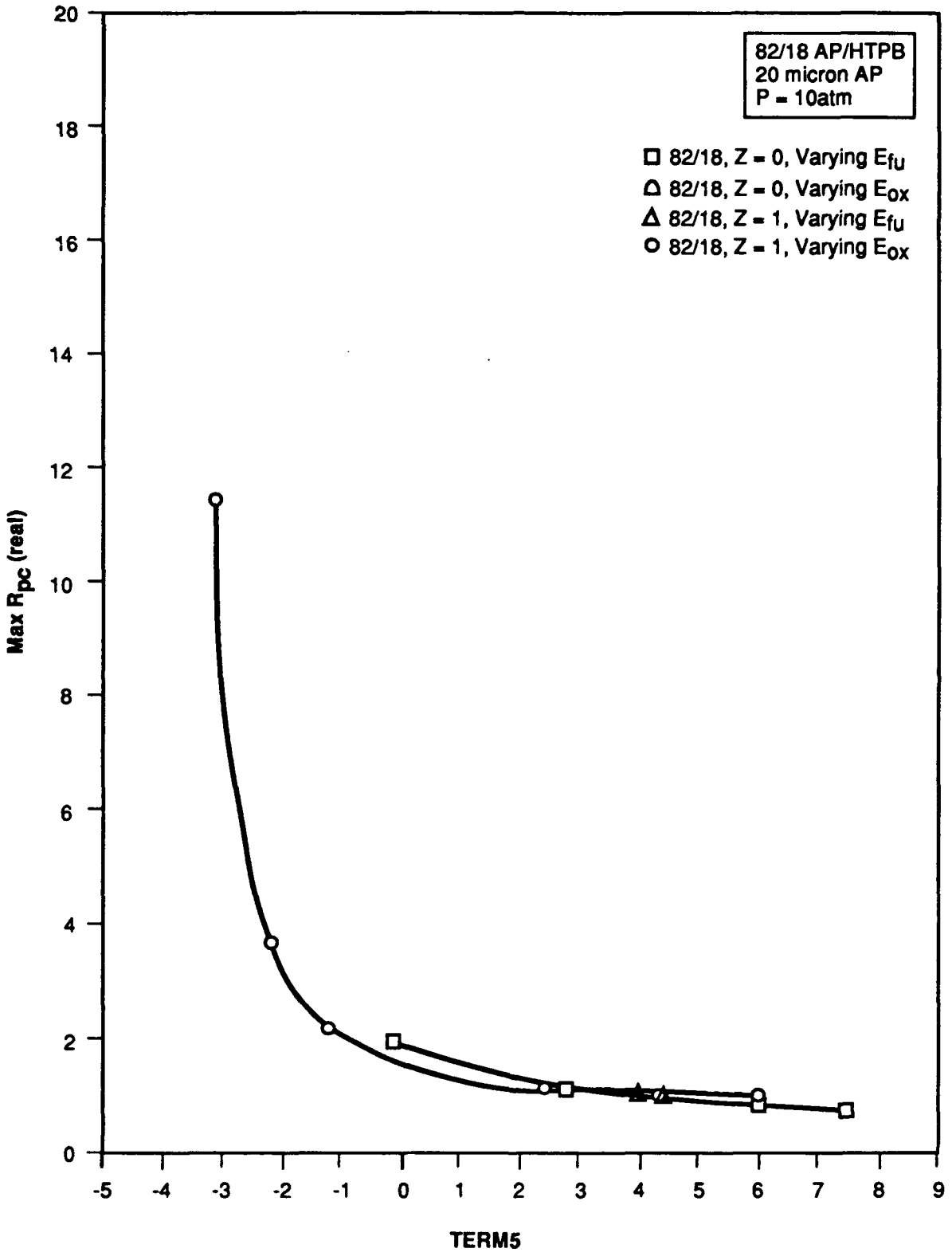

Figure 28. Maximum Value of Real Part of Pressure-Coupled Response vs. TERM5

1091-AFSOR

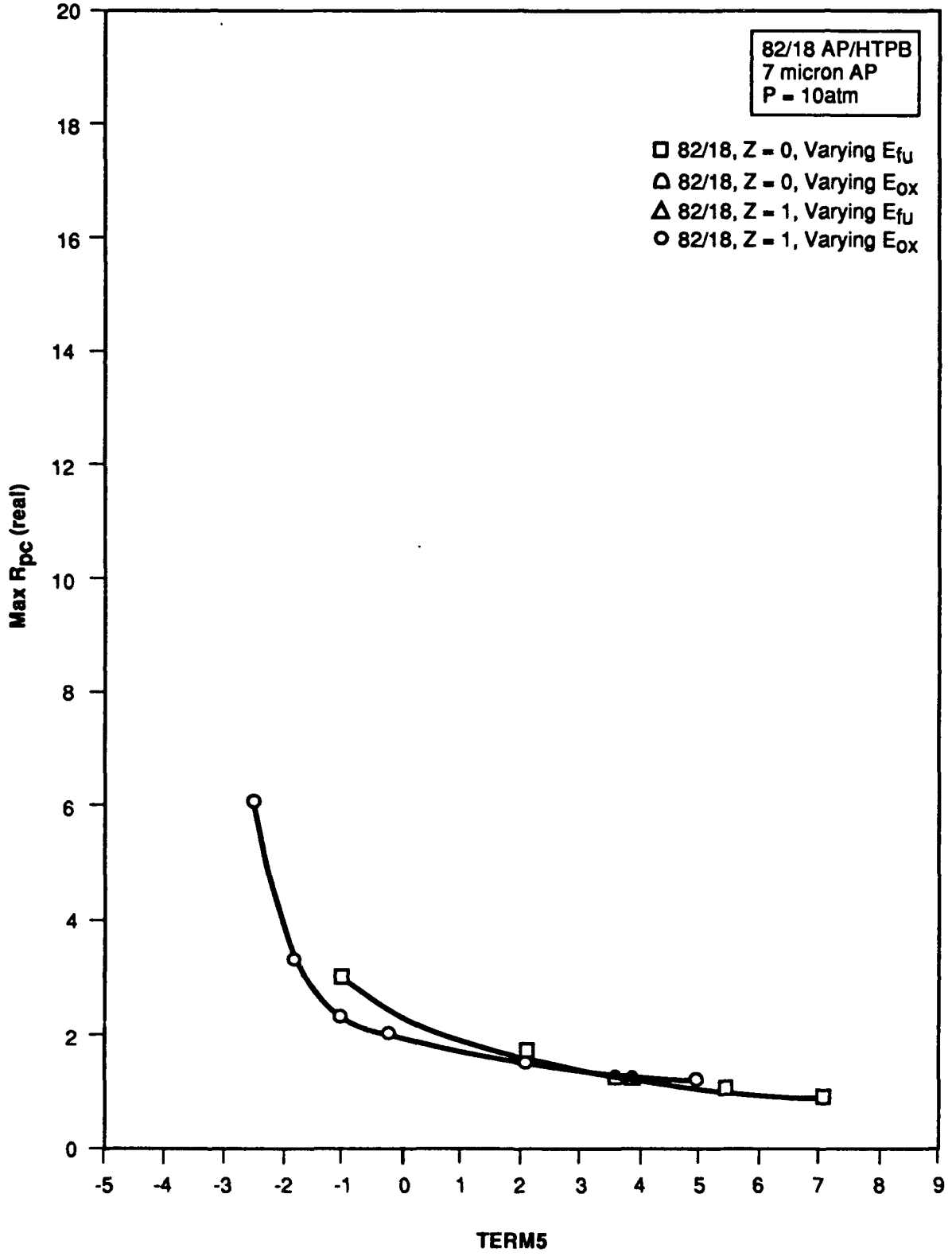

Figure 20. Maximum Value of Real Part of Pressure-Coupled Response vs. TERM5

1091-AFSOR

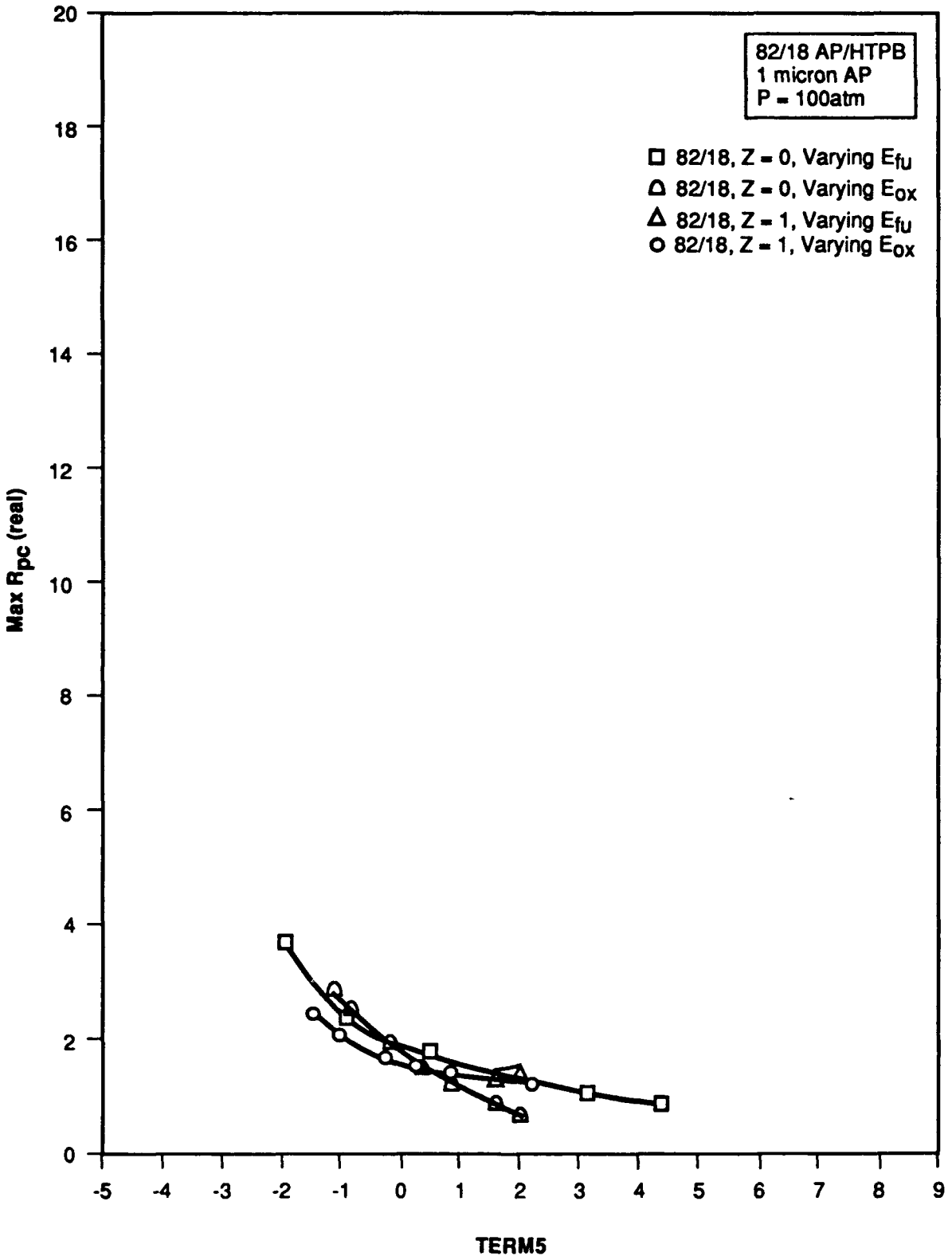

Figure 30. Maximum Value of Real Part of Pressure-Coupled Response vs. TERM5

1091-AFSOR

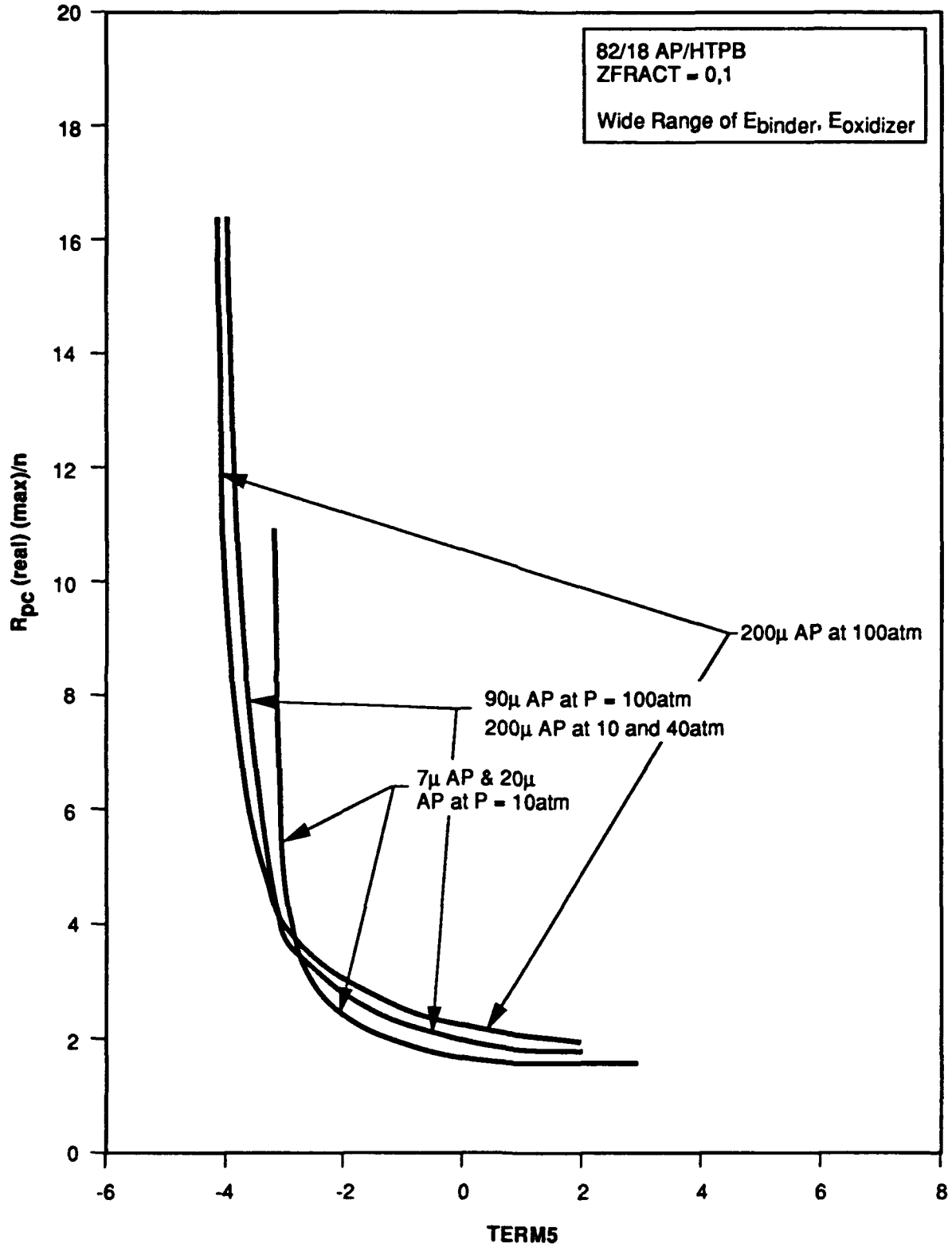

Figure 31. Dependence of Maximum Values of Real Part of Pressure-Coupled Response Divided By BR Exponent on TERM5 for Several Pressure-AP Size Combinations 1091-AFSOR

Identification of factors leading to changes in TERM5 (and thus in maximum value of the real part of the pressure-coupled response) with changes in $E_{OXIDIZER}$ (at a fixed value of E_{BINDER}) and changes in E_{BINDER} (at a fixed value of $E_{OXIDIZER}$) is of interest. Examination of computer printout details for various cases in combination with Equation 52 (with recognition that $f_1 = (m'/\bar{m})/T_s'$, $L = \partial q_{fdbk}/\partial T_s$ (for constant T_f,P) and $f_4 = dQ_{gas}/dT_s$ results in such definition for various pressure-particle size combinations, both for ZFRACT = 0 and ZFRACT = 1, as presented in the remaining pages of this section. As may be seen, several factors contribute to changes in TERM5 with changes in $E_{OXIDIZER}$ and E_{BINDER} (all other parameters being held constant); the relative importance of these factors is seen to vary from case to case, negating the possibility of encompassing generalizations.

82/18 AP/HTPB 1μ AP P = 100 atm

1. E_{fuel} up from 14500 to 2700 at E_{OX} = 22000 (ΔE gas from +7500 to -5000)

Z = 0	Effects on TERM5
Stabilizing changes in $\frac{\partial Q_{surf}}{\partial \bar{T}_s}$ (more negative)	+0.9
Stabilizing changes in $\frac{\partial Q_{gas}}{\partial \bar{T}_s}$ (positive → negative)	+3.8
Stabilizing changes in $\frac{\partial q_{fdbk}}{\partial \bar{T}_s}$ (more negative)	+2.2

Net Effect: Stabilizing

Z = 1

Slightly stabilizing changes in $\frac{\partial q_{fdbk}}{\partial \bar{T}_s}$ (more negative) +1.0

Slightly destabilizing changes in $\frac{m'}{\bar{m}\, T_s'}$ (more positive) -1.1

Net Effect: Negligible

2. E_{OX} down from 24000 to 10000 at E_{fuel} = 16900 (ΔE goes from +7100 to -6900)

Z = 0

Very destabilizing changes in $\frac{\partial Q_{surf}}{\partial \bar{T}_s}$ (negative → positive) -9.1

Stabilizing changes in $\frac{m'}{\bar{m}\, T_s'}$ (less positive) +2.7

Very stabilizing change in $\frac{\partial Q_{gas}}{\partial \bar{T}_s}$ (positive → negative) +10.8

Net Effect: Stabilizing

Z = 1

Very destabilizing change in $\frac{\partial Q_{surf}}{\partial \bar{T}_s}$ (negative → positive) -10.1

Stabilizing change in $\frac{m'}{\bar{m}\, T_s'}$ (less positive) +2.3

Stabilizing change in $\frac{\partial Q_{gas}}{\partial \bar{T}_s}$ (positive → negative) +6.5

Destabilizing change in $\frac{\partial q_{fdbk}}{\partial \bar{T}_s}$ (less negative) -2.0

Net Effect: Destabilizing

82/18 AP/HTPB 7μ AP P = 10 atm

1. E_{fuel} up from 14500 to 2700 at E_{OX} = 22000 (ΔE gas from +7500 to -5000)

Z = 0	Effects on TERM5
Stabilizing changes in $\frac{\partial Q_{surf}}{\partial \bar{T}_s}$ (more negative)	+1.6
Stabilizing changes in $\frac{\partial Q_{gas}}{\partial \bar{T}_s}$ (positive → negative)	+4.0
Stabilizing changes in $\frac{\partial q_{fdbk}}{\partial \bar{T}_s}$ (more negative)	+2.9

Net Effect: Stabilizing

Z = 1

No meaningful changes

Net Effect: Negligible

2. E_{OX} down from 24000 to 10000 at E_{fuel} = 16900 (ΔE goes from +7100 to -5900)

Z = 0

Very destabilizing changes in $\frac{\partial Q_{surf}}{\partial \bar{T}_s}$ (negative → positive)	-13.8
Stabilizing changes in $\frac{m'}{\bar{m}\, T_s'}$ (less positive)	+1.6
Very stabilizing change in $\frac{\partial Q_{gas}}{\partial \bar{T}_s}$ (positive → negative)	+12.6

Net Effect: Slightly Stabilizing

Z = 1

Very destabilizing change in $\frac{\partial Q_{surf}}{\partial \bar{T}_s}$ (negative → positive) -15.5

Stabilizing change in $\frac{m'}{\bar{m}\ T_s'}$ (less positive) +2.3

Stabilizing change in $\frac{\partial Q_{gas}}{\partial \bar{T}_s}$ (positive → negative) +8.1

Destabilizing change in $\frac{\partial q_{fdbk}}{\partial \bar{T}_s}$ (less negative) -4.2

Net Effect: Destabilizing

82/18 AP/HTPB 20μ AP P = 10 atm

1. E_{fuel} up from 14500 to 27000 at E_{OX} = 22000 (ΔE gas from +7500 to -5000)

Z = 0	Effects on TERM5
Stabilizing changes in $\frac{\partial Q_{surf}}{\partial \bar{T}_s}$ (more negative)	+1.6
Stabilizing changes in $\frac{\partial Q_{gas}}{\partial \bar{T}_s}$ (positive → negative)	+4.0
Stabilizing changes in $\frac{\partial q_{fdbk}}{\partial \bar{T}_s}$ (more negative)	+2.3

Net Effect: Stabilizing

Z = 1

No meaningful changes

Net Effect: Negligible

2. E_{OX} down from 24000 to 10000 at E_{fuel} = 16900 (ΔE goes from +7100 to -5900)

Z = 0

Stabilizing Change in A (lower absolute value)	+0.8
Destabilizing changes in $\frac{\partial Q_{surf}}{\partial T_s}$ (negative → positive)	-14.1
Stabilizing changes in $\frac{m'}{\bar{m}\ T_s'}$ (less positive)	+1.5
Very stabilizing change in $\frac{\partial Q_{gas}}{\partial T_s}$ (positive → negative)	+12.0
Destabilizing change in $\frac{\partial q_{fdbk}}{\partial T_s}$ (less negative)	-1.7

Net Effect: Destabilizing

Z = 1

Stabilizing change in A (lower absolute value)	+1.1
Destabilizing change in $\frac{\partial Q_{surf}}{\partial T_s}$ (negative → positive)	-15.7
Stabilizing change in $\frac{m'}{\bar{m}\ T_s'}$ (less positive)	+1.9
Stabilizing change in $\frac{\partial Q_{gas}}{\partial T_s}$ (positive → negative)	+7.8
Destabilizing change in $\frac{\partial q_{fdbk}}{\partial T_s}$ (less negative)	-4.8

Net Effect: Destabilizing

82/18 AP/HTPB 90μ AP P = 100 atm

1. E_{fuel} up from 14500 to 27000 at E_{OX} = 22000 (ΔE gas from +7500 to -5000)

Z = 0	Effects on TERM5
Stabilizing changes in $\frac{\partial Q_{surf}}{\partial T_s}$ (more negative)	+1.5
Stabilizing changes in $\frac{\partial Q_{gas}}{\partial T_s}$ (positive → negative)	+0.8
Small destabilizing change in $\frac{\partial q_{fdbk}}{\partial T_s}$ (more negative)	-0.2
Net Effect: Stabilizing	
Z = 1	
Destabilizing changes in $\frac{\partial q_{fdbk}}{\partial T_s}$ (negative → positive)	-2.3
Net Effect: Destabilizing	

2. E_{OX} down from 24000 to 18750 at E_{fuel} = 16900 (ΔE goes from +7100 to +1850)

Z = 0	
Stabilizing change in A (lower absolute value)	+0.2
Destabilizing changes in $\frac{\partial Q_{surf}}{\partial T_s}$ (negative → positive)	-5.3

Stabilizing changes in $\frac{\partial Q_{gas}}{\partial \bar{T}_s}$ (positive → negative) +1.0

Stabilizing change in $\frac{\partial q_{fdbk}}{\partial \bar{T}_s}$ (less positive) +1.5

Net Effect: Destabilizing

Z = 1

Stabilizing change in A (lower absolute value) +0.4

Destabilizing change in $\frac{\partial Q_{surf}}{\partial \bar{T}_s}$ (negative → positive) -5.9

Stabilizing change in $\frac{\partial Q_{gas}}{\partial \bar{T}_s}$ (positive → negative) +0.6

Stabilizing change in $\frac{\partial q_{fdbk}}{\partial \bar{T}_s}$ (positive → negative) +0.5

Net Effect: Destabilizing

82/18 AP/HTPB 200μ AP P = 100 atm

1. E_{fuel} up from 14500 to 27000 at E_{ox} = 22000 (ΔE gas from +7500 to -5000)

Z = 0	Effects on TERM5
Stabilizing changes in $\frac{\partial Q_{surf}}{\partial \bar{T}_s}$ (more negative)	+1.5
Stabilizing changes in $\frac{\partial Q_{gas}}{\partial \bar{T}_s}$ (positive → negative)	+0.3
Destabilizing changes in $\frac{\partial q_{fdbk}}{\partial \bar{T}_s}$ (more positive)	-0.2

Net Effect: Stabilizing

Z = 1

Destabilizing changes in $\frac{\partial q_{fdbk}}{\partial \bar{T}_s}$ (more positive) -2.05

Net Effect: Destabilizing

2. E_{fuel} goes from 28000 to 21500 at E_{fuel} = 16900 (ΔE goes from +11100 to +4600)

Z = 2

Stabilizing changes in A (lower absolute value) +0.3

Very destabilizing changes in $\frac{\partial Q_{surf}}{\partial \bar{T}_s}$ (less negative) -6.8

Stabilizing changes in $\frac{\partial Q_{gas}}{\partial \bar{T}_s}$ (less positive) +0.5

Stabilizing changes in $\frac{\partial q_{fdbk}}{\partial \bar{T}_s}$ (less positive) +2.8

Net Effect: Destabilizing

Z = 1

Stabilizing changes in A (lower absolute value) +0.5

Very destabilizing effects in $\frac{\partial Q_{surf}}{\partial \bar{T}_s}$ (less negative) -7.5

Stabilizing changes in $\frac{\partial Q_{gas}}{\partial \bar{T}_s}$ (less positive) +0.3

Stabilizing changes in $\frac{\partial q_{fdbk}}{\partial \bar{T}_s}$ (less positive) +1.7

Net Effect: Destabilizing

6.2 Variant II - Calculations with ZFRACT Being a Function of a Characteristic Oscillation Time - Burn Time Ratio

As with the studies involving input values of ZFRACT (presented in the last section), discussions of studies using an expression relating ZFRACT to the ratio of characteristic oscillation time to characteristic time for passage of the combustion front through a thickness of propellant equal to one oxidizer particle diameter are broken into two parts, calculations with baseline values of the oxidizer and fuel ablation activation energies, and examination of the effects of various values of these activation energies on pressure-coupled response functions. In both cases, the following relationship between ZFRACT (degree of surface area adjustment during oscillations) and the time ratio (TIMRAT) was utilized:

$$\text{ZFRACT} = 0.0 \text{ for TIMRAT} < 0.1$$

$$\text{ZFRACT} = \frac{\ln(\text{TIMRAT}) - \ln(0.1)}{\ln(10) - \ln(0.1)} \text{ for } 0.1 < \text{TIMRAT} < 10 \qquad (53)$$

$$\text{ZFRACT} = 1.0 \text{ for TIMRAT} > 10.0$$

(Other expressions could obviously be used in further studies, but should not offset the conclusions drawn in any major way.) As indicated earlier, use of an oscillation-frequency-dependent expression for ZFRACT of course precludes development of closed-form expressions for the pressure-coupled response functions for any given pressure-propellant combination.

6.2.1 Calculations Using Baseline Ablation Activation Energies

Plots of predicted values of the real part of the pressure-coupled response versus dimensionless frequency, w_p, (Equation 26) are presented in Figures 32-42 (for pressures of 10, 40, and 100 atm) for various AP/HTPB ratios and AP particle sizes. Included on each figure (one figure per AP/HTPB ratio - AP size combination) are expressions relating the oscillation frequency to the dimensionless value used as the abscissa for each pressure. Since ZFRACT decreases (less surface area adjustment) with increasing frequency, these curves in most cases have somewhat different shapes than the

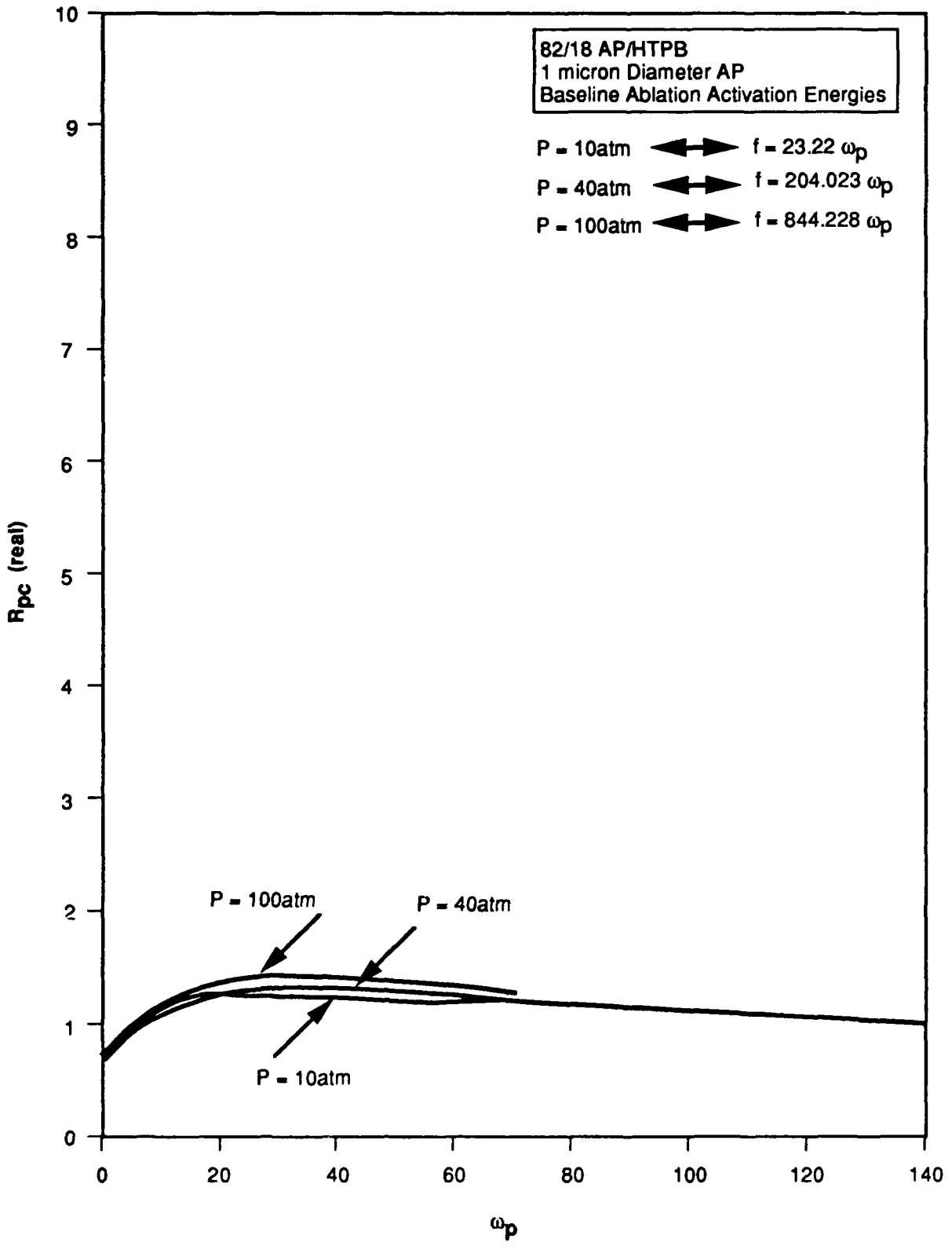

Figure 32. Real Part of Pressure-Coupled Response vs. Dimensionless Frequency

1091-AFSOR

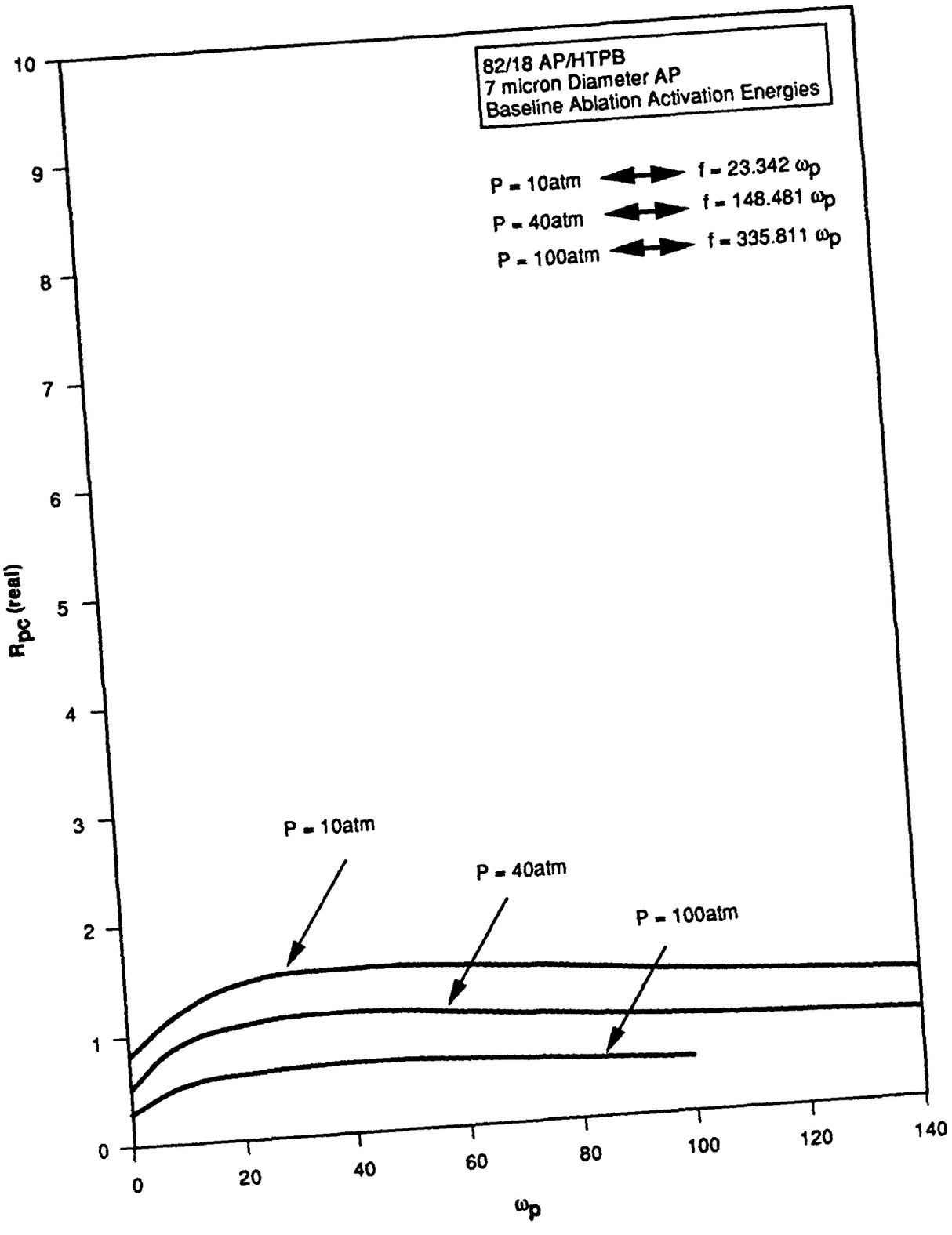

Figure 33. Real Part of Pressure-Coupled Response vs. Dimensionless Frequency

1091-AFSOR

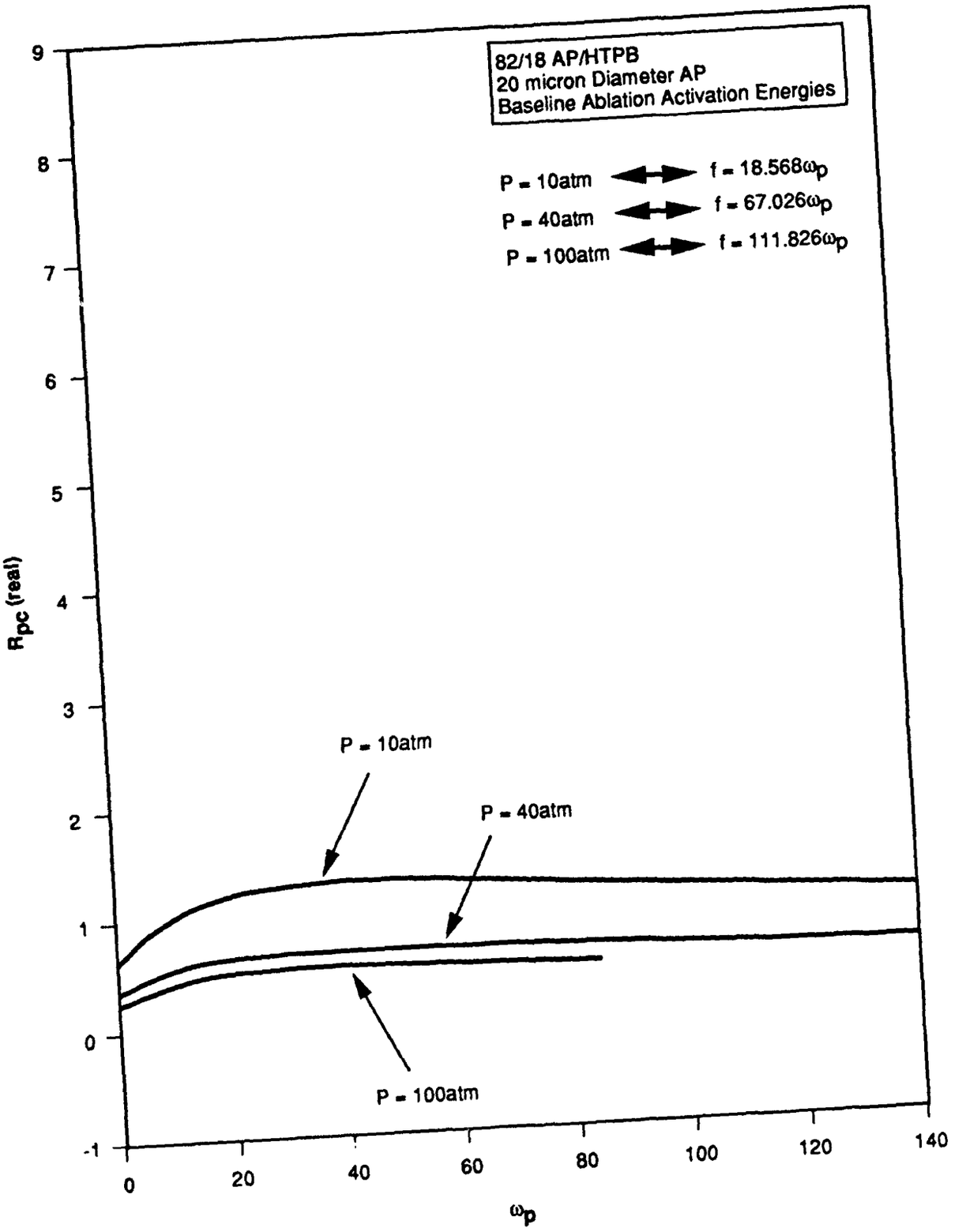

Figure 34. Real Part of Pressure-Coupled Response vs. Dimensionless Frequency

1091-AFSOR

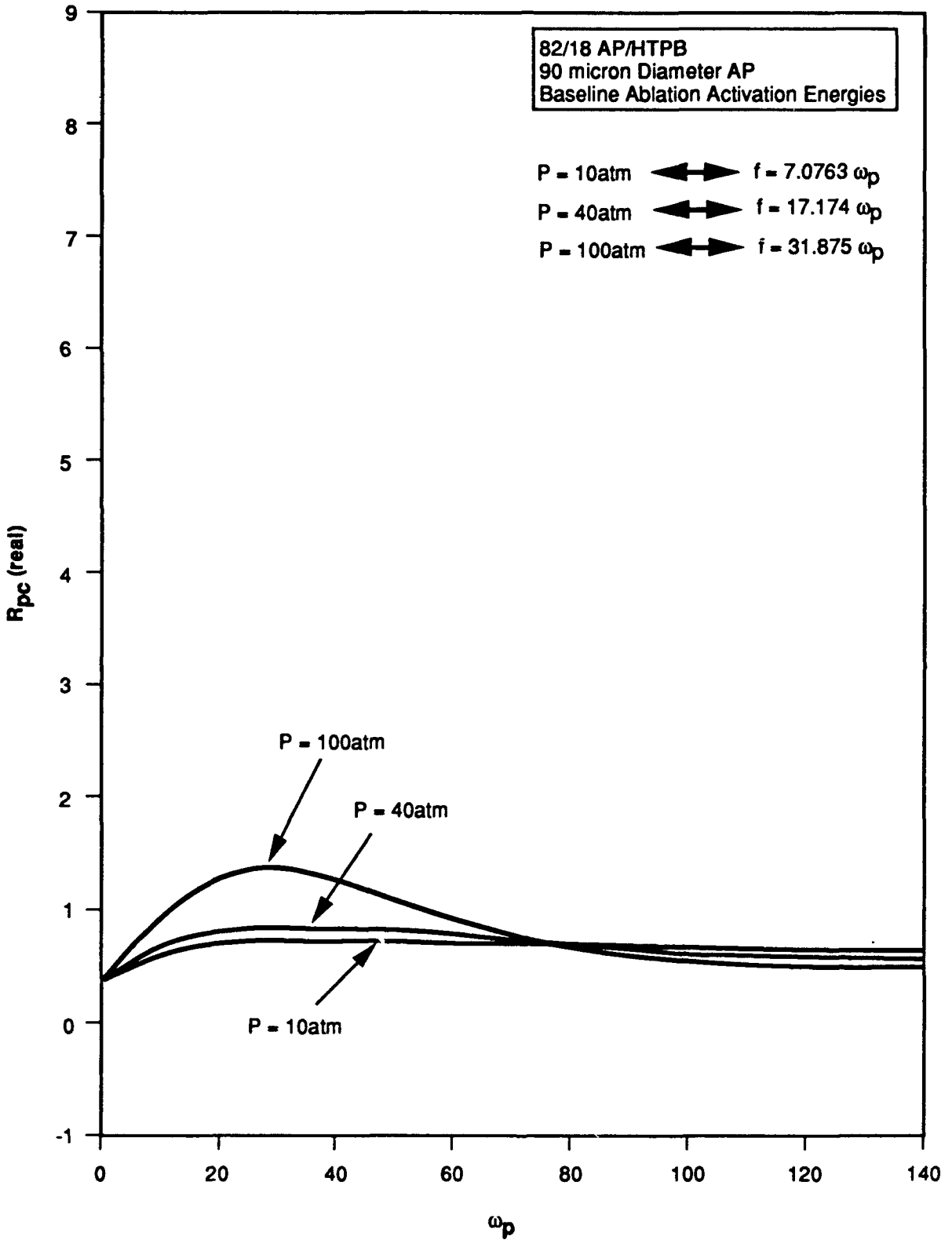

Figure 35. Real Part of Pressure-Coupled Response vs. Dimensionless Frequency

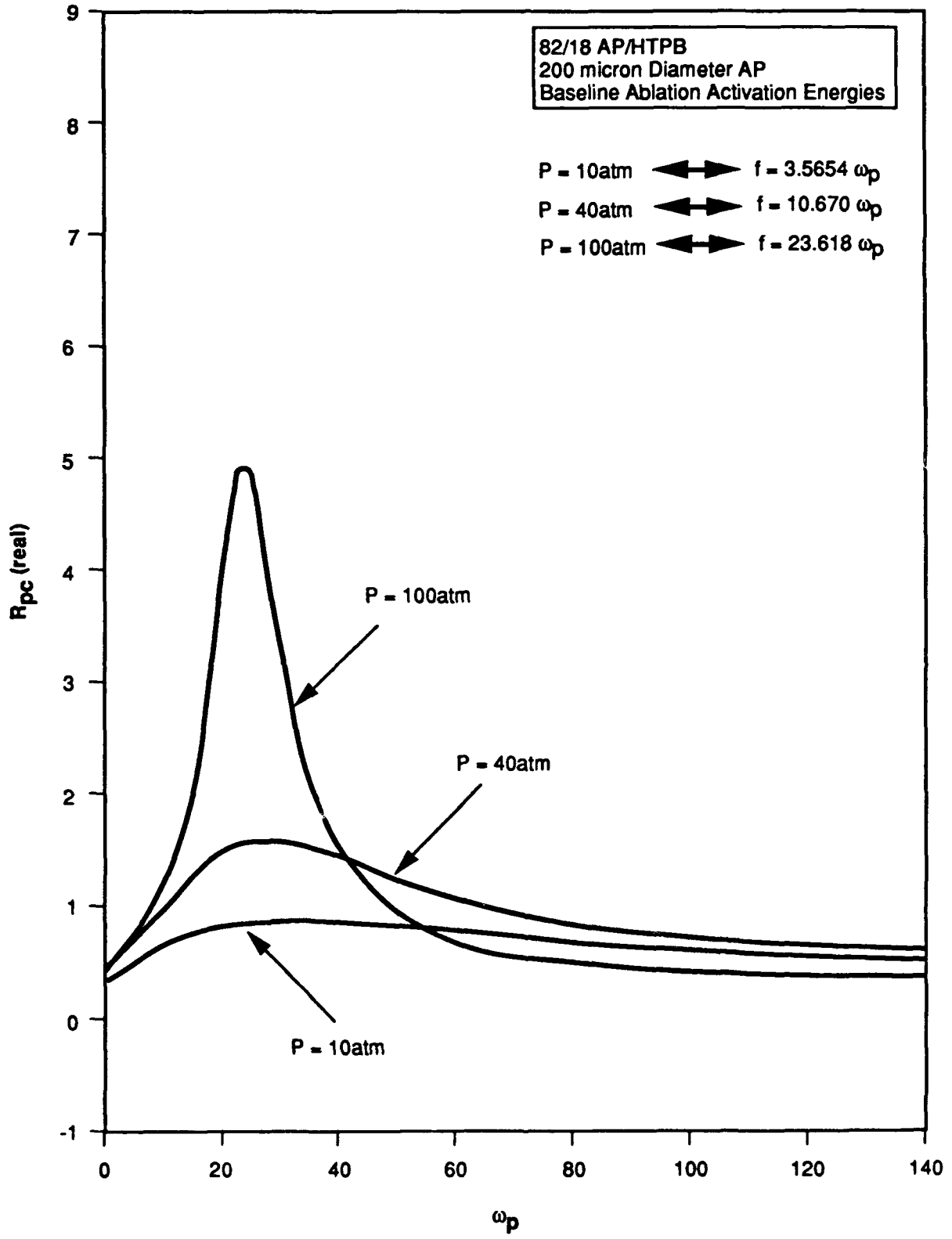

Figure 36. Real Part of Pressure-Coupled Response vs. Dimensionless Frequency

1091-AFSOR

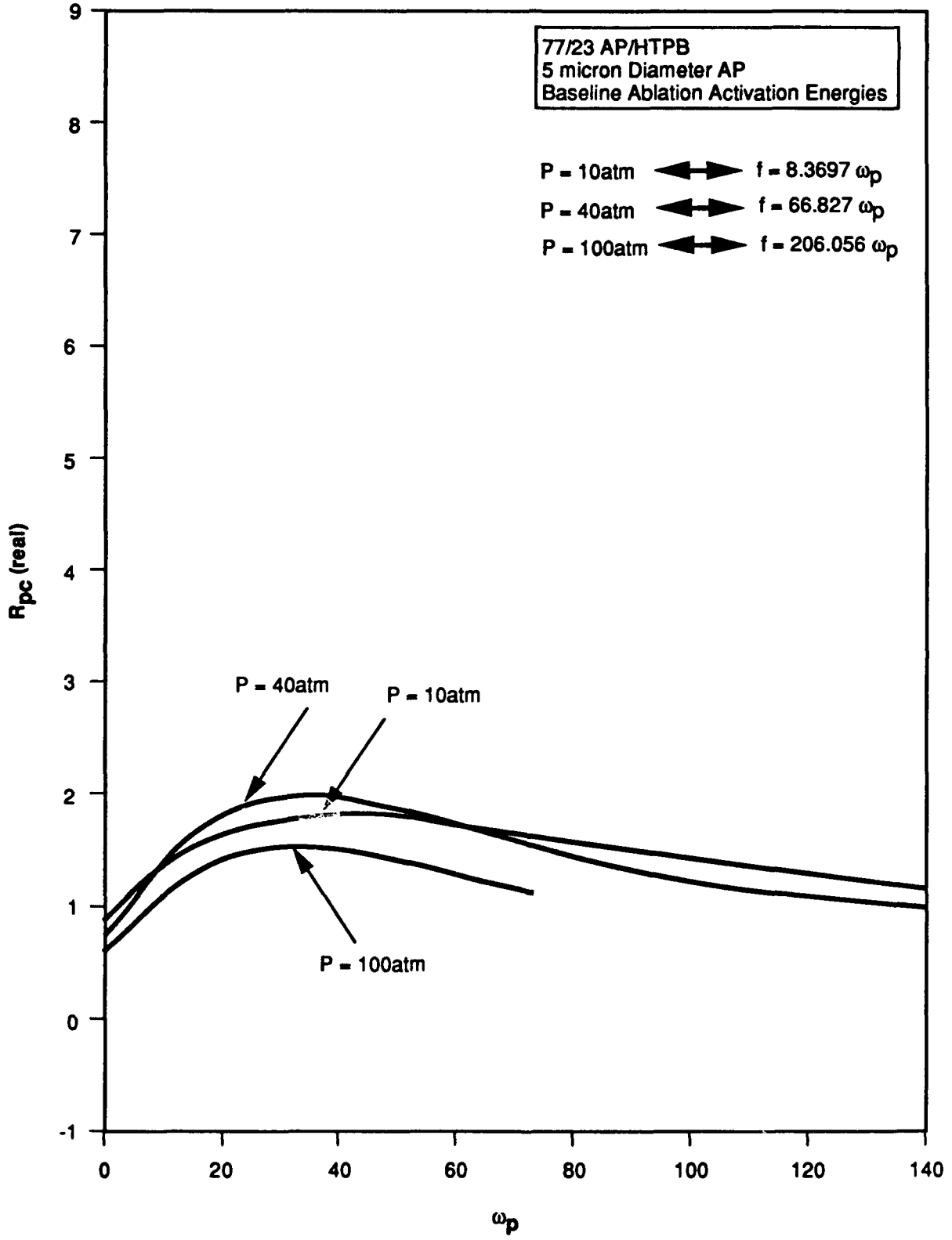

Figure 37. Real Part of Pressure-Coupled Response vs. Dimensionless Frequency

1091-AFSOR

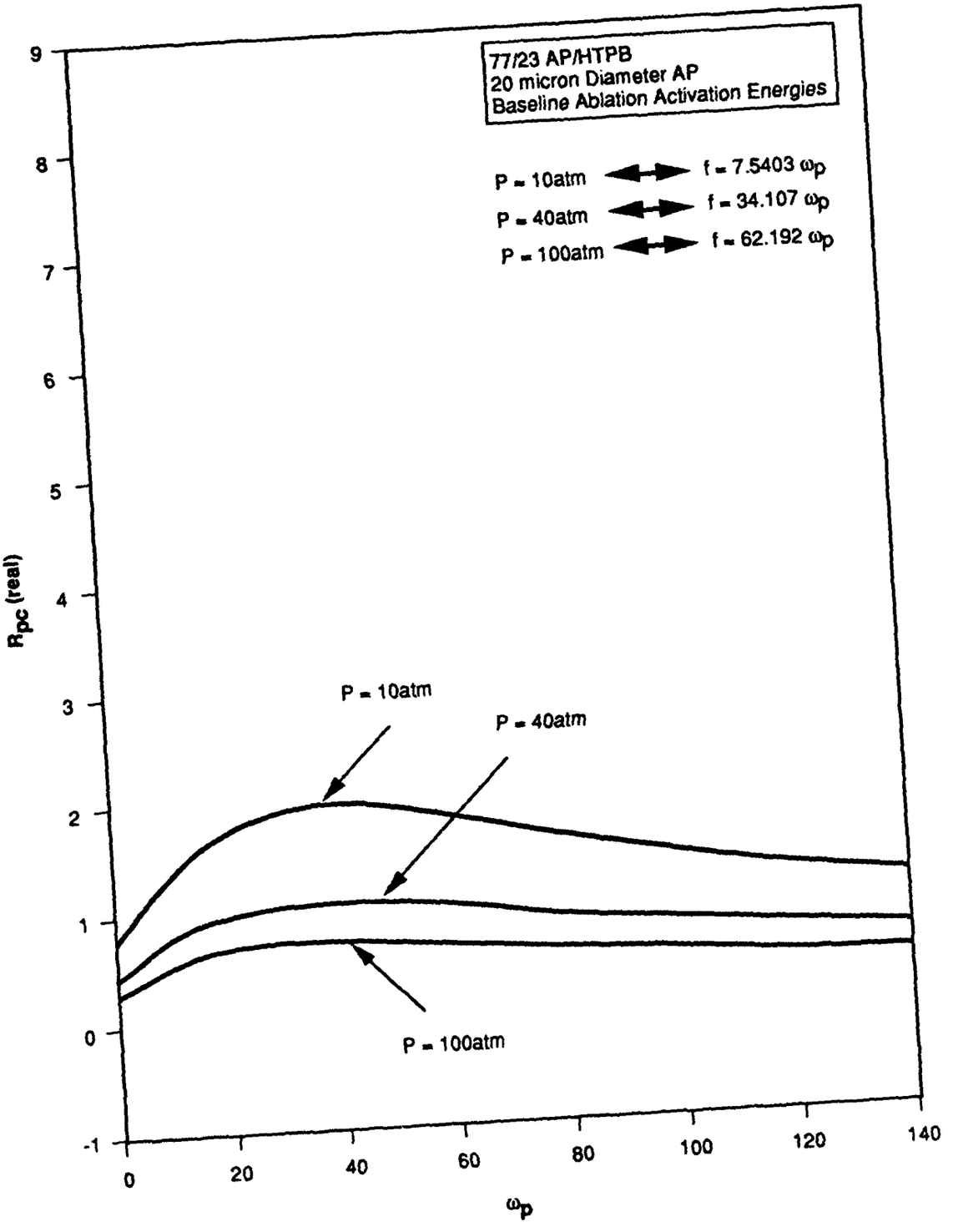

Figure 38. Real Part of Pressure-Coupled Response vs. Dimensionless Frequency

1091-AFSOR

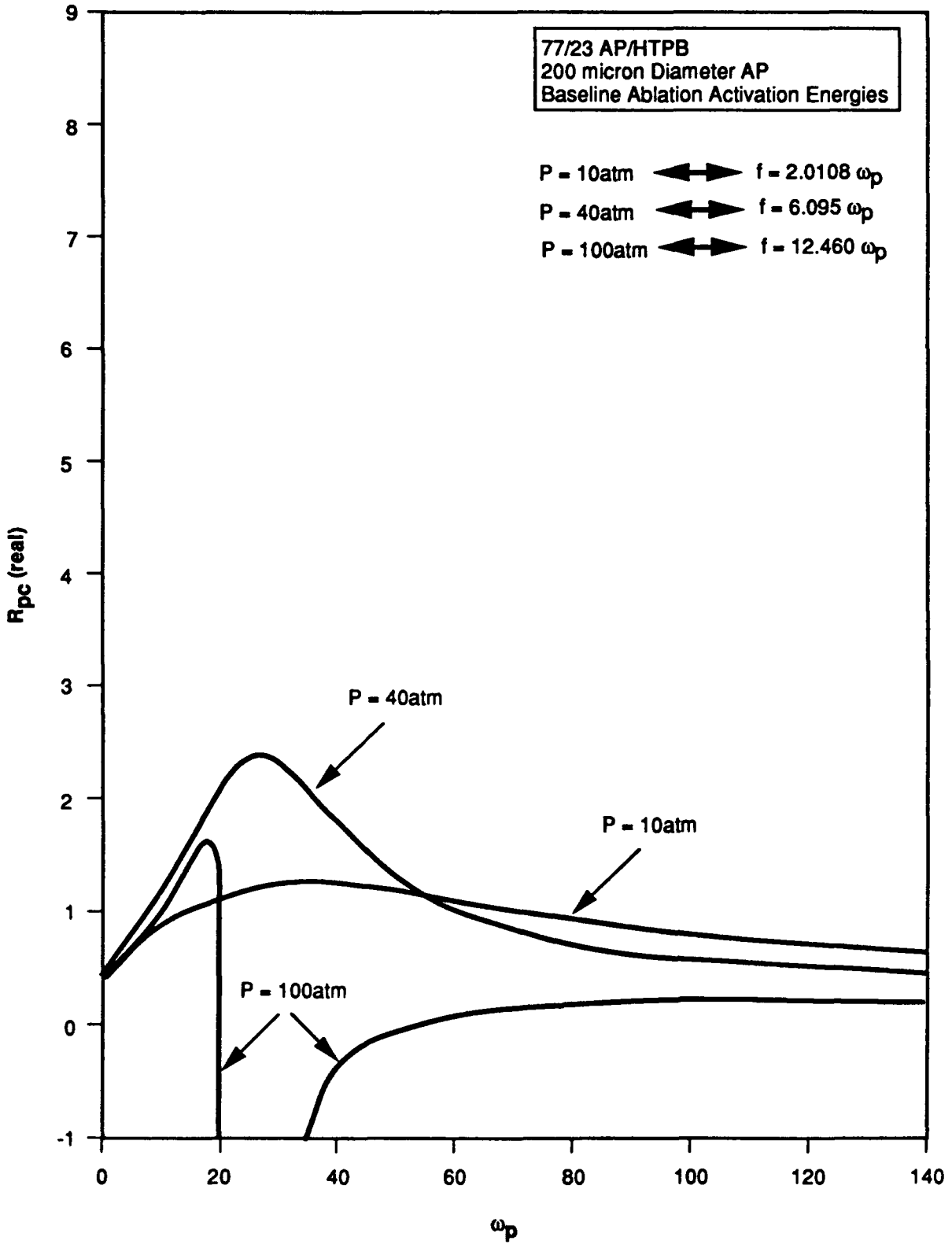

Figure 39. Real Part of Pressure-Coupled Response vs. Dimensionless Frequency

1091-AFSOR

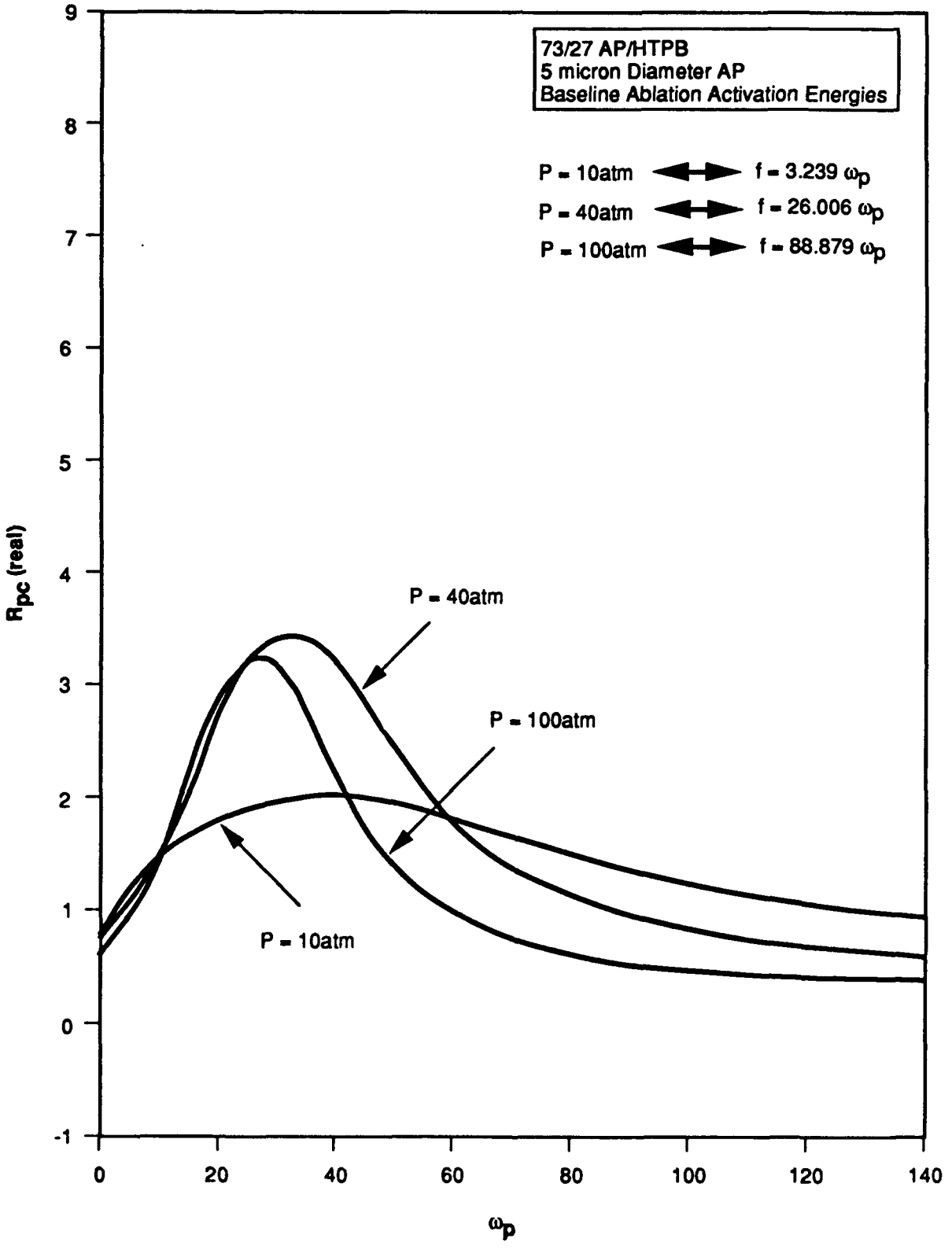

Figure 40. Real Part of Pressure-Coupled Response vs. Dimensionless Frequency

1091-AFSOR

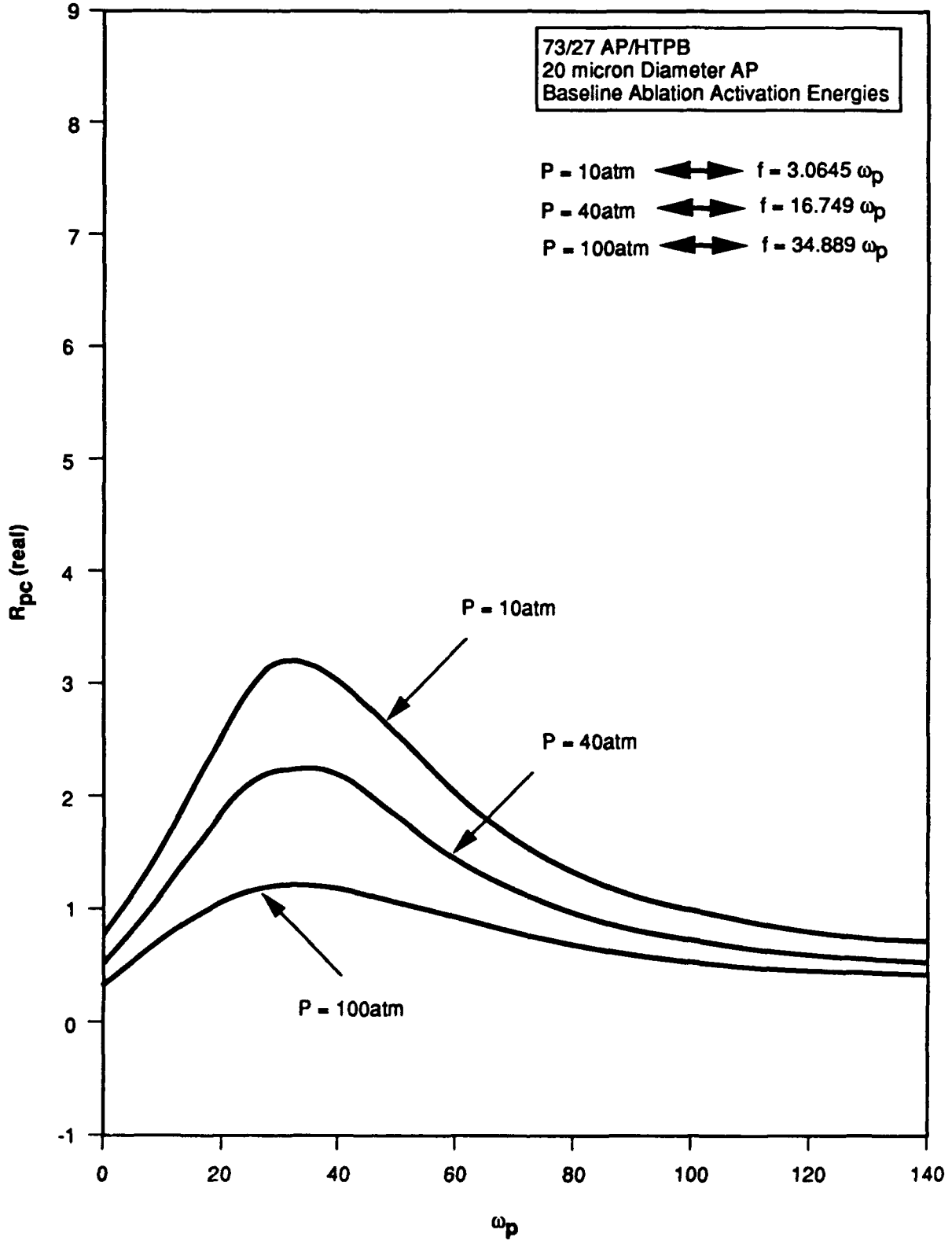

Figure 41. Real Part of Pressure-Coupled Response vs. Dimensionless Frequency

1091-AFSOR

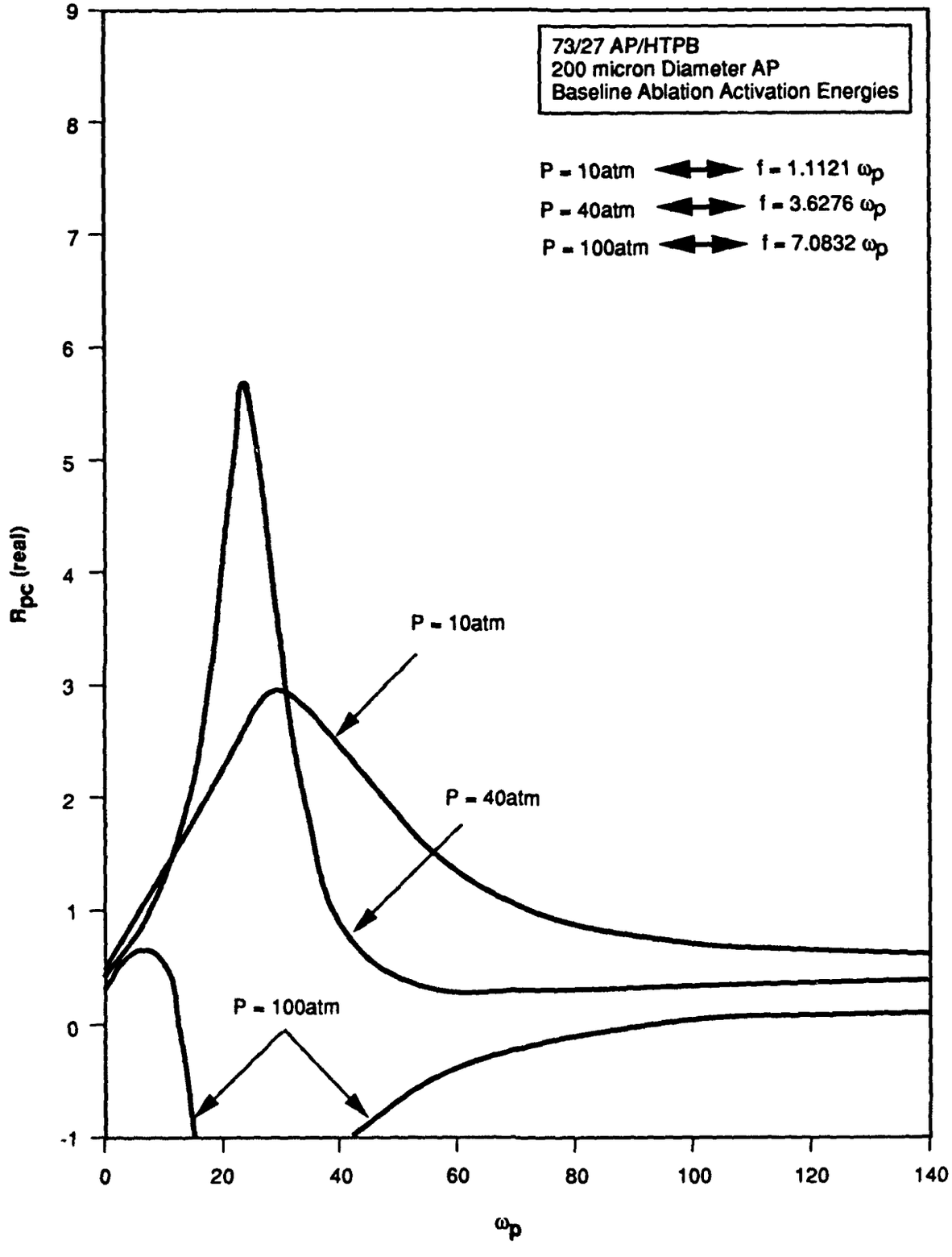

Figure 42. Real Part of Pressure-Coupled Response vs. Dimensionless Frequency

1091-AFSOR

curves of Figures 5-8, where ZFRACT was held constant for each curve. At the lowest frequencies, the response values correspond to ZFRACT = 1.0 values on the previous graphs; while at the highest frequencies, they are closer to the ZFRACT = 0 values. That is, these curves tend to track across the curves shown earlier, moving from the top curve to the bottom curve as frequency increases (left to right). (Detailed computer printouts include ZFRACT values at each frequency, permitting quantitative demonstration of this behavior.) As may be seen from Figures 32-34, the pressure-coupled responses for the 1-, 7-, and 20-micron AP, 82/18 AP/HTPB cases are fairly low, without any sharp peaks. As the AP size is increased to 90 and 200 microns for the 82/18 cases, the pressure-coupled response versus dimensionless frequency curves begin to exhibit significant peaks (Figures 35 and 36), particularly at high pressure. With 77/23 AP/HTPB formulations, increased sensitivity to pressure oscillations is seen (Figure 37-39); this is particularly strong for the 200 micron AP case. In fact, for the 200 micron AP case at P = 100 atm, the formulation is actually intrinsically unstable (the dive in the response to very low negative values is indicative of such intrinsic instability). Finally, with 73/27 AP/HTPB formulations, the responses are still higher; again, intrinsic instability is predicted for the 200-micron-AP, P = 100 atm case.

6.2.2 Effects of Changes in Activation Energies of Fuel and Oxidizer Ablation Processes

Plots of the calculated real part of the pressure-coupled response versus oscillation frequency are presented in Figures 43-60 for various values of oxidizer ablation activation energy (at constant fuel ablation activation energy) and various values of fuel ablation activation energy (at constant oxidizer ablation activation energy) for several AP/HTPB ratio-pressure-oxidizer particle size combinations. The maximum values of this real part of the pressure-coupled response, extracted from these plots, are next plotted against oxidizer ablation activation energy for various AP/HTPB ratio-pressure-AP size combinations in Figures 61-70, and against fuel ablation activation energy in Figures 71-80. The following discussion will be concentrated on the results depicted in Figures 61-80.

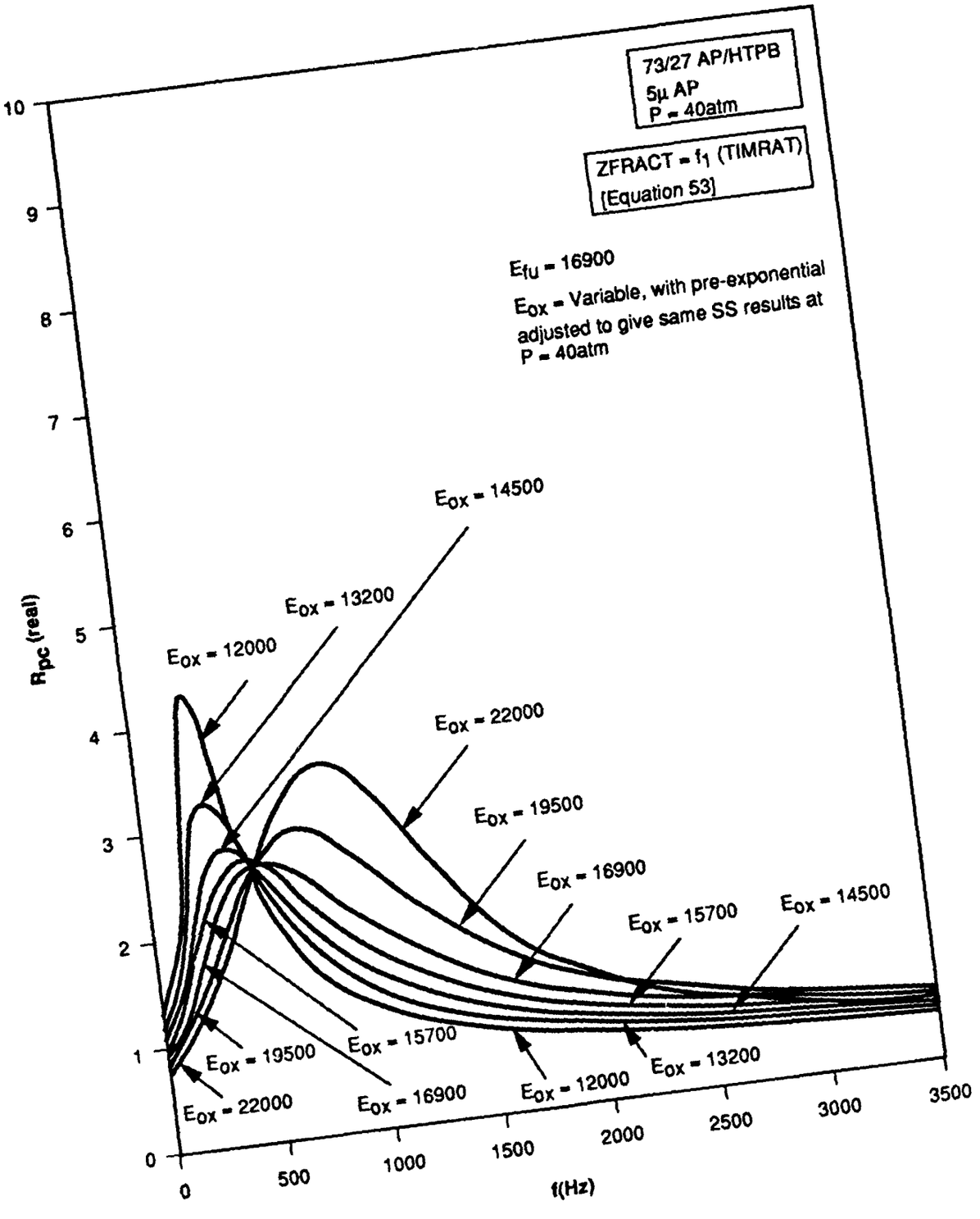

1091-AFSOR

Figure 43. Real Part of Pressure-Coupled Response vs. Oscillation Frequency

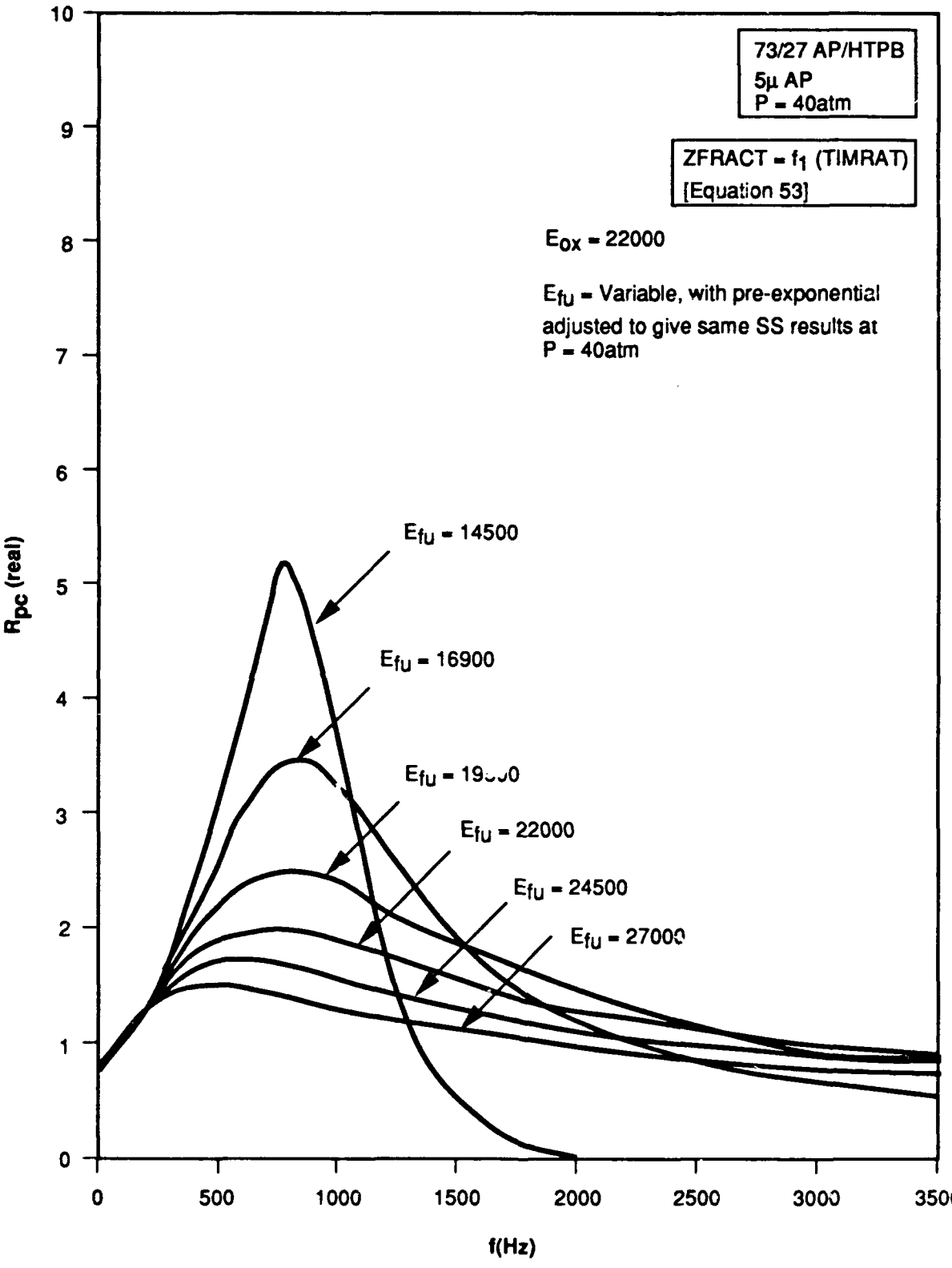

Figure 44. Real Part of Pressure-Coupled Response vs. Oscillation Frequency

1091-AFSOR

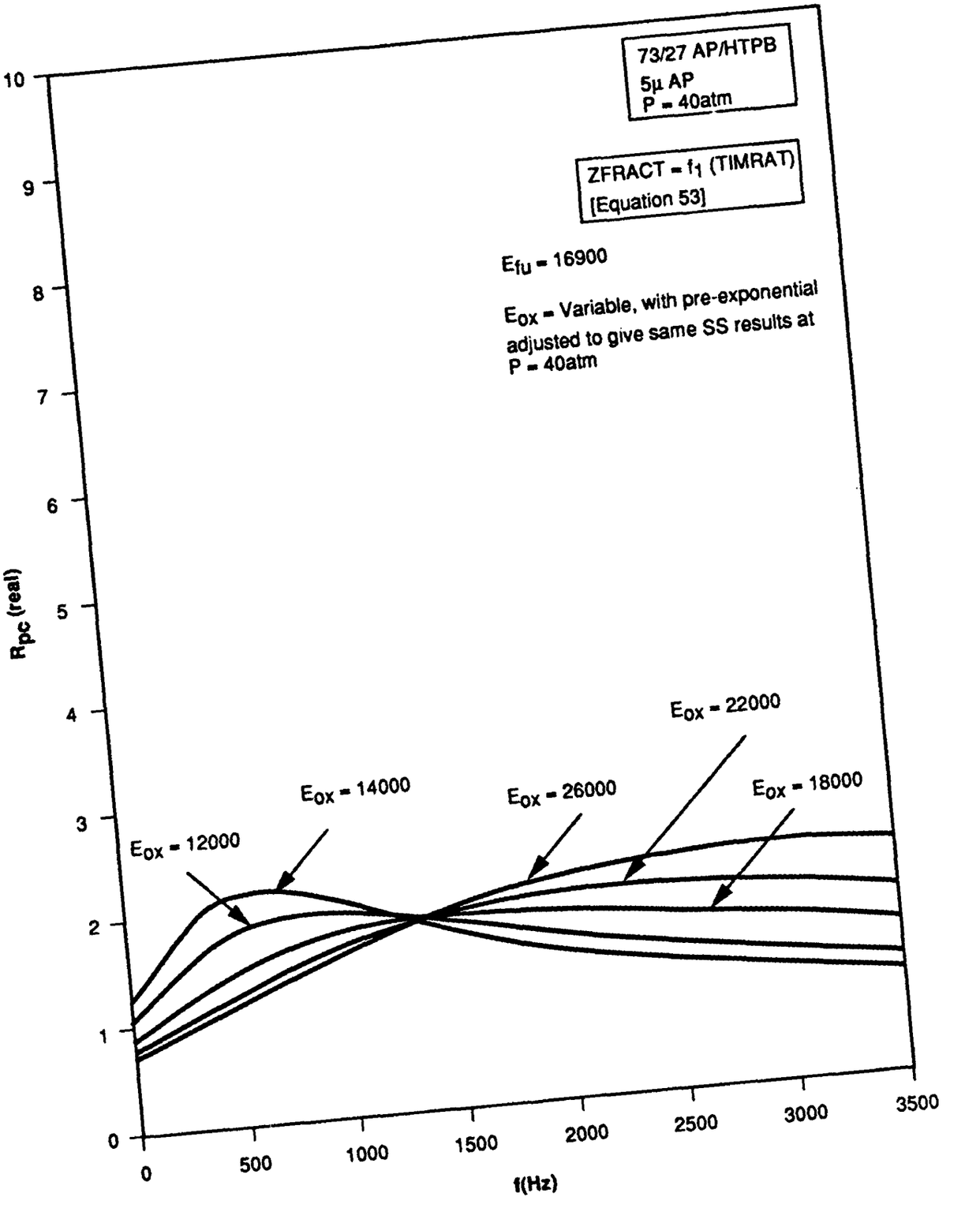

Figure 45. Real Part of Pressure-Coupled Response vs. Oscillation Frequency

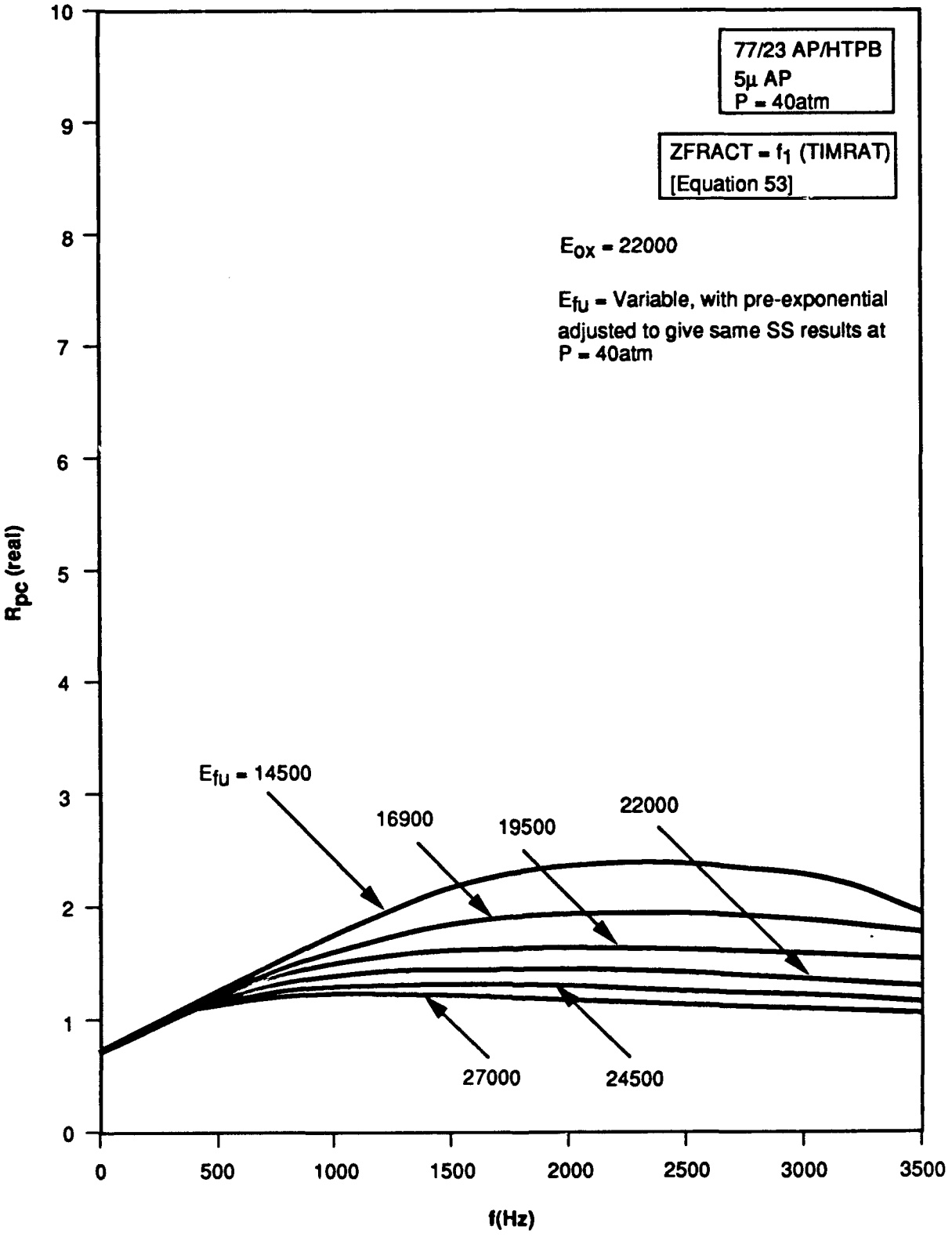

Figure 46. Real Part of Pressure-Coupled Response vs. Oscillation Frequency

1091-AFSOR

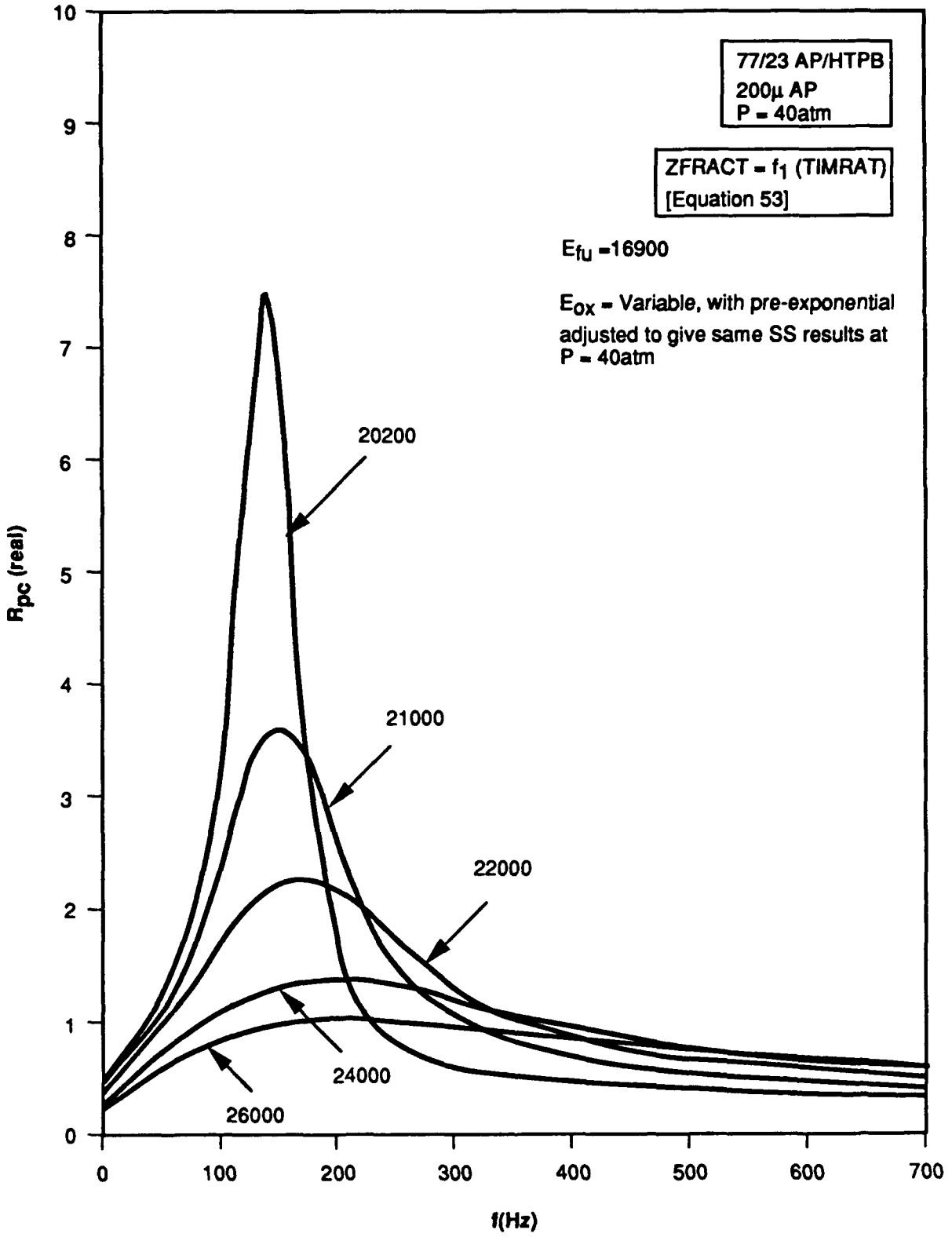

Figure 47. Real Part of Pressure-Coupled Response vs. Oscillation Frequency

1091-AFSOR

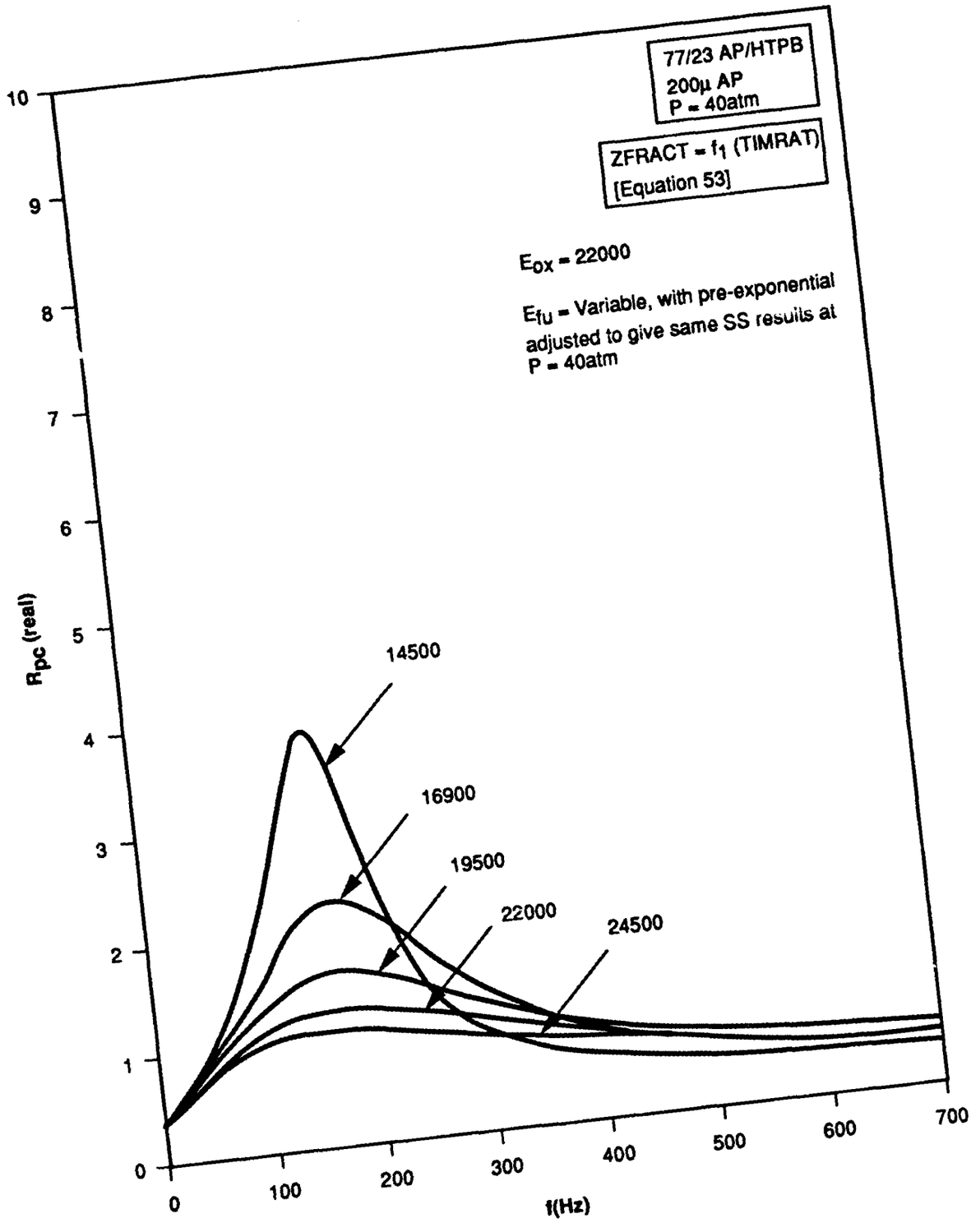

Figure 48. Real Part of Pressure-Coupled Response vs. Oscillation Frequency

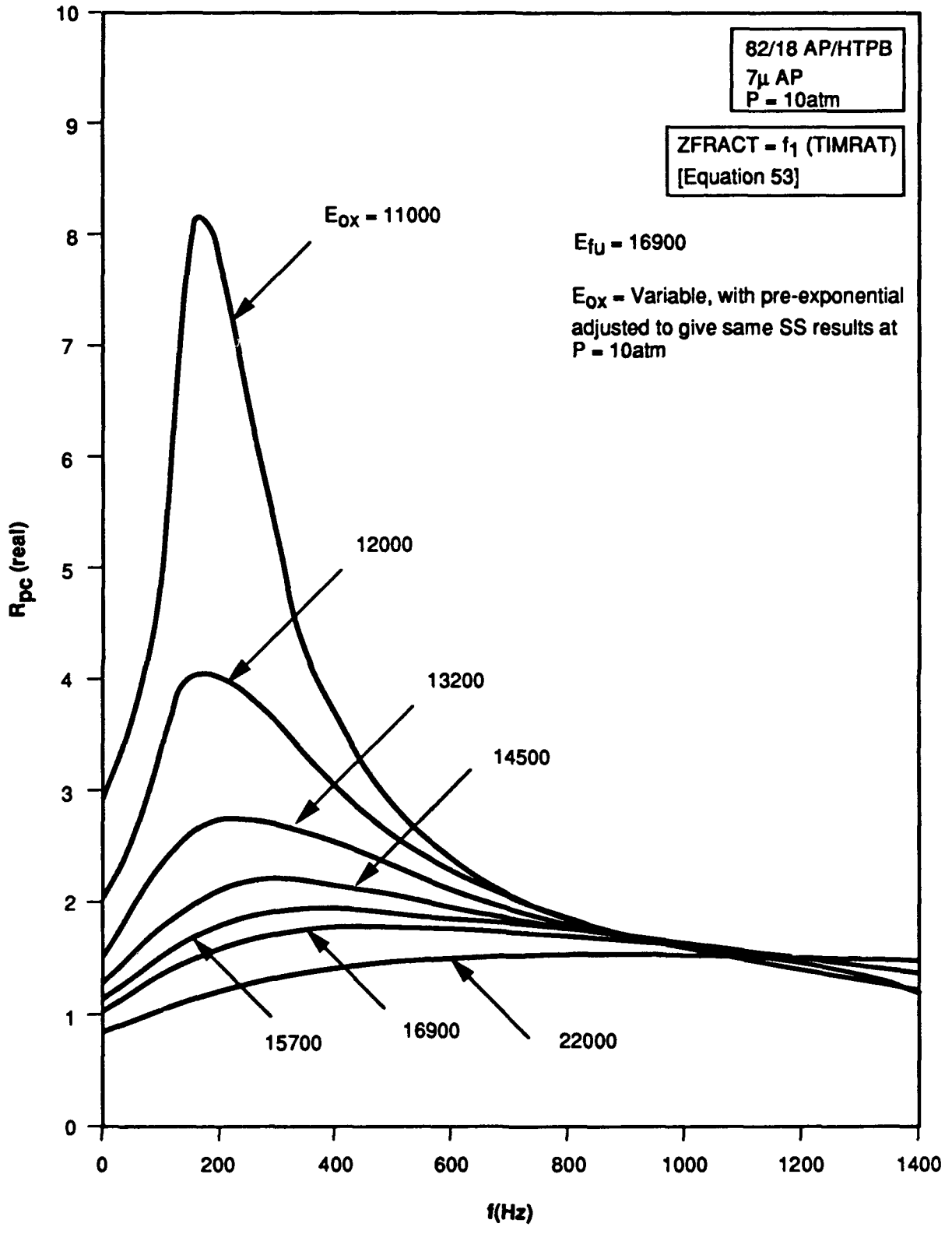

Figure 49. Real Part of Pressure-Coupled Response vs. Oscillation Frequency

1091-AFSOR

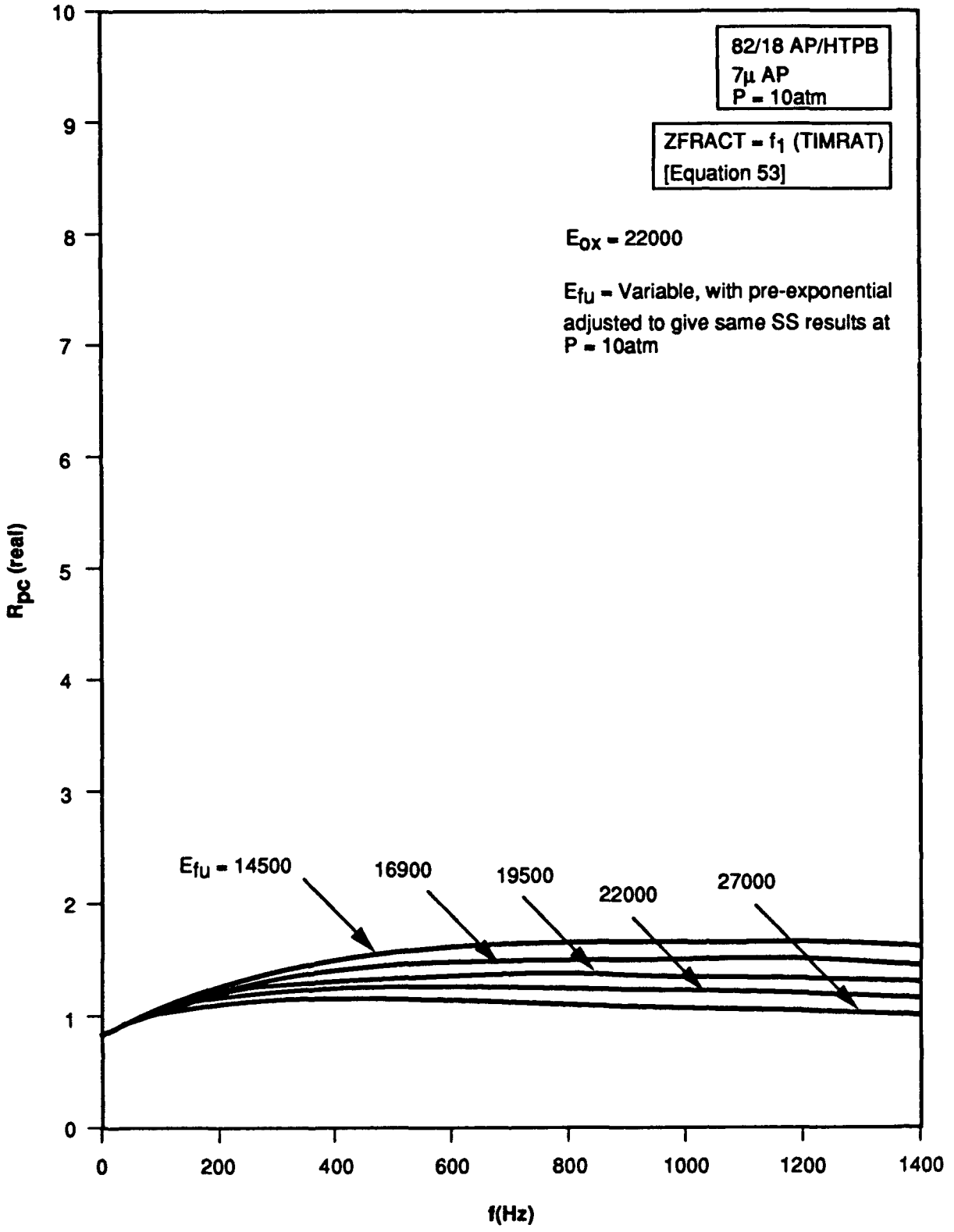

Figure 50. Real Part of Pressure-Coupled Response vs. Oscillation Frequency

1091-AFSOR

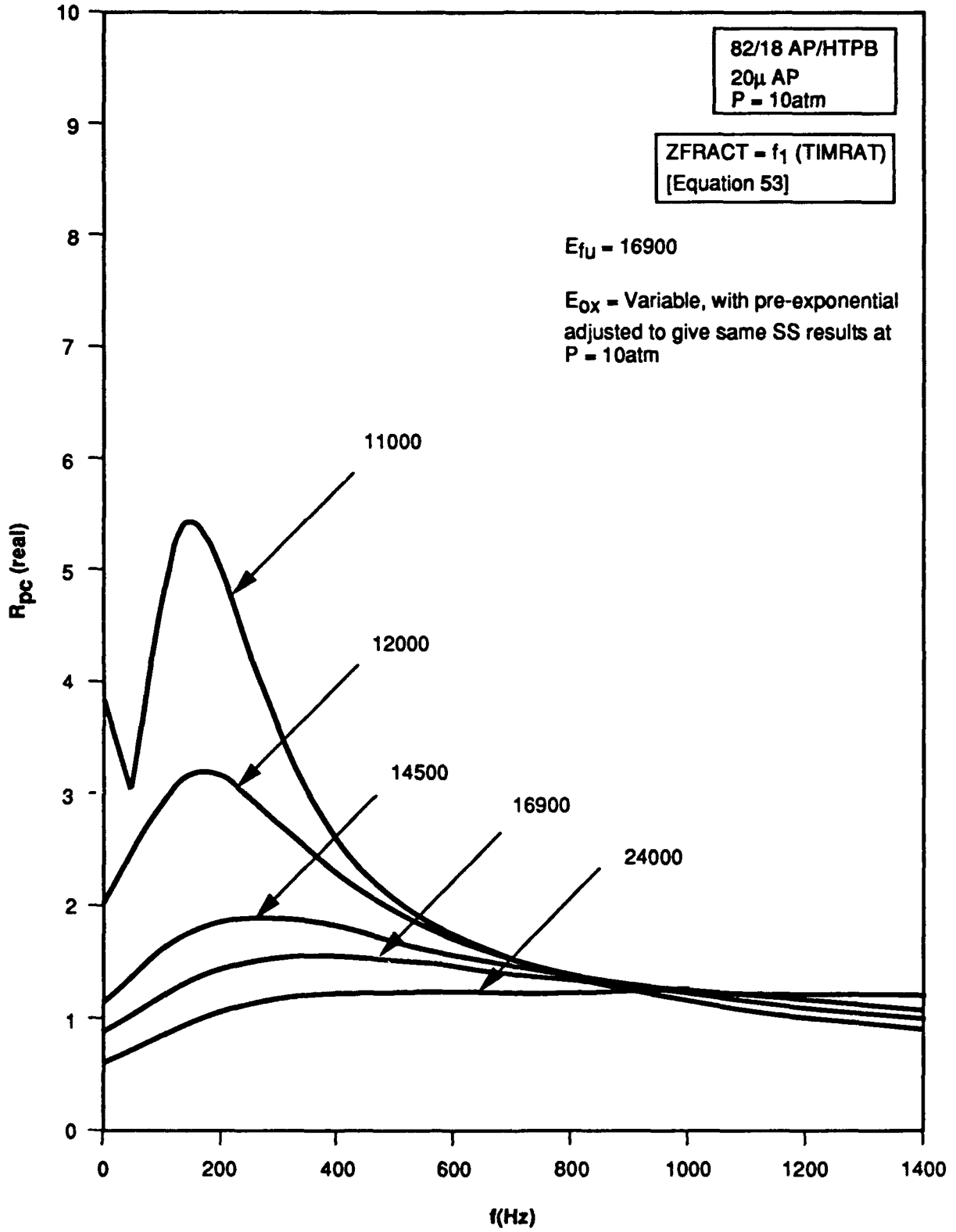

Figure 51. Real Part of Pressure-Coupled Response vs. Oscillation Frequency

1091-AFSOR

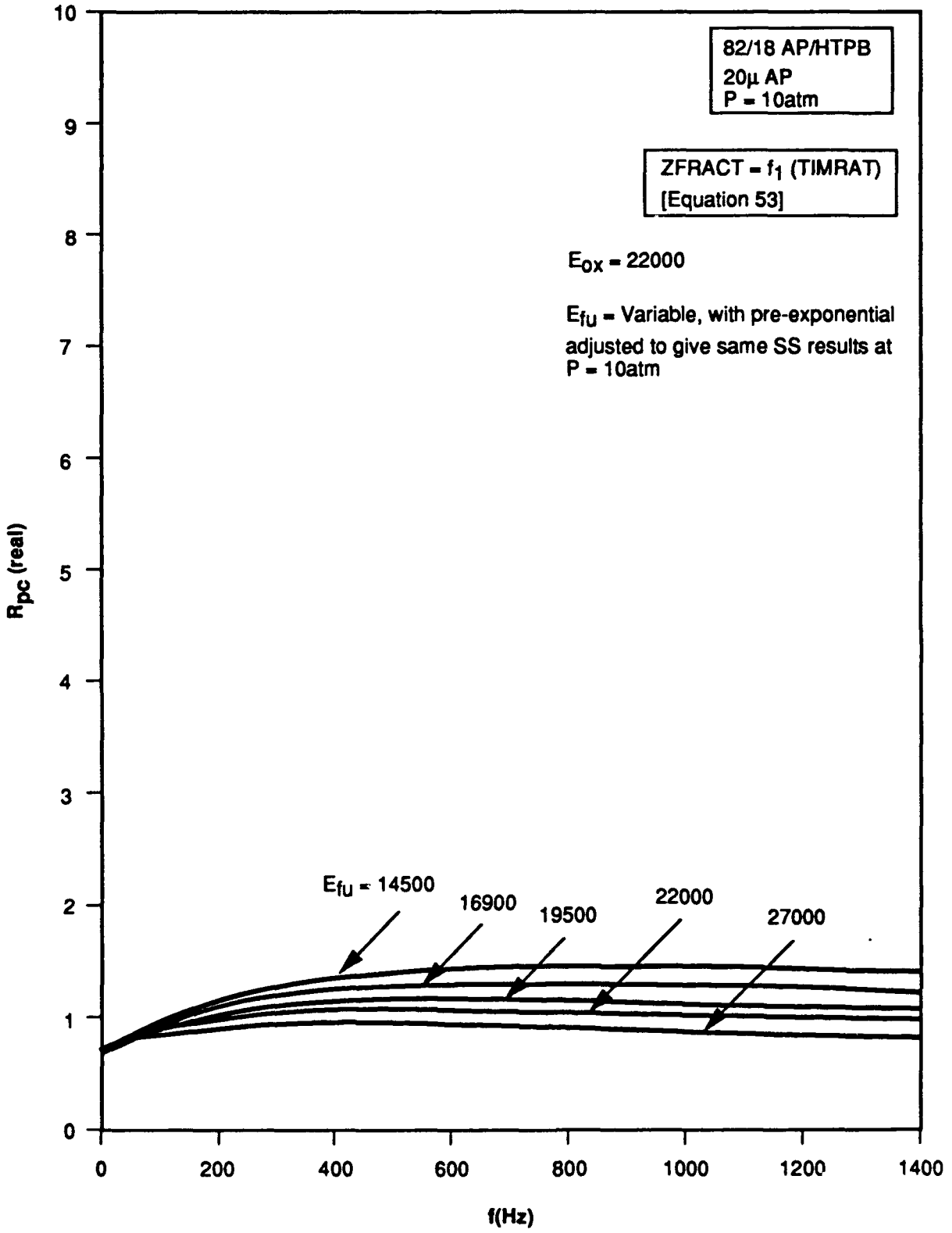

Figure 52. Real Part of Pressure-Coupled Response vs. Oscillation Frequency

1091-AFSOR

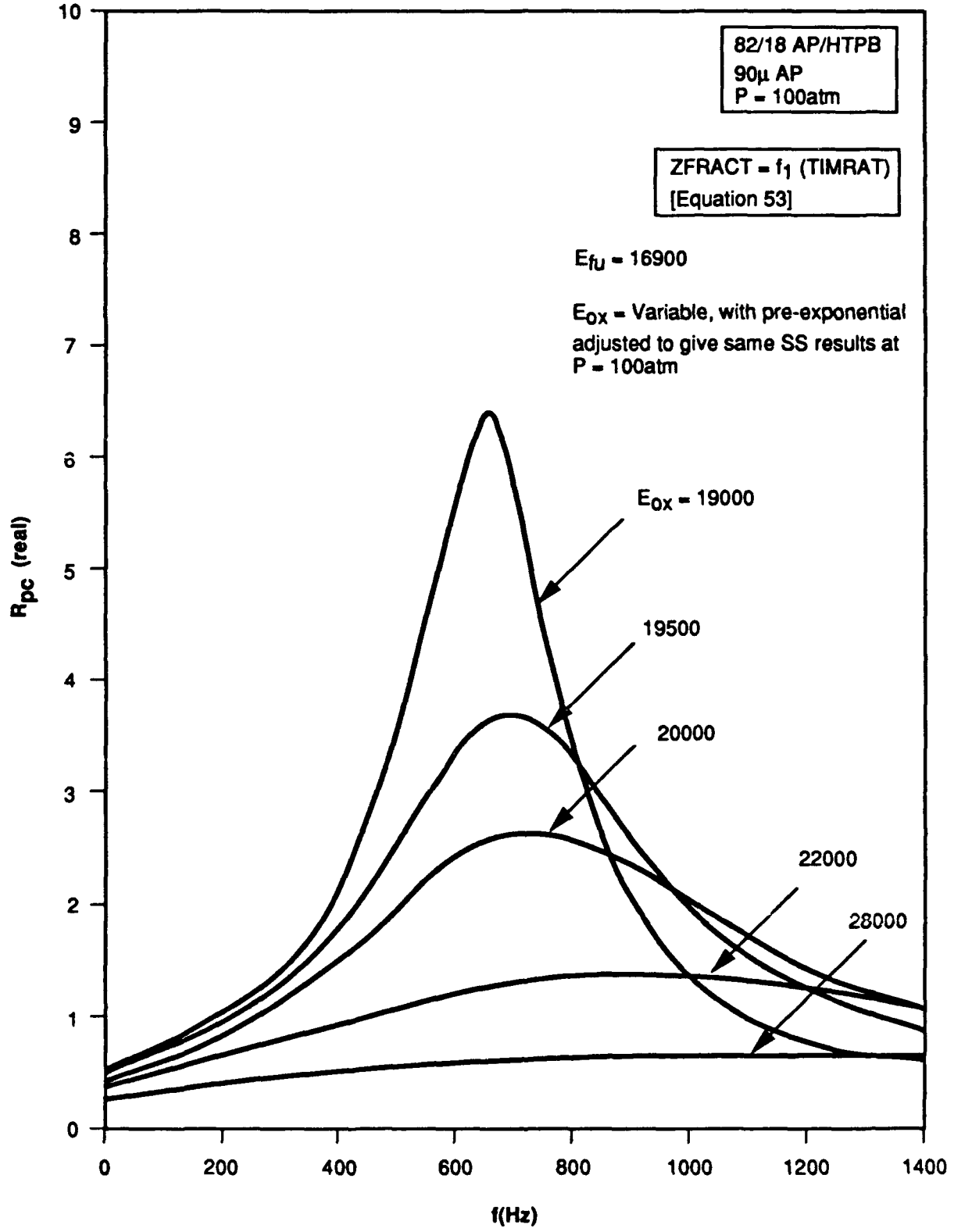

Figure 53. Real Part of Pressure-Coupled Response vs. Oscillation Frequency

1091-AFSOR

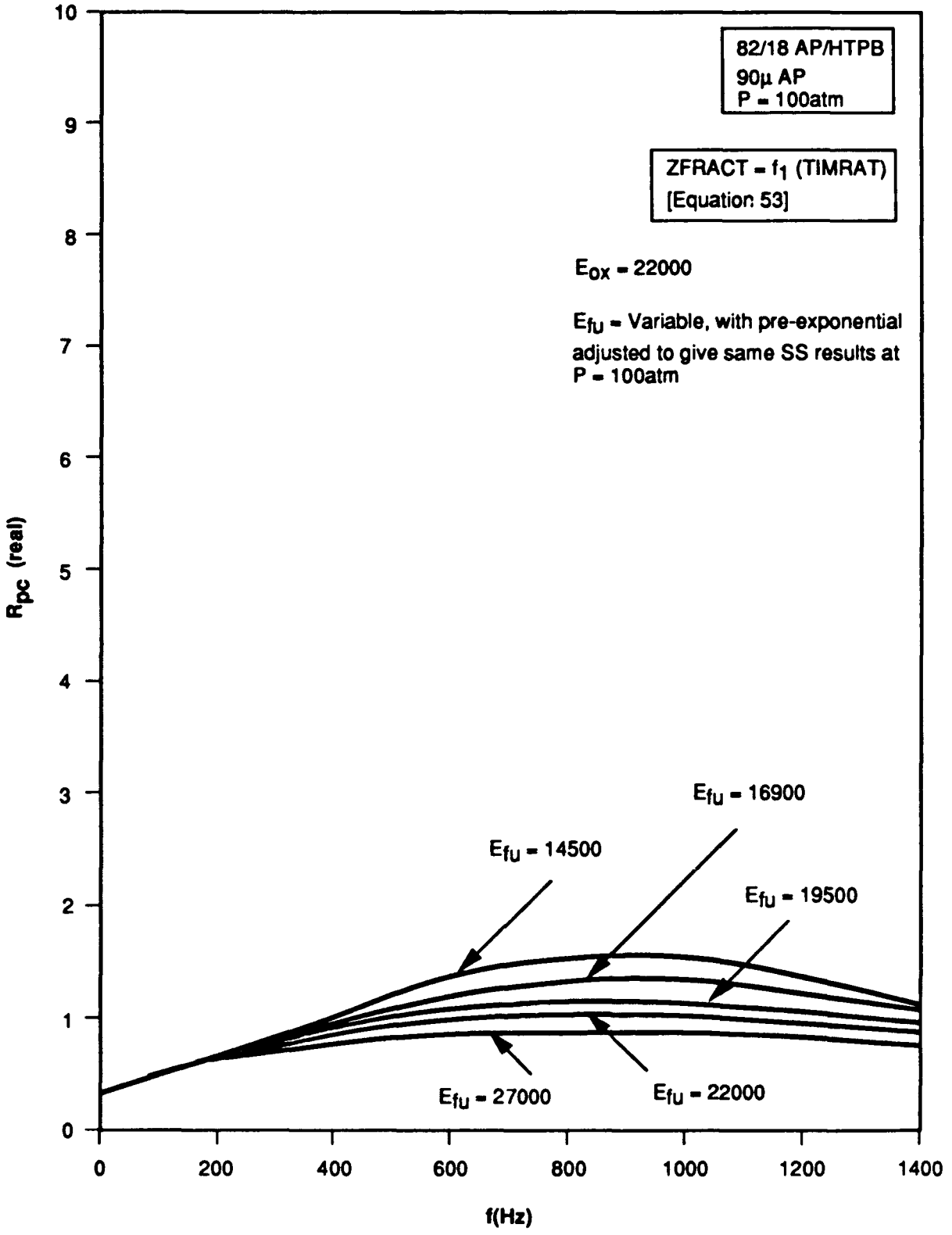

Figure 54. Real Part of Pressure-Coupled Response vs. Oscillation Frequency

1091-AFSOR

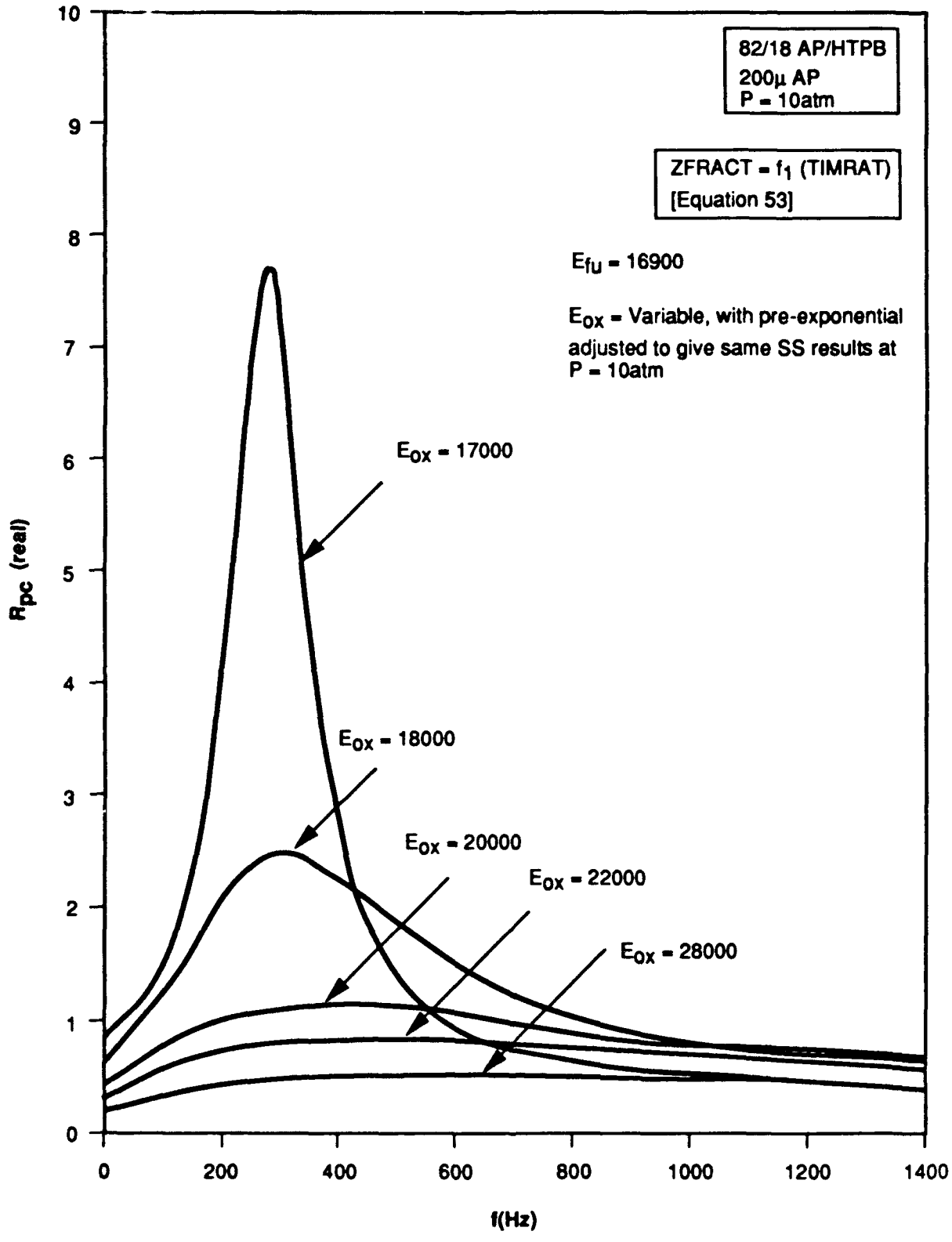

Figure 55. Real Part of Pressure-Coupled Response vs. Oscillation Frequency

1091-AFSOR

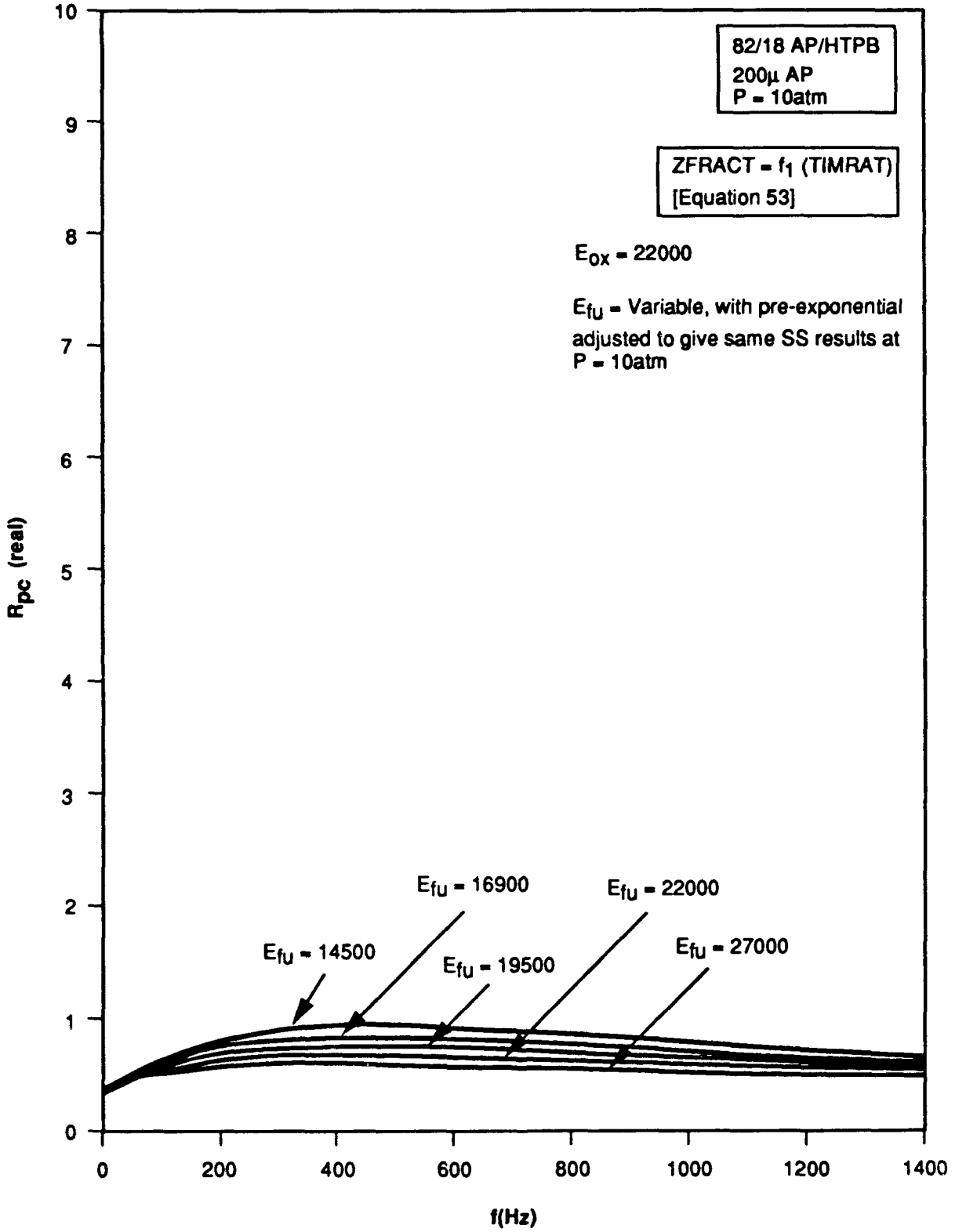

Figure 56. Real Part of Pressure-Coupled Response vs. Oscillation Frequency

1091-AFSOR

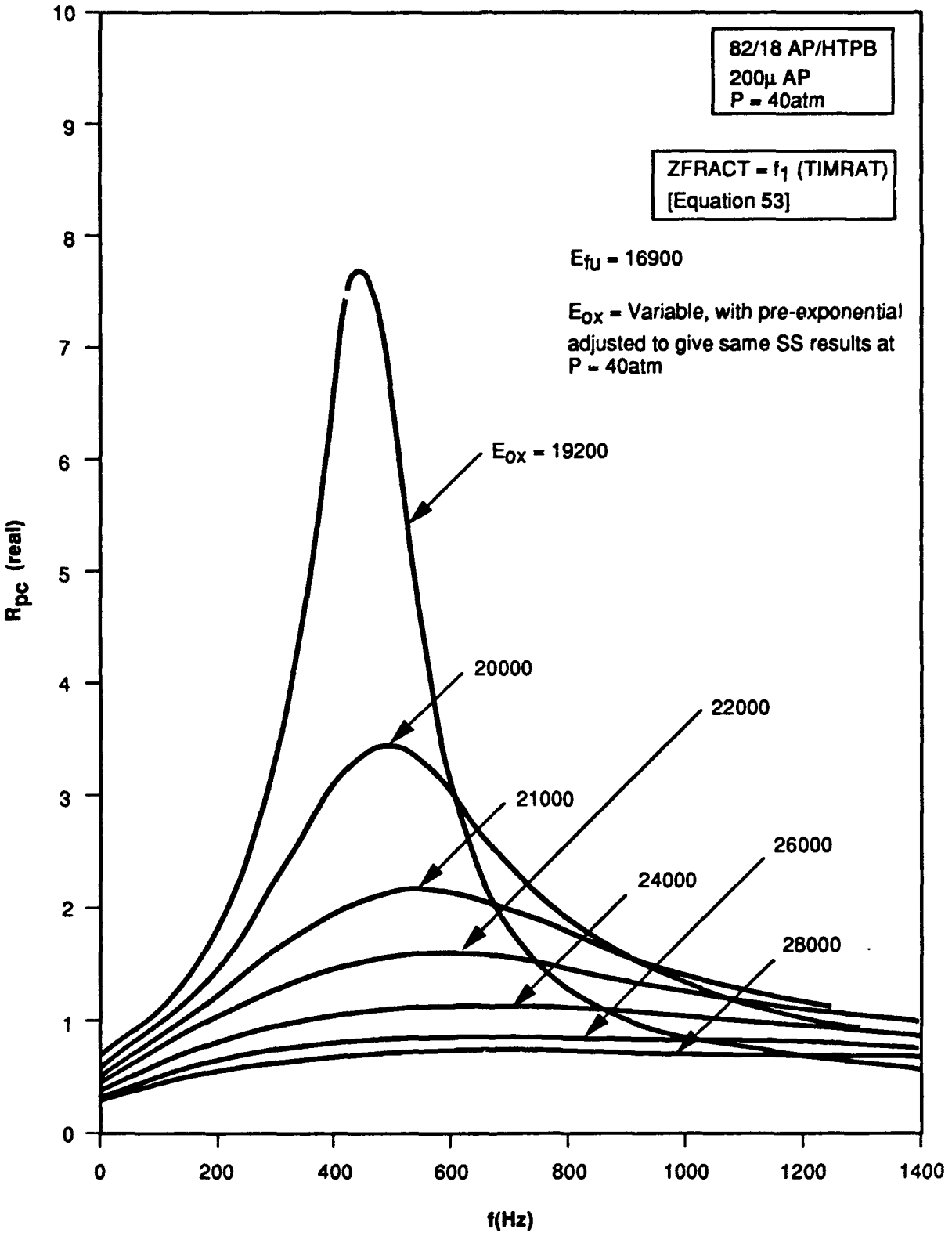

Figure 57. Real Part of Pressure-Coupled Response vs. Oscillation Frequency

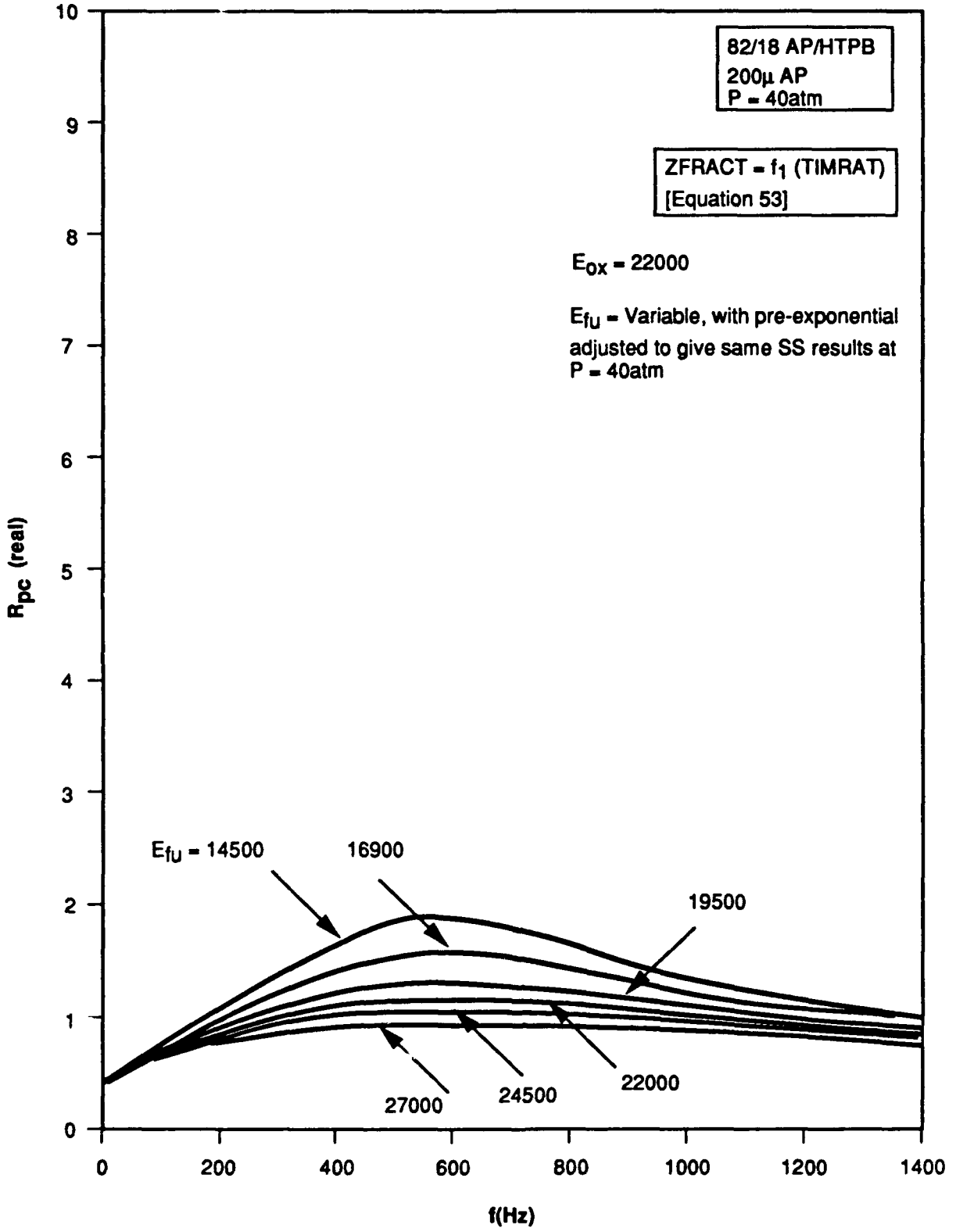

Figure 58. Real Part of Pressure-Coupled Response vs. Oscillation Frequency

1091-AFSOR

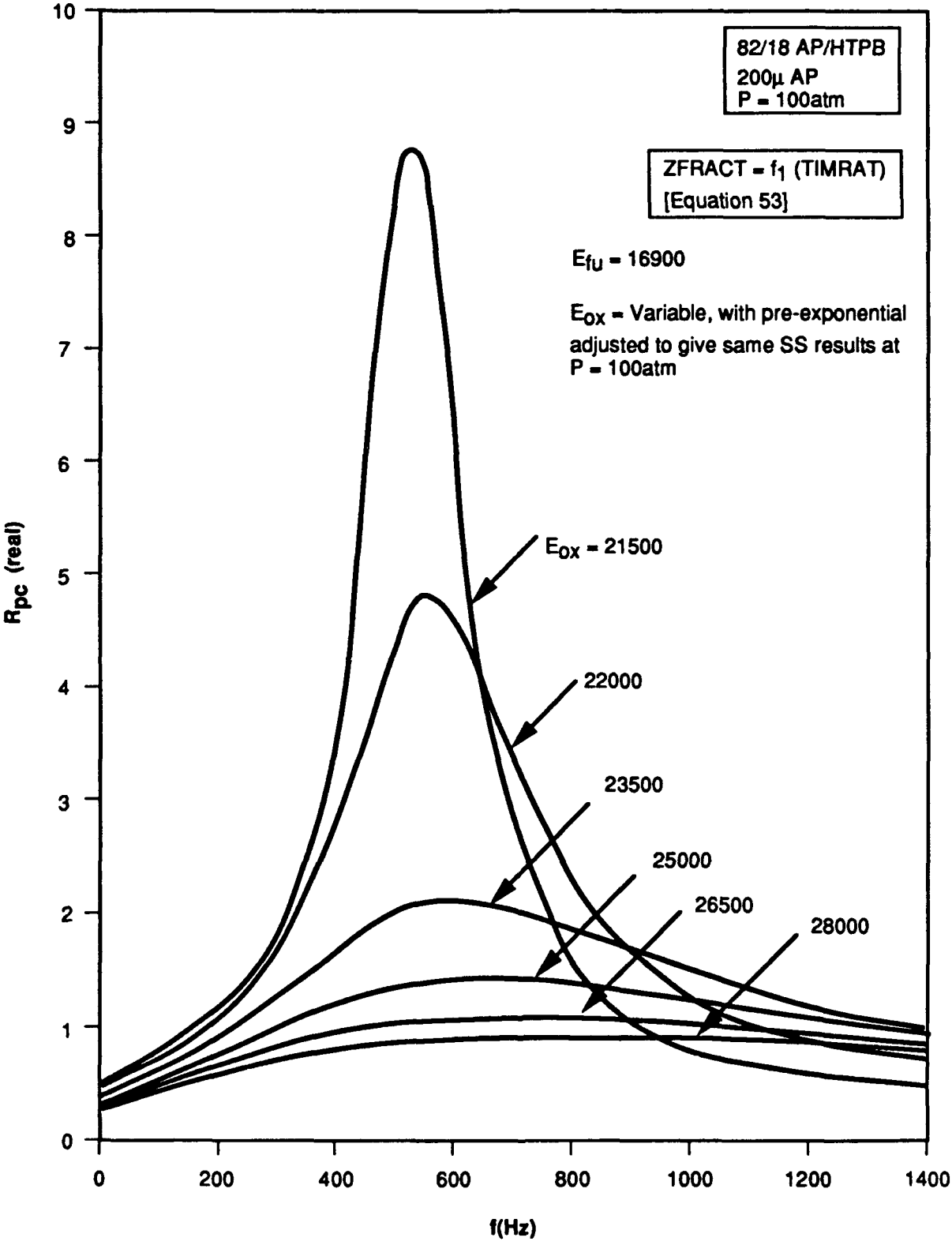

Figure 59. Real Part of Pressure-Coupled Response vs. Oscillation Frequency

1091-AFSOR

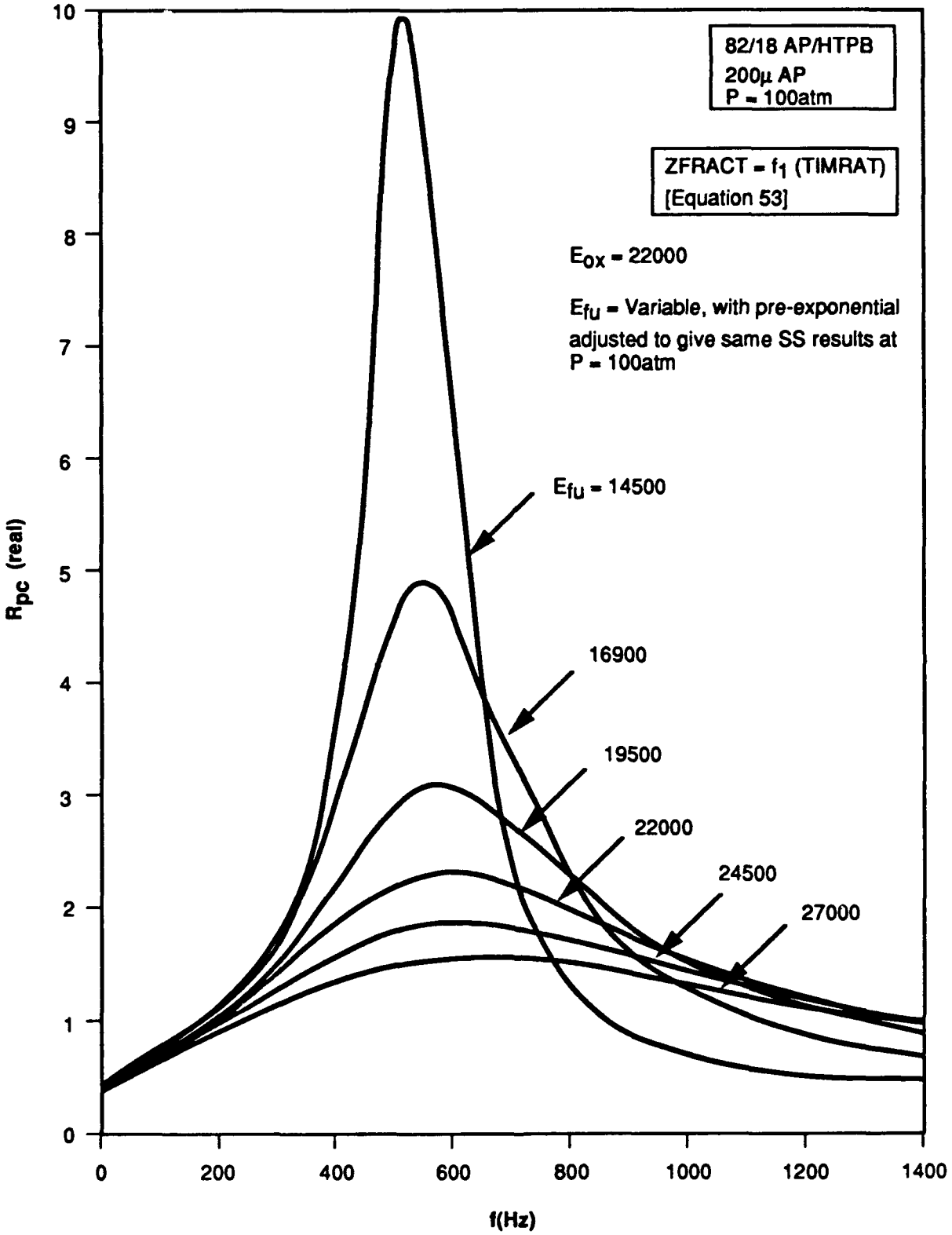

Figure 60. Real Part of Pressure-Coupled Response vs. Oscillation Frequency

1091-AFSOR

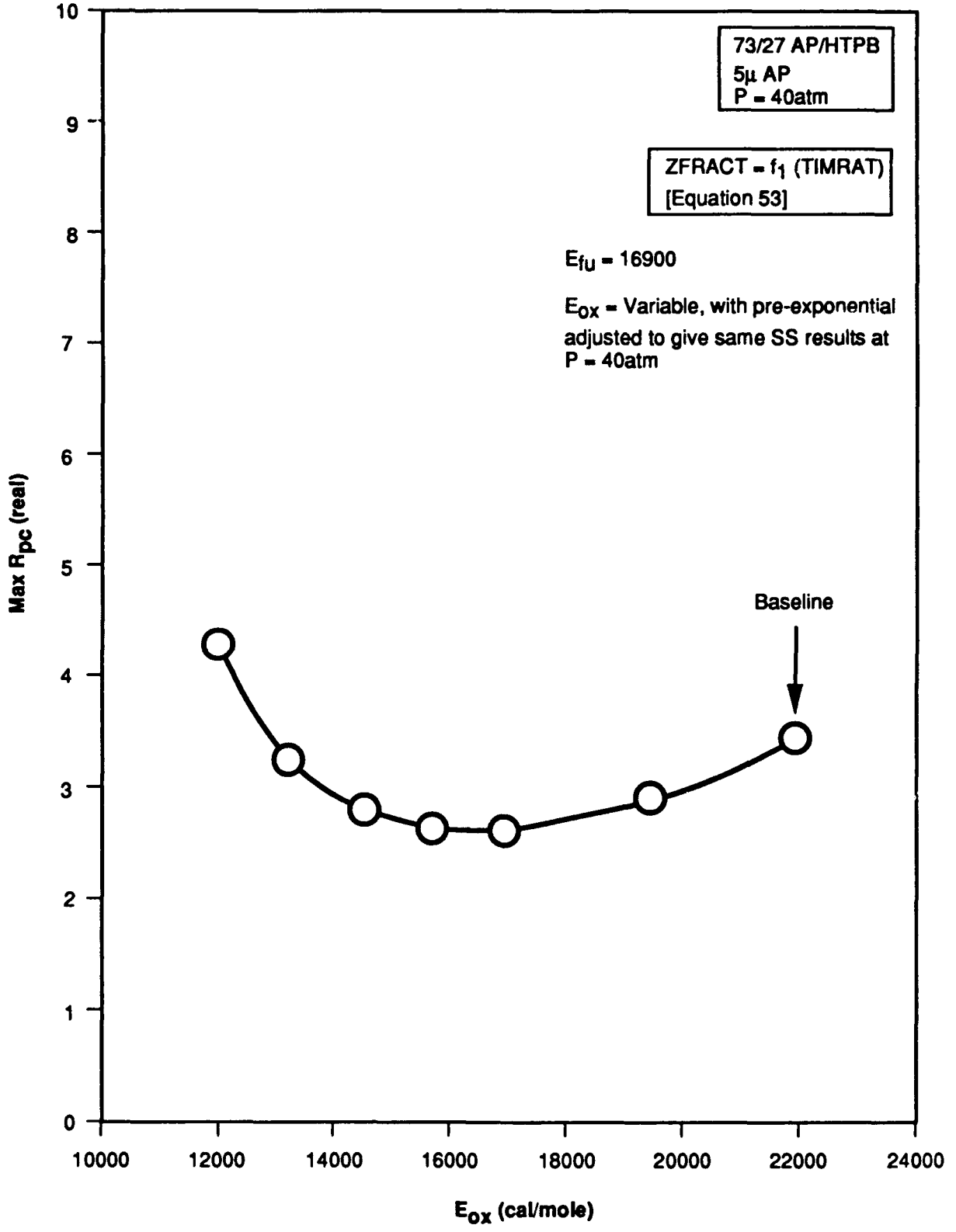

Figure 61. Dependence of Maximum Value of Pressure-Coupled Response on Oxidizer Ablation Activation Energy at Constant Fuel Ablation Activation Energy

1091-AFSOR

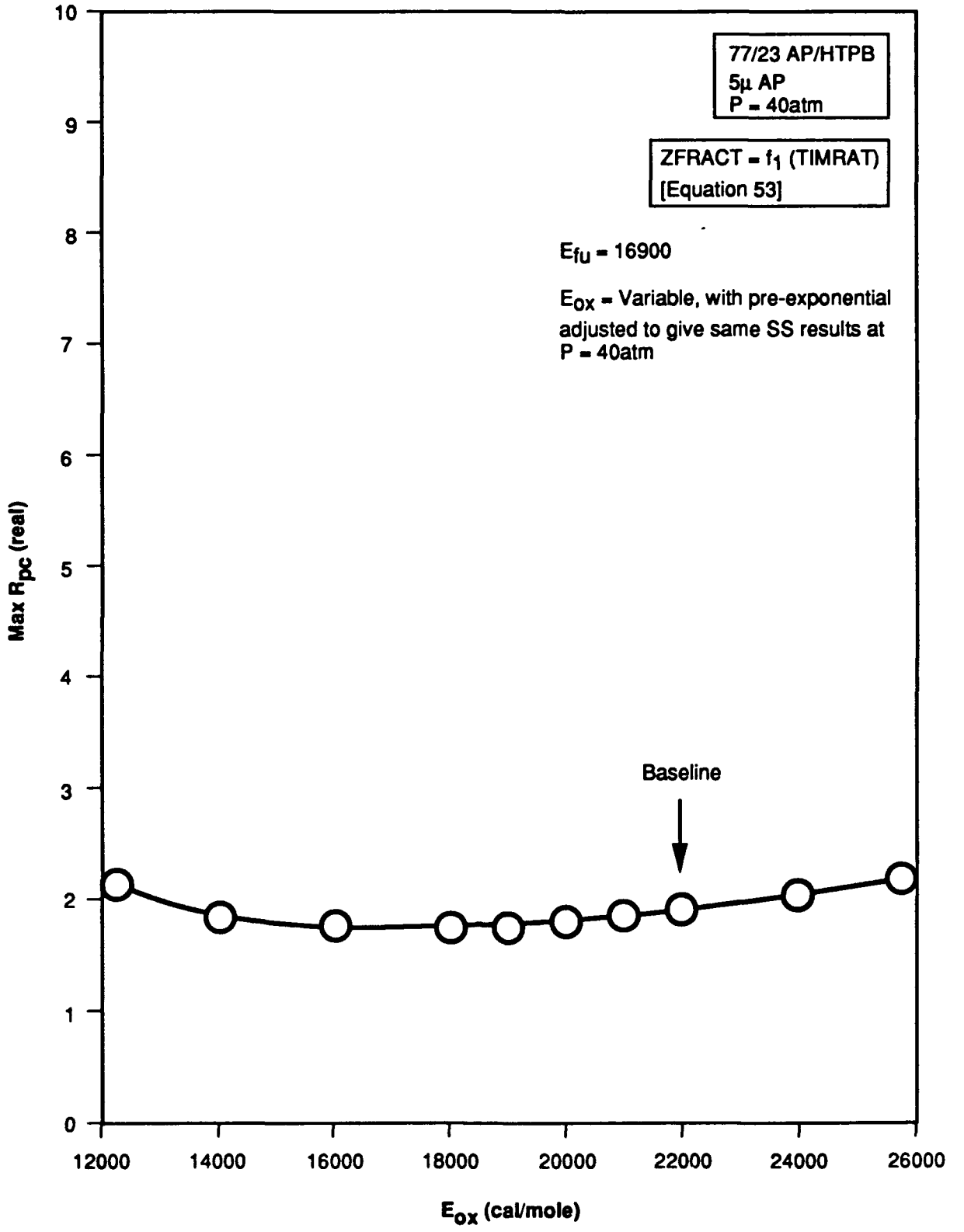

Figure 62. Dependence of Maximum Value of Pressure-Coupled Response on Oxidizer Ablation Activation Energy at Constant Fuel Ablation Activation Energy

1091-AFSOR

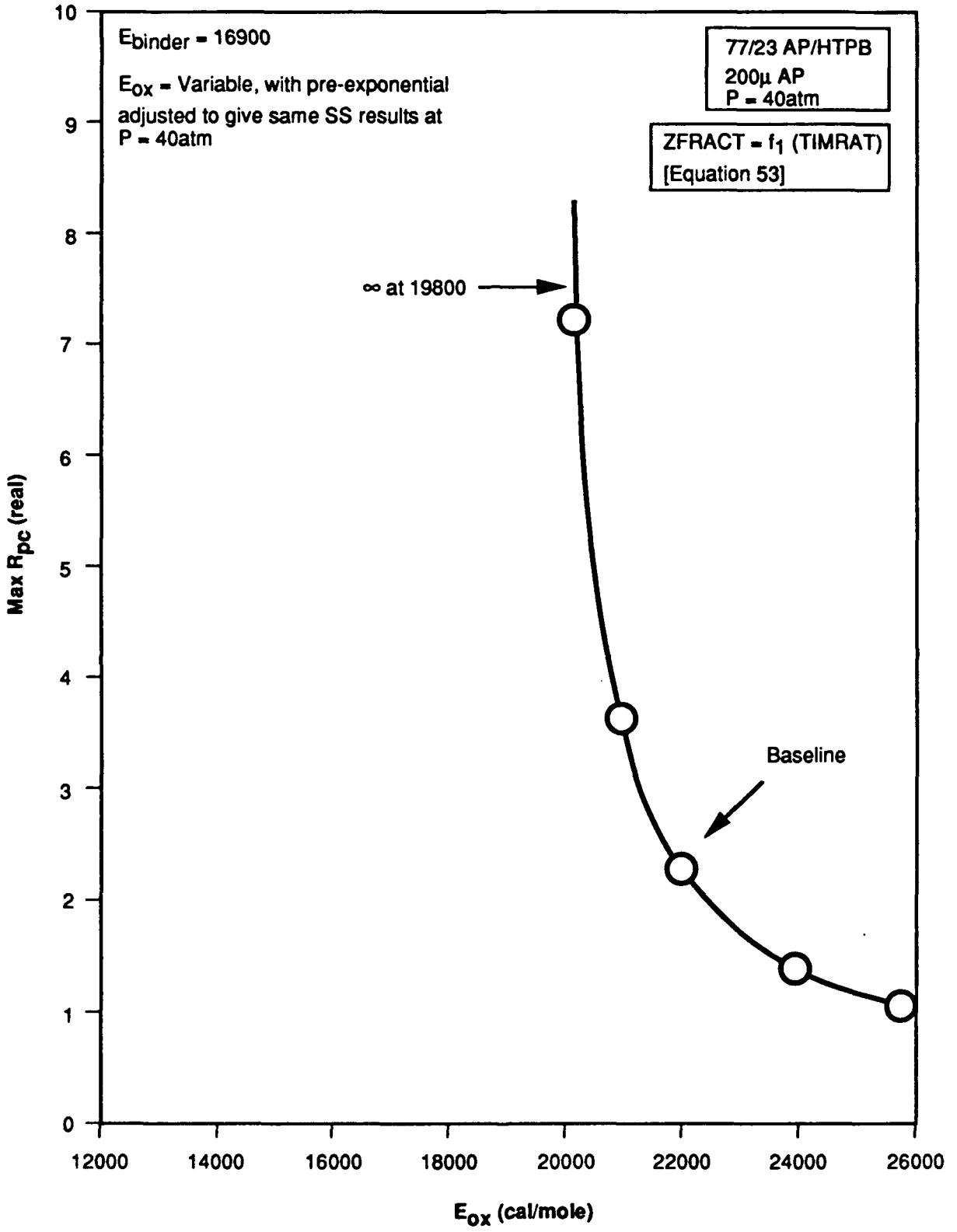

Figure 63. Dependence of Maximum Value of Pressure-Coupled Response on Oxidizer Ablation Activation Energy at Constant Fuel Ablation Activation Energy

1091-AFSOR

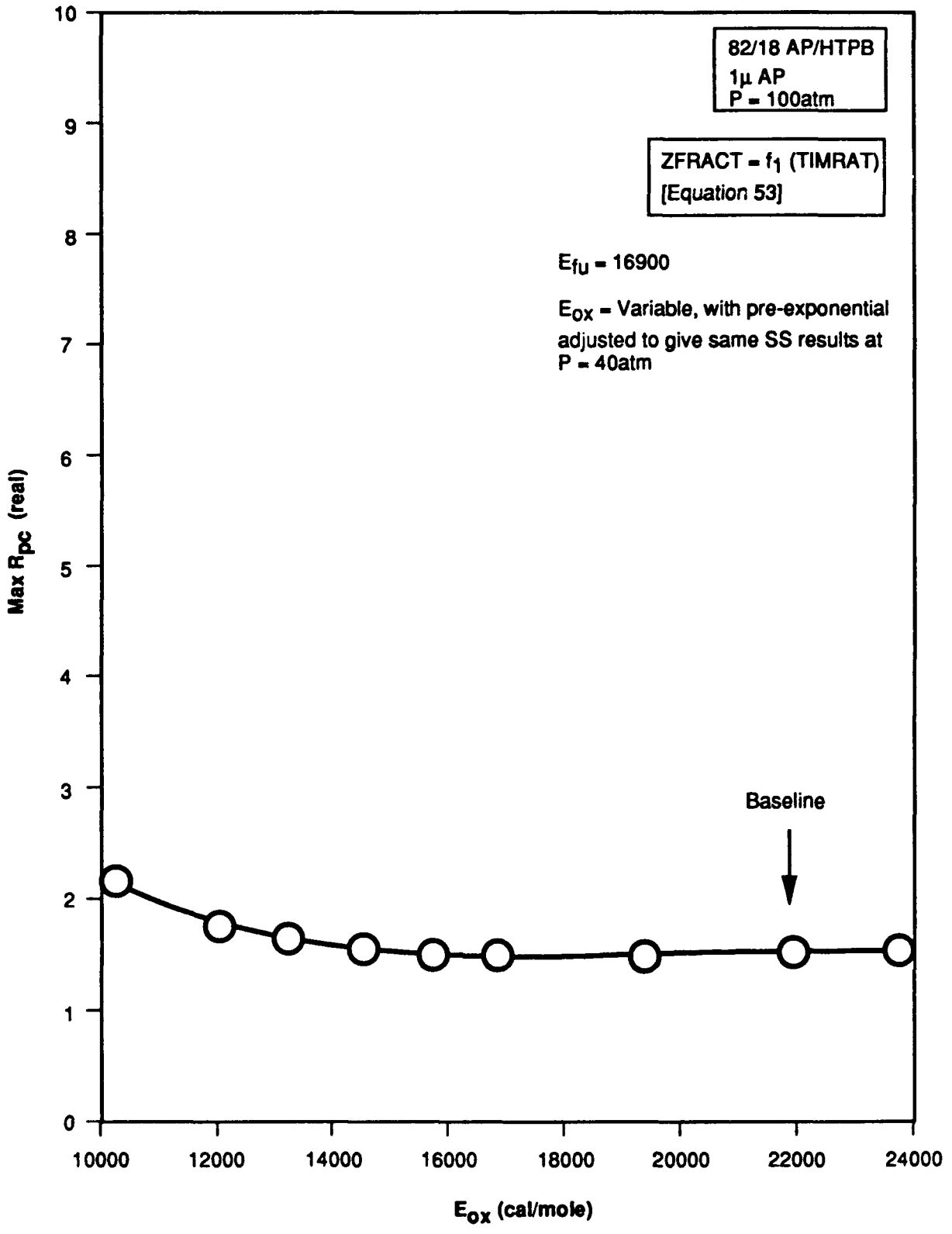

Figure 64. Dependence of Maximum Value of Pressure-Coupled Response on Oxidizer Ablation Activation Energy at Constant Fuel Ablation Activation Energy

1091-AFSOR

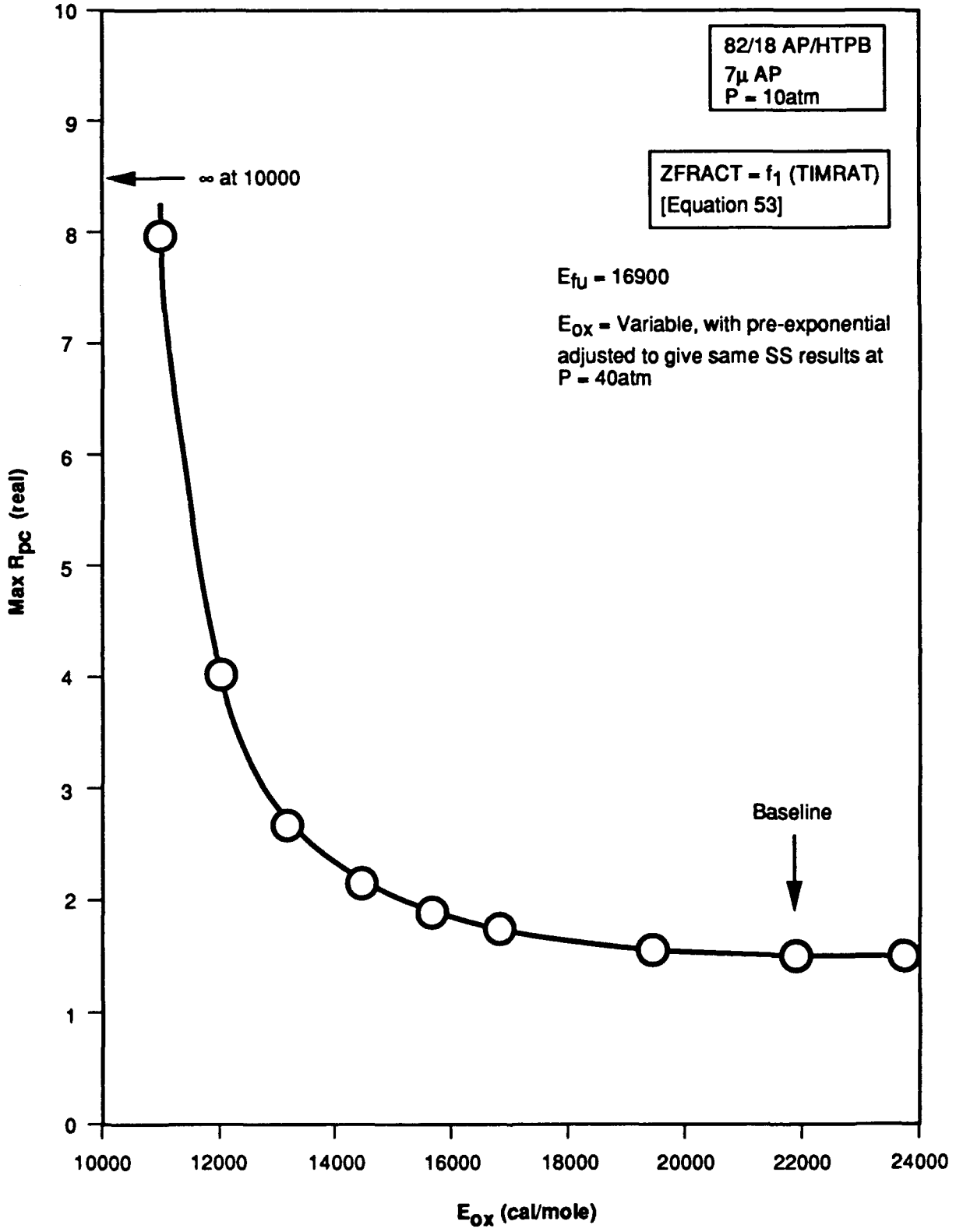

Figure 65. Dependence of Maximum Value of Pressure-Coupled Response on Oxidizer Ablation Activation Energy at Constant Fuel Ablation Activation Energy

1091-AFSOR

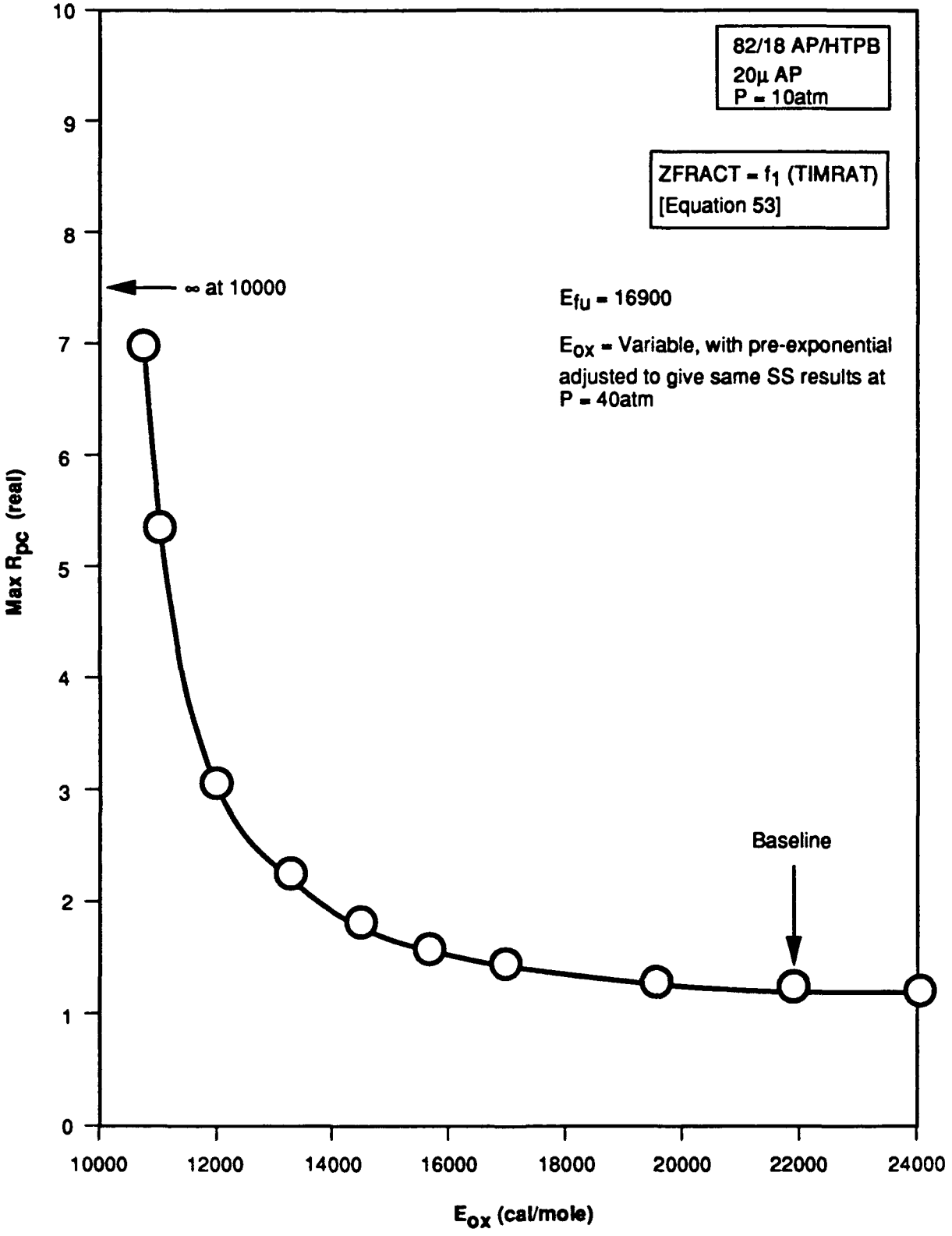

Figure 66. Dependence of Maximum Value of Pressure-Coupled Response on Oxidizer Ablation Activation Energy at Constant Fuel Ablation Activation Energy

1091-AFSOR

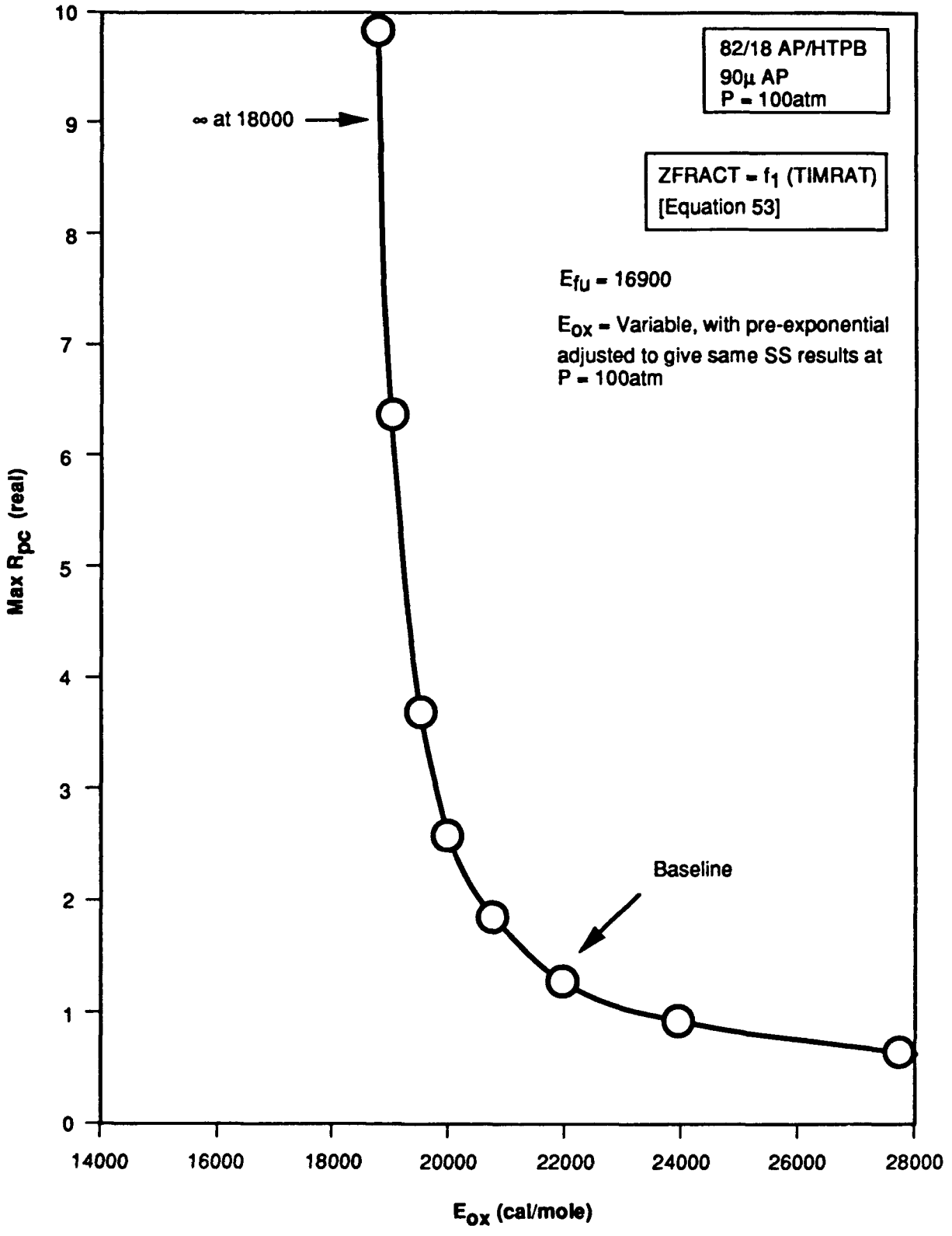

Figure 67. Dependence of Maximum Value of Pressure-Coupled Response on Oxidizer Ablation Activation Energy at Constant Fuel Ablation Activation Energy

1091-AFSOR

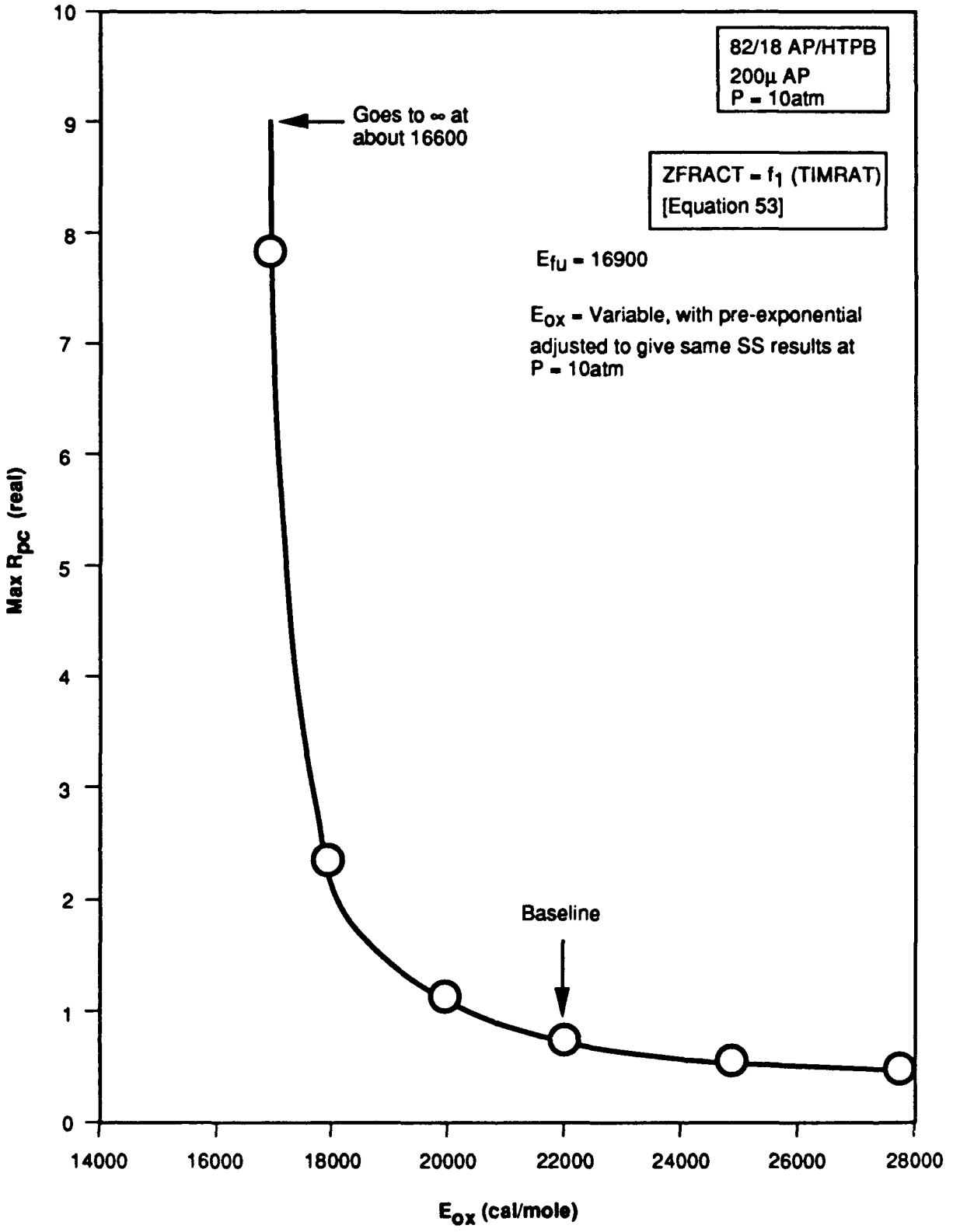

Figure 68. Dependence of Maximum Value of Pressure-Coupled Response on Oxidizer Ablation Activation Energy at Constant Fuel Ablation Activation Energy

1091-AFSOR

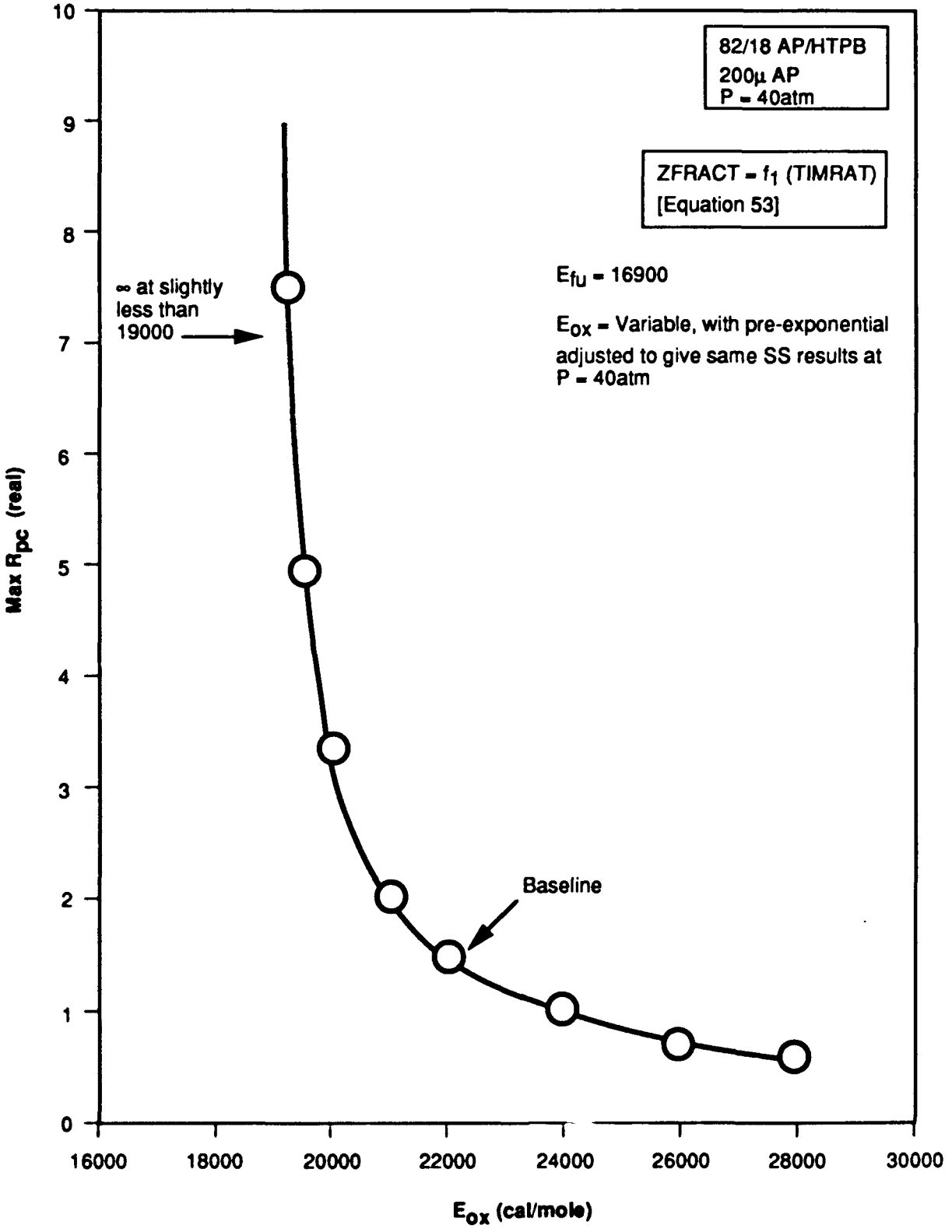

Figure 69. Dependence of Maximum Value of Pressure-Coupled Response on Oxidizer Ablation Activation Energy at Constant Fuel Ablation Activation Energy

1091-AFSOR

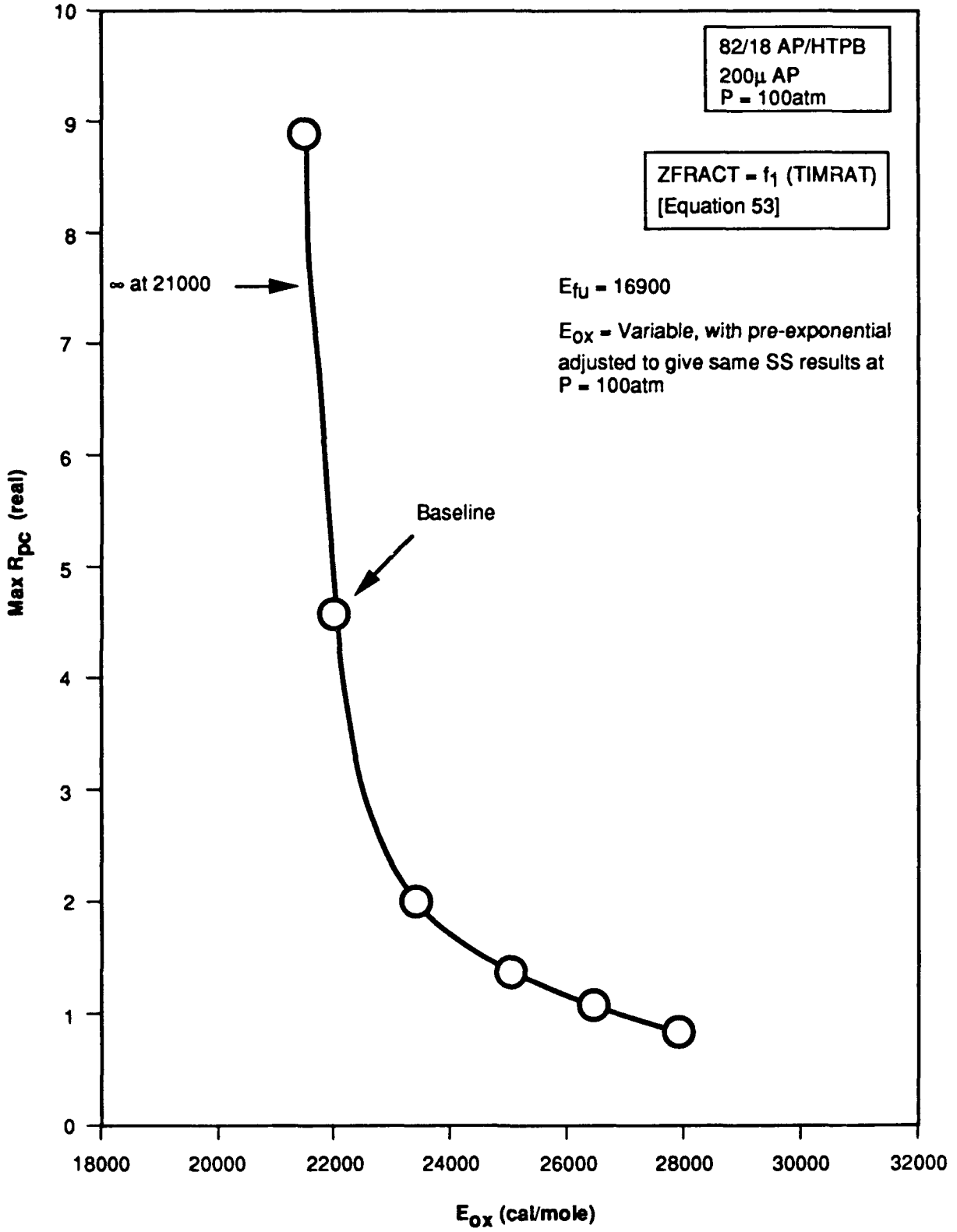

Figure 70. Dependence of Maximum Value of Pressure-Coupled Response on Oxidizer Ablation Activation Energy at Constant Fuel Ablation Activation Energy

1091-AFSOR

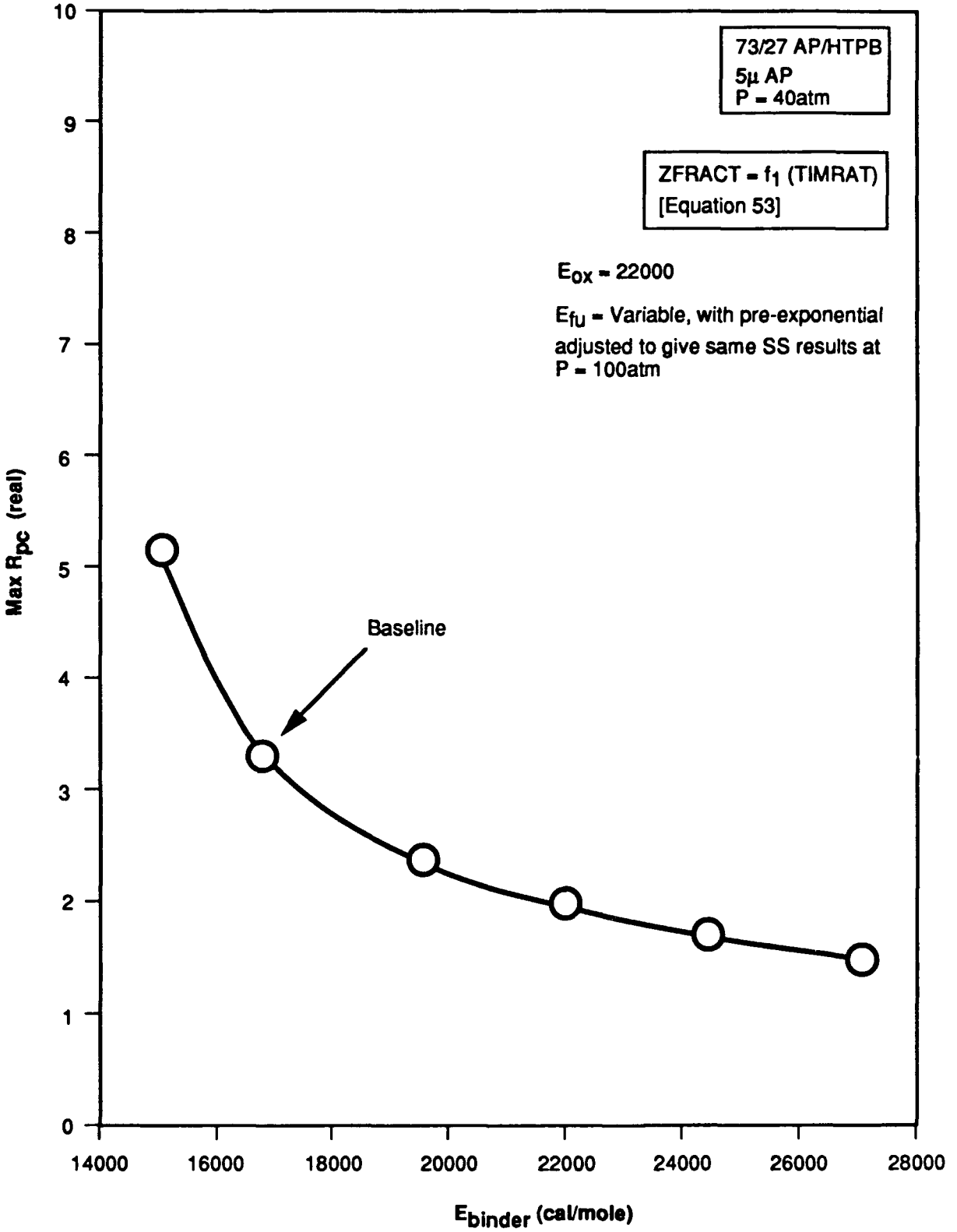

Figure 71. Dependence of Maximum Value of Pressure-Coupled Response on Fuel Ablation Activition Energy at Constant Oxidizer Ablation Activation Energy

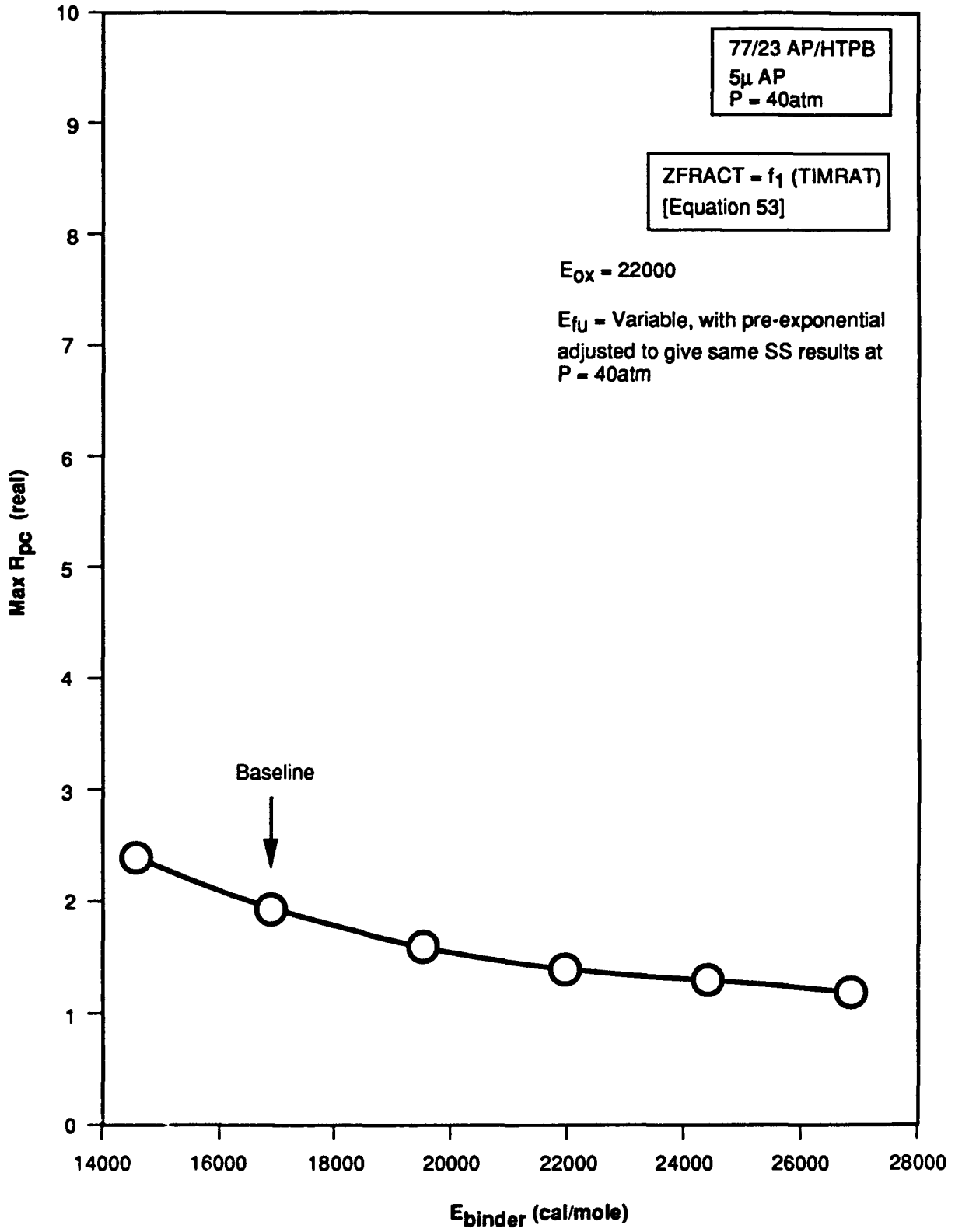

Figure 72. Dependence of Maximum Value of Pressure-Coupled Response on Fuel Ablation Activation Energy at Constant Oxidizer Ablation Activation Energy

1091-AFSOR

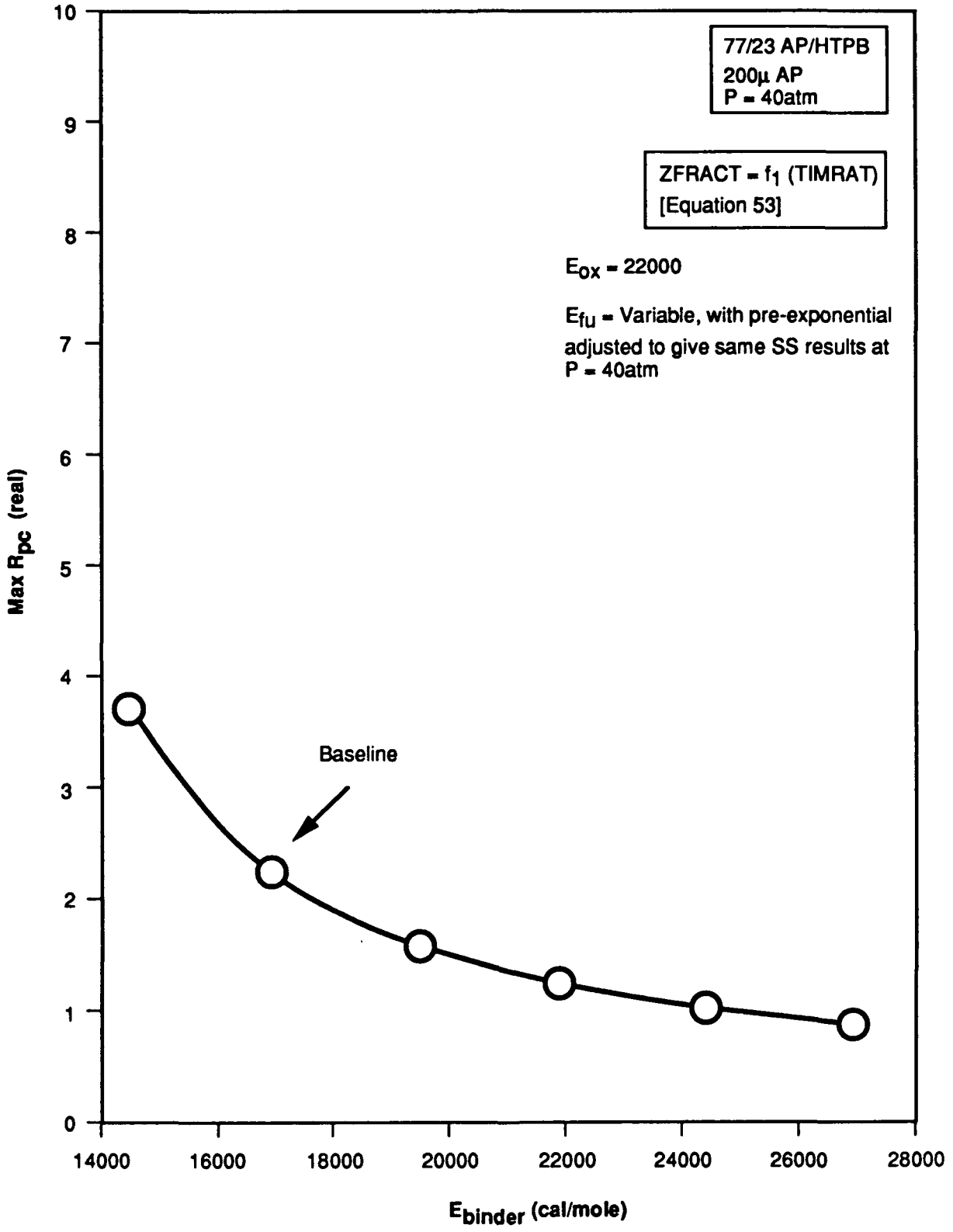

Figure 73. Dependence of Maximum Value of Pressure-Coupled Response on Fuel Ablation Activation Energy at Constant Oxidizer Ablation Activation Energy

1091-AFSOR

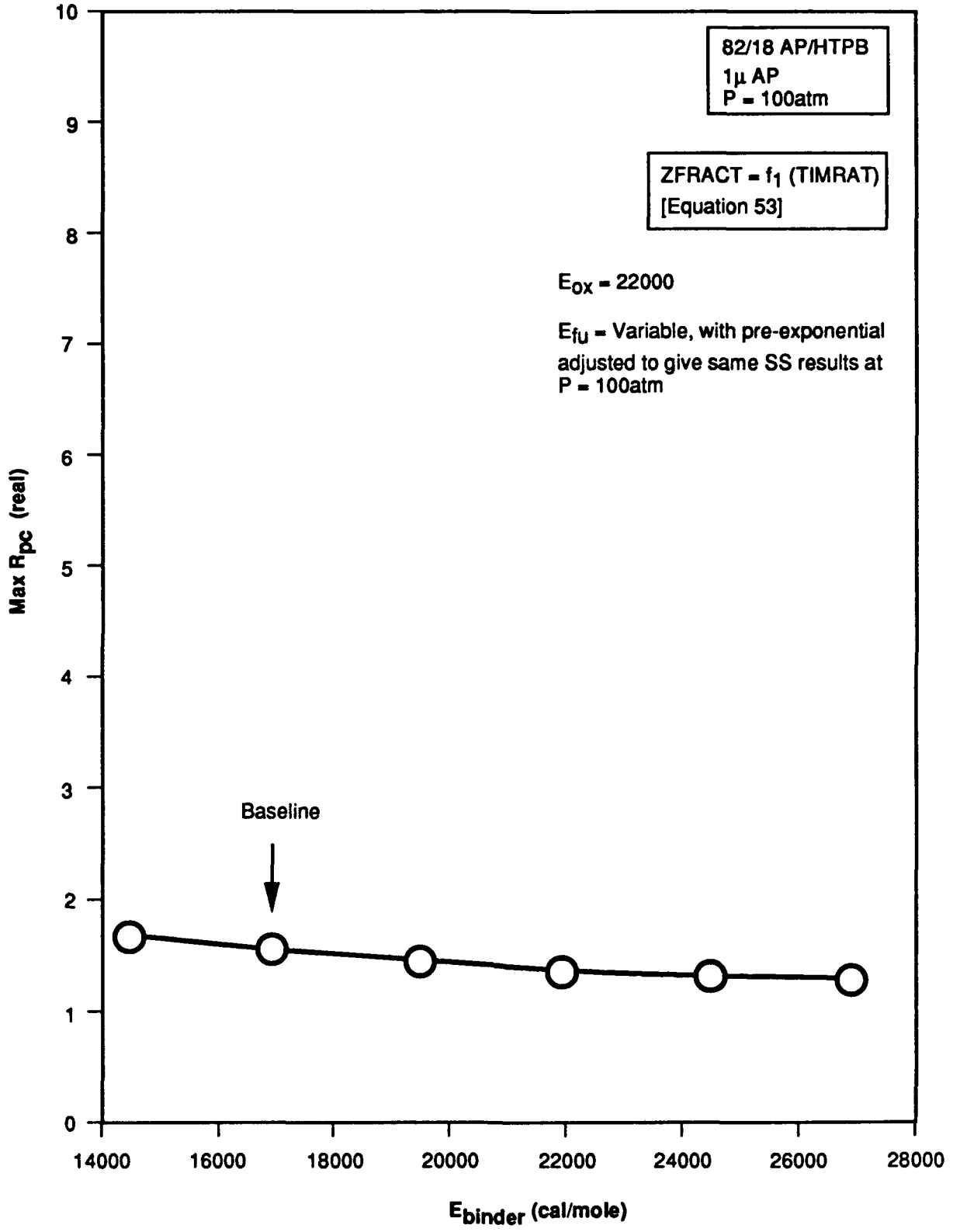

Figure 74. Dependence of Maximum Value of Pressure-Coupled Response on Fuel Ablation Activation Energy at Constant Oxidizer Ablation Activation Energy

1091-AFSOR

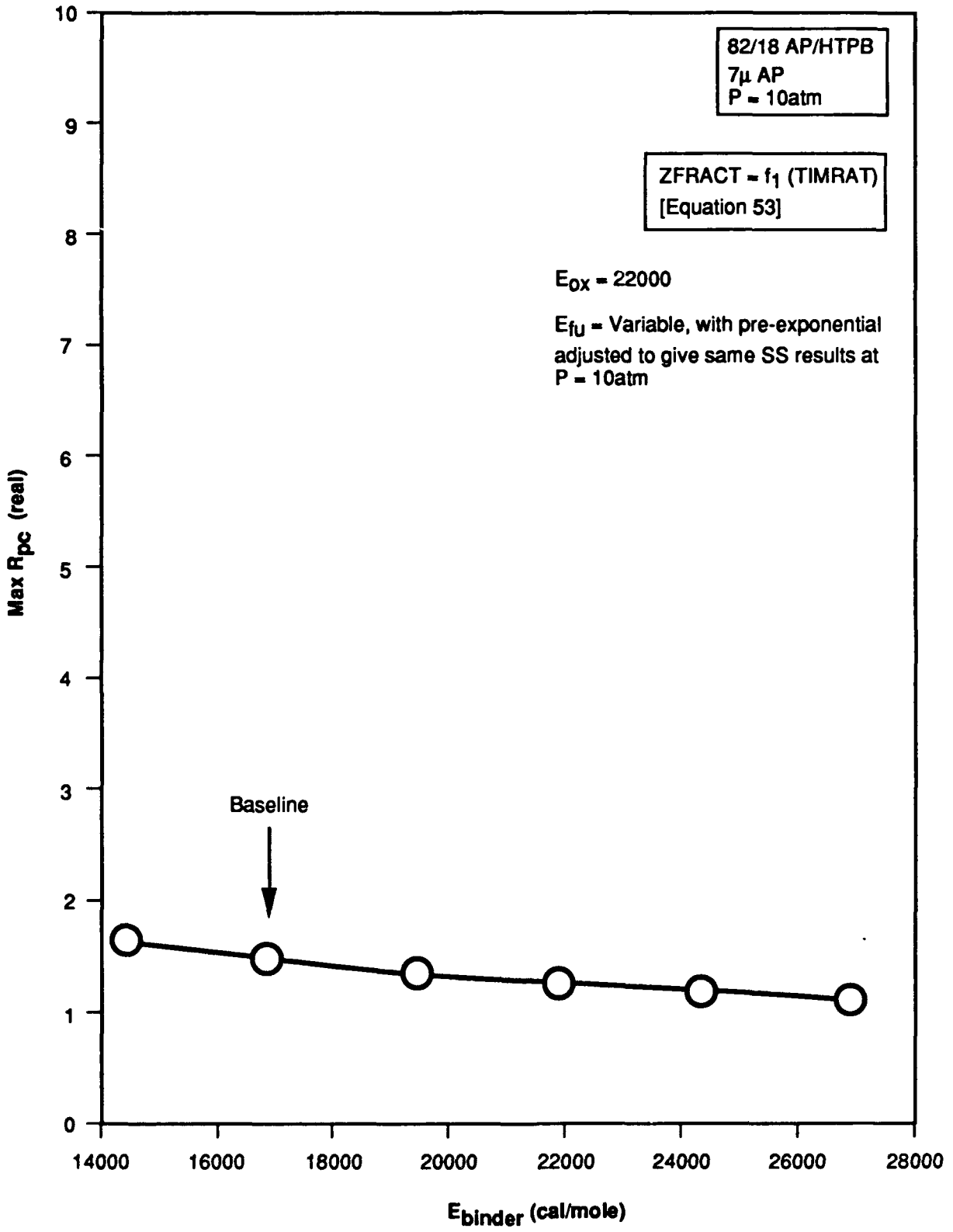

Figure 75. Dependence of Maximum Value of Pressure-Coupled Response on Fuel Ablation Activation Energy at Constant Oxidizer Ablation Activation Energy

1091-AFSOR

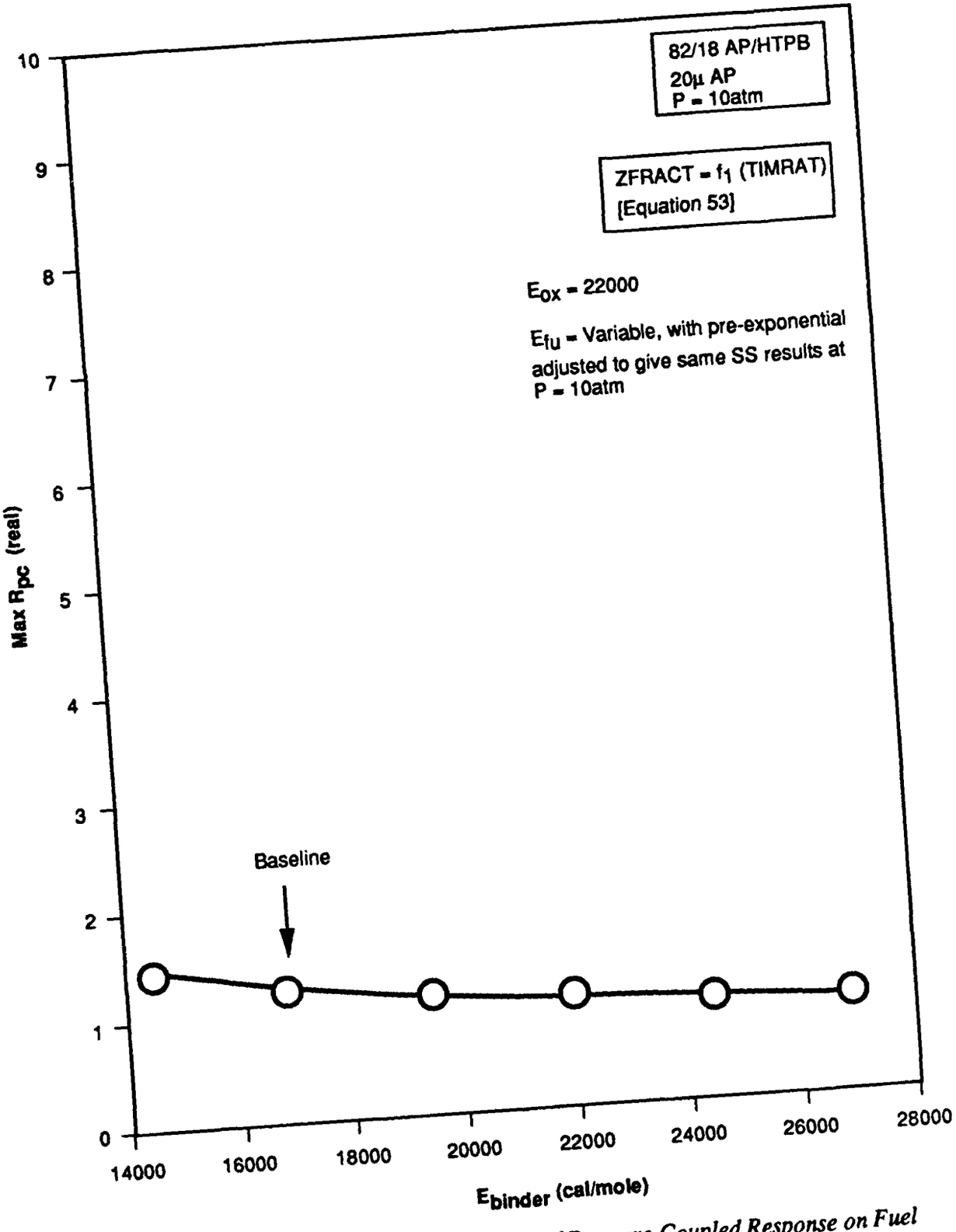

Figure 76. Dependence of Maximum Value of Pressure-Coupled Response on Fuel Ablation Activation Energy at Constant Oxidizer Ablation Activation Energy

1091-AFSOR

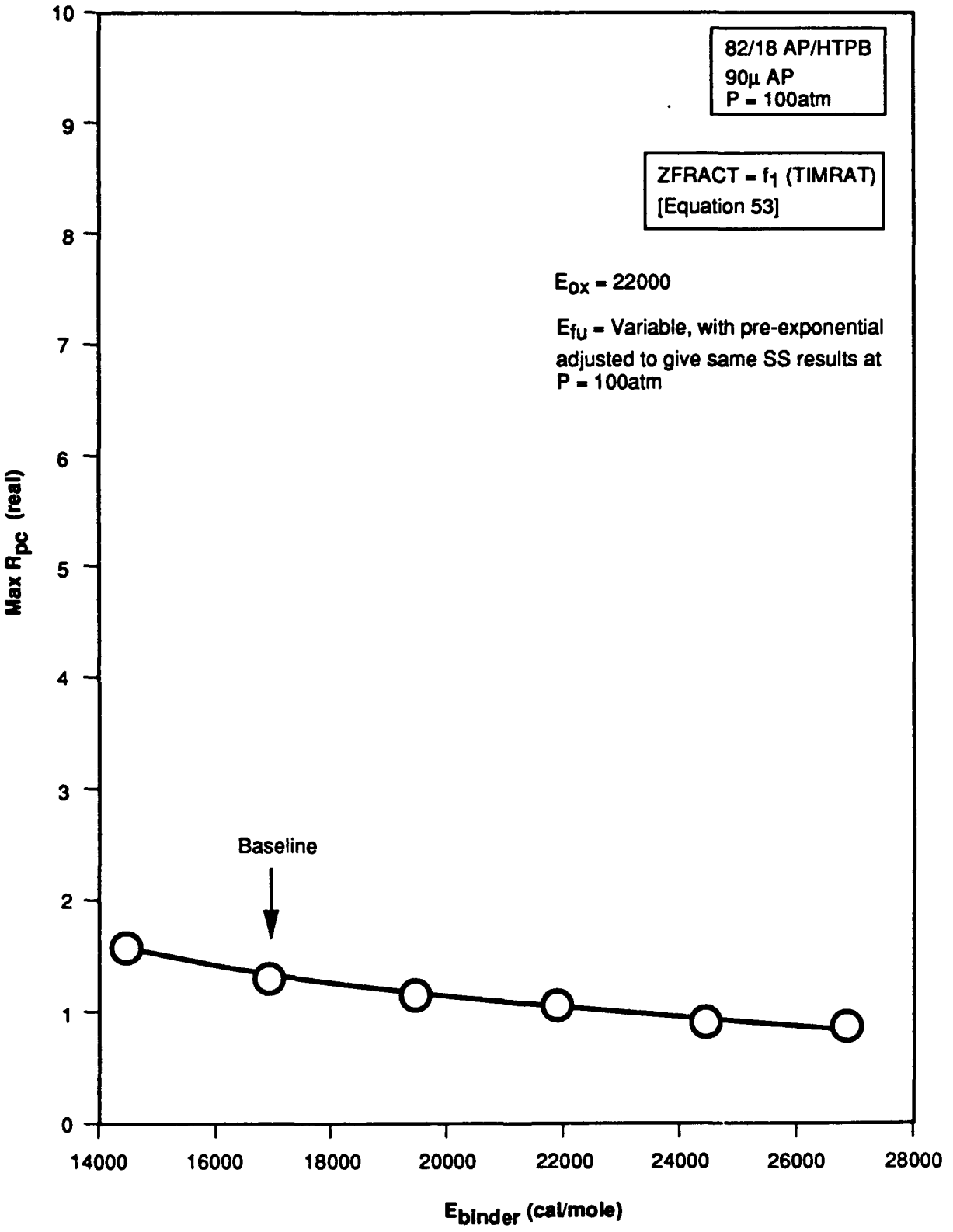

Figure 77. Dependence of Maximum Value of Pressure-Coupled Response on Fuel Ablation Activation Energy at Constant Oxidizer Ablation Activation Energy

1091-AFSOR

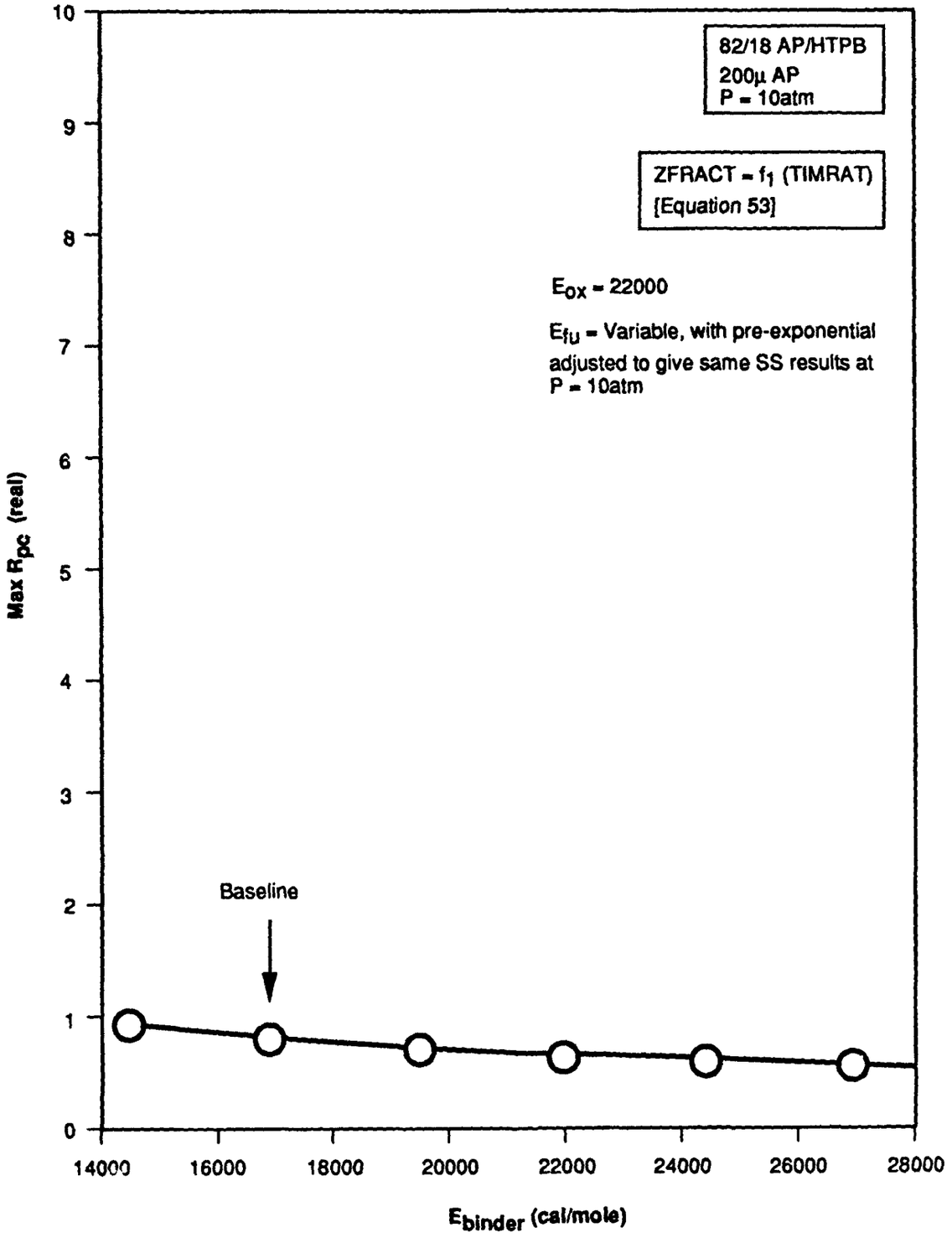

Figure 78. Dependence of Maximum Value of Pressure-Coupled Response on Fuel Ablation Activation Energy at Constant Oxidizer Ablation Activation Energy

1091-AFSOR

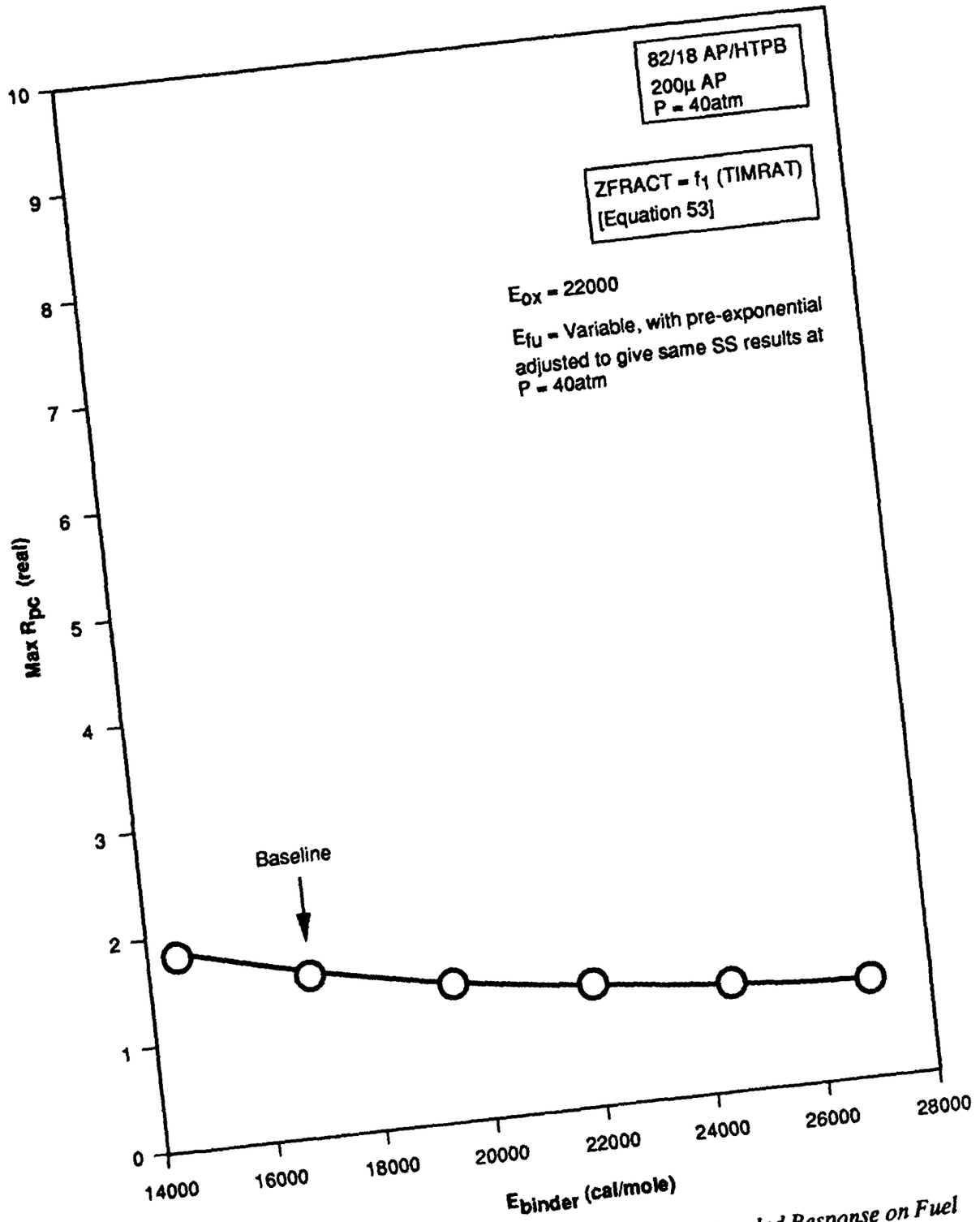

Figure 79. Dependence of Maximum Value of Pressure-Coupled Response on Fuel Ablation Activation Energy at Constant Oxidizer Ablation Activation Energy

1091-AFSOR

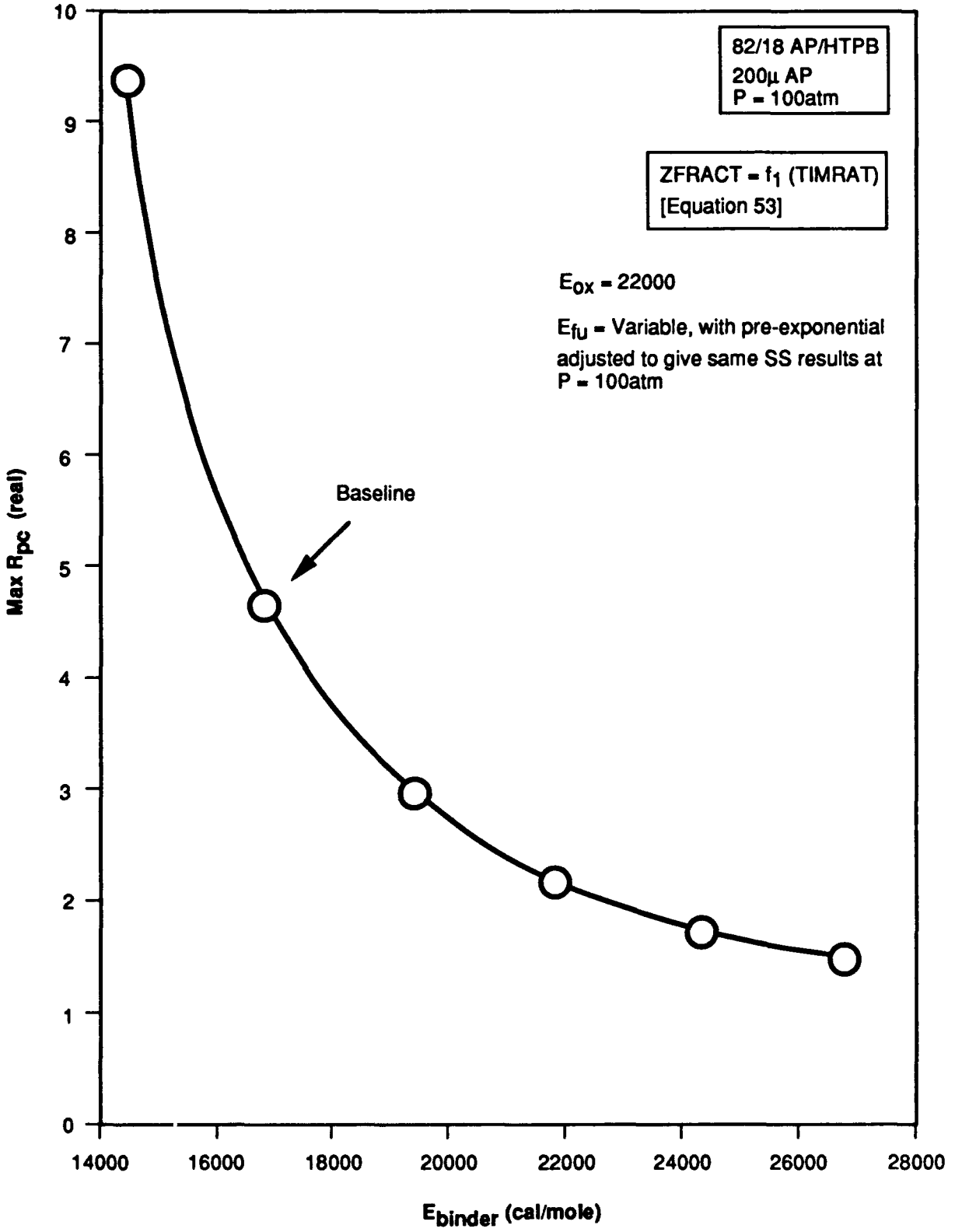

Figure 80. Dependence of Maximum Value of Pressure-Coupled Response on Fuel Ablation Activation Energy at Constant Oxidizer Ablation Activation Energy

1091-AFSOR

As may be seen from Figures 61-70, the maximum value of the real part of the pressure-coupled response decreases with increasing value of the oxidizer ablation activation energy (at fixed fuel ablation activation energy) for virtually every case examined, the only exceptions being the 73/27 AP/HTPB cases, which are not really of practical interest anyway. This result is opposite of predictions made with the preliminary model (References 3-5) developed in the 1980 time period and discussed earlier; in that preliminary model it should be recalled that the pressure-coupled response real parts were predicted to <u>increase</u> with increasing oxidizer ablation activation energy at fixed binder ablation activation energy. Careful examination of the computer printouts indicate that this change comes about as a result of treatment of the condensed-phase heat release depending on various parameters (not treated in the preliminary model) in the current modeling effort; these factors appear to more than compensate for the effects of the relative ablation activation energies on the degree of oscillation of oxidizer/fuel ratio of gas pockets leaving the propellant surface, which by themselves tend to lead to lower response of the propellant burning rate to pressure oscillations with decreased values of $E_{OXIDIZER} - E_{BINDER}$. It is also important to note that for most cases (with the exception of 200-micron-AP cases) little benefit (in terms of reduced real part of the pressure-coupled response) is available via variation of the oxidizer ablation activation energy at the fixed baseline values of the fuel ablation activation energy. For the 200-micron-AP cases, considerable reduction of the maximum real part of the response function <u>can</u> be obtained by <u>increasing</u> $E_{OXIDIZER}$ (opposite of what was predicted with the preliminary model!)

Figures 71-80 show that the predicted maxima in the real parts of the pressure-coupled responses decrease with increasing values of the binder ablation activation energy (at fixed oxidizer ablation activation energy) for all cases examined, in qualitative agreement with the preliminary studies of References 3-5. However, the magnitude of these decreases, particularly for the more practical 82/18 AP/HTPB cases, are considerably less than predicted in the preliminary studies, indicating that little benefit is likely to be achieved through tailoring of the binder ablation activation energies.

7.0 CONCLUSIONS

Based on the parametric studies with the current model to date, it appears that, for most cases, little benefit in terms of reduced sensitivity of burning rate to pressure oscillations is likely to be obtained via variation of fuel or oxidizer ablation activation energies. However, it must be acknowledged that the parametric studies to date are fairly limited in scope; further studies with simultaneous variation of oxidizer and fuel ablation activation energies might reveal favorable combinations for reduction of pressure-coupled response as might different assumptions regarding changes in pre-exponential factors accompanying changes in actuation energies. (Recall that it was assumed in the parametric studies to date that the pre-exponentials would vary with the activation energies in such a manner as to give constant steady-state burning rate at the pressure of interest; other scenarios can obviously be examined with this model, though interpretation of the results will be obviously more complex in terms of what is being held constant in the comparisons.) Thus, it may be concluded that although preliminary exercise of the unsteady-state burning-rate model developed in this study indicates that the proposed approach of reducing pressure-coupled response functions via modification of the kinetics of the oxidizer and fuel ablation processes has rather limited promise, further numerical studies with this model might well prove beneficial. Experimental studies should be conducted to verify the preliminary conclusions.

8.0 REFERENCES

1. Culick, F. E. C., "Combustion Instability in Solid Rocket Motors, Vol. II: A Guide for Motor Designers," Chemical Propulsion Information Agency, Laurel, MD, CPIA Publication 290, Jan., 1981.

2. Summerfield, M., Caveny, L. H., Battista, R., Kubota, N., Gostintsev, Y. A., and Isoda, H., "Theory of Dynamic Extinguishment of Solid Propellants With Special Reference to Non-Steady Heat Feedback Law," J. Spacecraft and Rockets, 8, 3, p. 251, (1971).

3. King, M. K., "Composite Propellant Combustion Modeling: Pressure-Coupled Response Functions," AIAA/SAE/ASME 16th Joint Propulsion Conference, Hartford, CT, AIAA Paper 80-1124, July, 1980.

4. King, M. K., "Examination of Alternate Approaches For Utilizing Steady-State Propellant Combustion Model Parameters in Calculation of Pressure-Coupled Response Functions," 18th JANNAF Combustion Meeting, Pasadena, CA, Oct., 1981, CPIA Publication 347, Vol. III, p. 21.

5. King, M. K., "Modeling of Pressure-Coupled Response Functions of Solid Propellants," 19th Int. Symposium on Combustion, Haifa, Israel, Aug., 1982, The Combustion Institute, Pittsburgh, PA, p. 707, 1982.

6. King. M. K., "Model for Steady-State Combustion of Unimodal Composite Solid Propellants," AIAA 16th Aerospace Sciences Meeting, Huntsville, AL, AIAA Paper 78-216, Jan., 1978.

7. King, M. K., "A Model of the Effects of Pressure and Crossflow Velocity on Composite Propellant Burning Rate," AIAA/SAE/ASME 15th Joint Propulsion Conference, Las Vegas, NV, AIAA Paper 79-1171, June, 1979.

8. King, M. K., "Experimental and Theoretical Study of the Effects of Pressure and Crossflow on Composite Propellant Burning Rate," 18th Int. Symposium on Combustion, Waterloo, Canada, Aug., 1980, The Combustion Institute, Pittsburgh, PA, p. 207, 1981.

9. King, M. K., "Predicted and Measured Effects of Pressure and Crossflow Velocity on Composite Propellant Burning Rate," 17th JANNAF Combustion Meeting, Langley, VA, Sept., 1980, CPIA Publication 329, Vol. I, p. 99.

10. Beckstead, M. W., Derr, R. L., and Price, C. F., "The Combustion of Solid Monopropellants and Composite Propellants," 13th Int. Symposium on Combustion, The Combustion Institute, Pittsburgh, PA, p. 1047, 1971.

11. Waesche, R. H. W., and Wenograd, J., "Calculation of Solid Propellant Burning Rates From Condensed-Phase Decomposition Kinetics," AIAA 7th Aerospace Sciences Meeting, AIAA Paper 69-145, Jan., 1969.

12. Burke, S. P., and Schumann, T. E. W., "Diffusion Flames," Industrial Engineering and Chemistry, 20, 10, p. 998, Oct., 1928.

APPENDIX A

Tabulations of R_{pc} expressions and maximum values of the real part of the pressure-coupled response as a function of binder ablation activation energy (at constant oxidizer ablation activation energy) and as a function of oxidizer ablation activation energy (at constant fuel ablation activation energy)

82/18 AP/HTPB 1μ AP P = 100 atm ZFRACT = 0.0

E_{OX} = 22000

E_{BINDER}	R_{PC} Expression	Max $R_{PC}^{(real)}$
14500	$R_{PC} = \frac{7.51682}{\lambda + \frac{6.73817}{\lambda} - 2.06327}$	3.53
16900	$R_{PC} = \frac{7.67438}{\lambda + \frac{6.87912}{\lambda} - 0.82536}$	2.26
19500	$R_{PC} = \frac{7.84455}{\lambda + \frac{7.03181}{\lambda} + 0.52148}$	1.64
22000	$R_{PC} = \frac{8.00872}{\lambda + \frac{7.17864}{\lambda} + 1.81977}$	1.31
24500	$R_{PC} = \frac{8.17270}{\lambda + \frac{7.32548}{\lambda} + 3.12085}$	1.10
27000	$R_{PC} = \frac{8.33655}{\lambda + \frac{7.47233}{\lambda} + 4.42385}$	0.95

82/18 AP/HTPB 1μ AP P = 100 atm ZFRACT = 1.0

E_{OX} = 22000

E_{BINDER}	R_{PC} Expression	Max $R_{PC}^{(real)}$
14500	$R_{PC} = \frac{7.22121}{\lambda + \frac{6.47319}{\lambda} + 1.58292}$	1.27
16900	$R_{PC} = \frac{7.53665}{\lambda + \frac{6.75565}{\lambda} + 1.62544}$	1.30
19500	$R_{PC} = \frac{7.87856}{\lambda + \frac{7.06229}{\lambda} + 1.67042}$	1.33
22000	$R_{PC} = \frac{8.21082}{\lambda + \frac{7.35980}{\lambda} + 1.71207}$	1.36
24500	$R_{PC} = \frac{8.54129}{\lambda + \frac{7.65586}{\lambda} + 1.75447}$	1.38
27000	$R_{PC} = \frac{8.87230}{\lambda + \frac{7.95254}{\lambda} + 1.79739}$	1.41

82/18 AP/HTPB 1μ AP P = 100 atm ZFRACT = 0.0

E_{OX} = 16900

E_{BINDER}	R_{PC} Expression	Max $R_{PC}^{(real)}$
24000	$R_{PC} = \frac{8.27121}{\lambda + \frac{7.41427}{\lambda} - 1.28076}$	2.68
22000	$R_{PC} = \frac{7.67438}{\lambda + \frac{6.87912}{\lambda} - 0.82536}$	2.26
19500	$R_{PC} = \frac{6.92786}{\lambda + \frac{6.21018}{\lambda} - 0.24807}$	1.83
16900	$R_{PC} = \frac{6.14555}{\lambda + \frac{5.51481}{\lambda} + 0.34919}$	1.47
15700	$R_{PC} = \frac{5.78849}{\lambda + \frac{5.19371}{\lambda} + 0.62634}$	1.33
14500	$R_{PC} = \frac{5.43114}{\lambda + \frac{4.87261}{\lambda} + 0.90209}$	1.20
13200	$R_{PC} = \frac{5.04408}{\lambda + \frac{4.52475}{\lambda} + 1.20543}$	1.07
12000	$R_{PC} = \frac{4.68673}{\lambda + \frac{4.20365}{\lambda} + 1.49120}$	0.96
10000	$R_{PC} = \frac{4.09097}{\lambda + \frac{3.66850}{\lambda} + 1.97779}$	0.79

82/18 AP/HTPB 1μ AP P = 100 atm ZFRACT = 1.0

E_{OX} = 16900

E_{BINDER}	R_{PC} Expression	Max $R_{PC}^{(real)}$
24000	$R_{PC} = \frac{8.02618}{\lambda + \frac{7.19462}{\lambda} + 2.14615}$	1.25
22000	$R_{PC} = \frac{7.53665}{\lambda + \frac{6.75566}{\lambda} + 1.62544}$	1.30
19500	$R_{PC} = \frac{6.92779}{\lambda + \frac{6.21012}{\lambda} + 0.96837}$	1.39
16900	$R_{PC} = \frac{6.29709}{\lambda + \frac{5.64455}{\lambda} + 0.28119}$	1.52
15700	$R_{PC} = \frac{5.87809}{\lambda + \frac{5.87809}{\lambda} + 0.002294}$	1.55
14500	$R_{PC} = \frac{5.59734}{\lambda + \frac{5.02172}{\lambda} - 0.29833}$	1.65
13200	$R_{PC} = \frac{5.29343}{\lambda + \frac{5.29343}{\lambda} - 0.64765}$	1.79
12000	$R_{PC} = \frac{5.01364}{\lambda + \frac{4.49686}{\lambda} - 0.97180}$	1.97
10000	$R_{PC} = \frac{4.55189}{\lambda + \frac{4.08182}{\lambda} - 1.51770}$	2.44

82/18 AP/HTPB 7μ AP P = 10 atm ZFRACT = 0.0

E_{OX} = 22000

E_{BINDER}	R_{PC} Expression	Max $R_{PC}^{(real)}$
14500	$R_{PC} = \frac{9.62518}{\lambda + \frac{7.49417}{\lambda} - 1.06186}$	2.89
16900	$R_{PC} = \frac{9.82654}{\lambda + \frac{7.65096}{\lambda} + 0.50946}$	1.99
19500	$R_{PC} = \frac{10.04453}{\lambda + \frac{7.82081}{\lambda} + 2.21404}$	1.50
22000	$R_{PC} = \frac{10.25358}{\lambda + \frac{7.98413}{\lambda} + 3.84654}$	1.23
24500	$R_{PC} = \frac{10.46331}{\lambda + \frac{8.14744}{\lambda} + 5.49289}$	1.04
27000	$R_{PC} = \frac{10.67303}{\lambda + \frac{8.31074}{\lambda} + 7.14231}$	0.91

82/18 AP/HTPB 7μ AP P = 10 atm ZFRACT = 1.0

E_{OX} = 22000

E_{BINDER}	R_{PC} Expression	Max $R_{PC}^{(real)}$
14500	$R_{PC} = \frac{10.89262}{\lambda + \frac{8.48100}{\lambda} + 3.85834}$	1.28
16900	$R_{PC} = \frac{10.74703}{\lambda + \frac{8.36765}{\lambda} + 3.80996}$	1.28
19500	$R_{PC} = \frac{10.61340}{\lambda + \frac{8.26374}{\lambda} + 3.76402}$	1.27
22000	$R_{PC} = \frac{10.50816}{\lambda + \frac{8.18236}{\lambda} + 3.72875}$	1.27
24500	$R_{PC} = \frac{10.42724}{\lambda + \frac{8.11935}{\lambda} + 3.69603}$	1.27
27000	$R_{PC} = \frac{10.37006}{\lambda + \frac{8.07483}{\lambda} + 3.66935}$	1.27

82/18 AP/HTPB 7μ AP P = 10 atm ZFRACT = 0.0

E_{OX} = 16900

E_{BINDER}	R_{PC} Expression	Max $R_{PC}^{(real)}$
24000	$R_{PC} = \frac{10.59092}{\lambda + \frac{8.24613}{\lambda} + 0.45475}$	2.11
22000	$R_{PC} = \frac{9.82654}{\lambda + \frac{7.65096}{\lambda} + 0.50946}$	1.99
19500	$R_{PC} = \frac{8.87220}{\lambda + \frac{6.90696}{\lambda} + 0.57543}$	1.85
16900	$R_{PC} = \frac{7.87791}{\lambda + \frac{6.13323}{\lambda} + 0.66817}$	1.68
15700	$R_{PC} = \frac{7.41896}{\lambda + \frac{5.77612}{\lambda} + 0.71451}$	1.60
14500	$R_{PC} = \frac{6.96012}{\lambda + \frac{5.41901}{\lambda} + 0.76338}$	1.52
13200	$R_{PC} = \frac{6.46306}{\lambda + \frac{5.03215}{\lambda} + 0.81907}$	1.43
12000	$R_{PC} = \frac{6.00415}{\lambda + \frac{4.67502}{\lambda} + 0.87207}$	1.35
11000	$R_{PC} = \frac{5.62131}{\lambda + \frac{4.37741}{\lambda} + 0.91831}$	1.28

82/18 AP/HTPB 7μ AP P = 10 atm ZFRACT = 1.0

E_{BINDER}	R_{PC} Expression	Max $R_{PC}^{(real)}$
24000	$R_{PC} = \frac{11.85748}{\lambda + \frac{9.23228}{\lambda} + 5.05341}$	1.20
22000	$R_{PC} = \frac{10.74703}{\lambda + \frac{8.36765}{\lambda} + 3.80996}$	1.28
19500	$R_{PC} = \frac{9.41003}{\lambda + \frac{7.32566}{\lambda} + 2.24120}$	1.43
16900	$R_{PC} = \frac{8.02986}{\lambda + \frac{6.25152}{\lambda} + 0.59830}$	1.73
15700	$R_{PC} = \frac{7404999}{\lambda + \frac{5.76525}{\lambda} - 0.16435}$	1.97
14500	$R_{PC} = \frac{6.78779}{\lambda + \frac{5.28484}{\lambda} - 0.92930}$	2.39
13200	$R_{PC} = \frac{6.12771}{\lambda + \frac{4.77104}{\lambda} - 1.76064}$	3.30
12000	$R_{PC} = \frac{5.52511}{\lambda + \frac{4.30202}{\lambda} - 2.52811}$	5.90
11000	$R_{PC} = \frac{5.03852}{\lambda + \frac{3.92358}{\lambda} - 3.17608}$	-30-32

82/18 AP/HTPB 20μ AP P = 10 atm ZFRACT = 0.0

E_{OX} = 22000

E_{BINDER}	R_{PC} Expression	Max $R_{PC}^{(real)}$
14500	$R_{PC} = \frac{8.23249}{\lambda + \frac{7.52548}{\lambda} - 0.15744}$	1.94
16900	$R_{PC} = \frac{8.40476}{\lambda + \frac{7.68291}{\lambda} + 1.27501}$	1.47
19500	$R_{PC} = \frac{8.59134}{\lambda + \frac{7.85346}{\lambda} + 2.83319}$	1.18
22000	$R_{PC} = \frac{8.77074}{\lambda + \frac{8.01745}{\lambda} + 4.33767}$	0.99
24500	$R_{PC} = \frac{8.95089}{\lambda + \frac{8.18145}{\lambda} + 5.86113}$	0.86
27000	$R_{PC} = \frac{9.13030}{\lambda + \frac{8.34545}{\lambda} + 7.37783}$	0.76

82/18 AP/HTPB 20μ AP P = 10 atm ZFRACT = 1.0

E_{OX} = 22000

E_{BINDER}	R_{PC} Expression	Max $R_{PC}^{(real)}$
14500	$R_{PC} = \frac{9.15933}{\lambda + \frac{8.37272}{\lambda} + 4.45799}$	1.01
16900	$R_{PC} = \frac{9.09248}{\lambda + \frac{8.31156}{\lambda} + 4.36980}$	1.01
19500	$R_{PC} = \frac{9.04151}{\lambda + \frac{8.26497}{\lambda} + 4.28309}$	1.02
22000	$R_{PC} = \frac{9.01372}{\lambda + \frac{8.23957}{\lambda} + 4.20857}$	1.03
24500	$R_{PC} = \frac{9.00756}{\lambda + \frac{8.23325}{\lambda} + 4.13900}$	1.03
27000	$R_{PC} = \frac{9.02165}{\lambda + \frac{8.24614}{\lambda} + 4.08193}$	1.04

82/18 AP/HTPB 20μ AP P = 10 atm ZFRACT = 0.0

E_{OX} = 16900

E_{BINDER}	R_{PC} Expression	Max $R_{PC}^{(real)}$
24000	$R_{PC} = \frac{9.05858}{\lambda + \frac{8.28057}{\lambda} + 1.52498}$	1.48
22000	$R_{PC} = \frac{8.40476}{\lambda + \frac{7.68291}{\lambda} + 1.27501}$	1.47
19500	$R_{PC} = \frac{7.58766}{\lambda + \frac{6.93582}{\lambda} + 0.96903}$	1.46
16900	$R_{PC} = \frac{6.73653}{\lambda + \frac{6.15889}{\lambda} + 0.65713}$	1.44
14500	$R_{PC} = \frac{5.95291}{\lambda + \frac{5.44170}{\lambda} + 0.39053}$	1.41
13200	$R_{PC} = \frac{5.52827}{\lambda + \frac{5.05321}{\lambda} + 0.23632}$	1.40
12000	$R_{PC} = \frac{5.13584}{\lambda + \frac{4.69463}{\lambda} + 0.09731}$	1.39
11000	$R_{PC} = \frac{4.80997}{\lambda + \frac{4.39585}{\lambda} - 0.00182}$	1.38
10700	$R_{PC} = \frac{4.71206}{\lambda + \frac{4.30622}{\lambda} - 0.06620}$	1.39

82/18 AP/HTPB 20μ AP P = 10 atm ZFRACT = 1.0

E_{OX} = 16900

E_{BINDER}	R_{PC} Expression	Max $R_{PC}^{(real)}$
24000	$R_{PC} = \frac{9.99420}{\lambda + \frac{9.13583}{\lambda} + 5.83711}$	0.94
22000	$R_{PC} = \frac{9.09248}{\lambda + \frac{8.31155}{\lambda} + 4.36980}$	1.01
19500	$R_{PC} = \frac{7.99147}{\lambda + \frac{7.30504}{\lambda} + 2.52256}$	1.17
16900	$R_{PC} = \frac{6.86146}{\lambda + \frac{6.27310}{\lambda} + 0.59310}$	1.47
14500	$R_{PC} = \frac{5.86258}{\lambda + \frac{5.35913}{\lambda} - 1.20804}$	2.27
13200	$R_{PC} = \frac{5.33201}{\lambda + \frac{4.87382}{\lambda} - 2.18768}$	3.65
12000	$R_{PC} = \frac{4.84988}{\lambda + \frac{4.43324}{\lambda} - 3.09135}$	11.5
11000	$R_{PC} = \frac{4.44655}{\lambda + \frac{4.06373}{\lambda} - 3.84532}$	∞
10700	$R_{PC} = \frac{4.31590}{\lambda + \frac{3.94418}{\lambda} - 4.05345}$	∞

82/18 AP/HTPB 90μ AP P = 100 atm ZFRACT = 0.0

E_{OX} = 22000

E_{BINDER}	R_{PC} Expression	Max R_{PC}(real)
14500	$R_{PC} = \frac{2.58714}{\lambda + \frac{7.43368}{\lambda} - 2.83644}$	1.67
16900	$R_{PC} = \frac{2.64197}{\lambda + \frac{7.58930}{\lambda} - 2.48027}$	1.37
19500	$R_{PC} = \frac{2.70033}{\lambda + \frac{7.75785}{\lambda} - 2.09208}$	1.14
22000	$R_{PC} = \frac{2.75623}{\lambda + \frac{7.91987}{\lambda} - 1.71572}$	0.99
24500	$R_{PC} = \frac{2.81130}{\lambda + \frac{8.08184}{\lambda} - 1.33698}$	0.88
27000	$R_{PC} = \frac{2.86952}{\lambda + \frac{8.24373}{\lambda} - 0.95540}$	0.79

82/18 AP/HTPB 90μ AP P = 100 atm ZFRACT = 1.0

E_{OX} = 22000

E_{BINDER}	R_{PC} Expression	Max $R_{PC}^{(real)}$
14500	$R_{PC} = \frac{3.03954}{\lambda + \frac{8.73359}{\lambda} - 0.48777}$	0.72
16900	$R_{PC} = \frac{2.96894}{\lambda + \frac{8.52854}{\lambda} - 0.90409}$	0.80
19500	$R_{PC} = \frac{2.89115}{\lambda + \frac{8.30607}{\lambda} - 1.34409}$	0.89
22000	$R_{PC} = \frac{2.82471}{\lambda + \frac{8.11665}{\lambda} - 1.76287}$	1.01
24500	$R_{PC} = \frac{2.76329}{\lambda + \frac{7.94381}{\lambda} - 2.17554}$	1.19
27000	$R_{PC} = \frac{2.71645}{\lambda + \frac{7.80397}{\lambda} - 2.58686}$	1.44

82/18 AP/HTPB 90μ AP P = 100 atm ZFRACT = 0.0

E_{OX} = 16900

E_{BINDER}	R_{PC} Expression	Max $R_{PC}^{(real)}$
24000	$R_{PC} = \frac{2.84623}{\lambda + \frac{8.17966}{\lambda} - 1.54474}$	0.94
22000	$R_{PC} = \frac{2.64197}{\lambda + \frac{7.58930}{\lambda} - 2.48027}$	1.36
27050	$R_{PC} = \frac{2.51261}{\lambda + \frac{7.22034}{\lambda} - 3.07004}$	2.00
20000	$R_{PC} = \frac{2.43557}{\lambda + \frac{6.99895}{\lambda} - 3.42534}$	2.89
19500	$R_{PC} = \frac{2.38446}{\lambda + \frac{6.85136}{\lambda} - 3.66279}$	-4.15
19000	$R_{PC} = \frac{2.33304}{\lambda + \frac{6.70374}{\lambda} - 3.90127}$	-7.7
18750	$R_{PC} = \frac{2.30834}{\lambda + \frac{6.62991}{\lambda} - 4.02083}$	-15

82/18 AP/HTPB 92μ AP P = 100 atm ZFRACT = 1.0

E_{BINDER} = 16900

E_{BINDER}	R_{PC} Expression	Max $R_{PC}^{(real)}$
24000	$R_{PC} = \frac{3.29006}{\lambda + \frac{9.45517}{\lambda} + 0.68064}$	0.60
22000	$R_{PC} = \frac{2.96894}{\lambda + \frac{8.52854}{\lambda} - 0.90409}$	0.80
20750	$R_{PC} = \frac{2.76138}{\lambda + \frac{7.93521}{\lambda} - 1.89159}$	1.06
20000	$R_{PC} = \frac{2.64213}{\lambda + \frac{7.59252}{\lambda} - 2.48854}$	1.37
19500	$R_{PC} = \frac{2.56038}{\lambda + \frac{7.35681}{\lambda} - 2.88493}$	1.73
19000	$R_{PC} = \frac{2.48672}{\lambda + \frac{7.14534}{\lambda} - 3.28639}$	2.44
18750	$R_{PC} = \frac{2.45054}{\lambda + \frac{7.03834}{\lambda} - 3.48661}$	3.09

82/18 AP/HTPB 200μ AP P = 10 atm ZFRACT = 0.0

E_{OX} = 22000

E_{BINDER}	R_{PC} Expression	Max $R_{PC}^{(real)}$
14500	$R_{PC} = \frac{3.78394}{\lambda + \frac{7.80404}{\lambda} - 0.43012}$	0.94
16900	$R_{PC} = \frac{3.86325}{\lambda + \frac{7.96730}{\lambda} + 0.26616}$	0.81
19500	$R_{PC} = \frac{3.94853}{\lambda + \frac{8.14416}{\lambda} + 1.02351}$	0.71
22000	$R_{PC} = \frac{4.03174}{\lambda + \frac{8.31423}{\lambda} + 1.75970}$	0.63
24500	$R_{PC} = \frac{4.11418}{\lambda + \frac{8.48430}{\lambda} + 2.50210}$	0.58
27000	$R_{PC} = \frac{4.19665}{\lambda + \frac{8.65437}{\lambda} + 3.25130}$	0.53

82/18 AP/HTPB 200μ AP P = 10 atm ZFRACT = 1.0

E_{OX} = 22000

E_{BINDER}	R_{PC} Expression	Max $R_{PC}^{(real)}$
14500	$R_{PC} = \frac{3.45944}{\lambda + \frac{7.13478}{\lambda} + 1.80716}$	0.57
16900	$R_{PC} = \frac{3.67393}{\lambda + \frac{7.57685}{\lambda} + 1.74305}$	0.60
19500	$R_{PC} = \frac{3.91405}{\lambda + \frac{8.07303}{\lambda} + 1.67644}$	0.63
22000	$R_{PC} = \frac{4.15538}{\lambda + \frac{8.56918}{\lambda} + 1.61828}$	0.66
24500	$R_{PC} = \frac{4.40485}{\lambda + \frac{9.08372}{\lambda} + 1.56219}$	0.70
27000	$R_{PC} = \frac{4.66315}{\lambda + \frac{9.61638}{\lambda} + 1.51073}$	0.73

82/18 AP/HTPB 200μ AP P = 10 atm ZFRACT = 0.0

E_{OX} = 16900

E_{BINDER}	R_{PC} Expression	Max $R_{PC}^{(real)}$
28000	$R_{PC} = \frac{4.76502}{\lambda + \frac{9.82666}{\lambda} + 4.94054}$	0.48
25000	$R_{PC} = \frac{4.31405}{\lambda + \frac{8.89698}{\lambda} + 2.61423}$	0.59
22000	$R_{PC} = \frac{3.86325}{\lambda + \frac{7.96730}{\lambda} + 0.26616}$	0.81
20000	$R_{PC} = \frac{3.56274}{\lambda + \frac{7.34751}{\lambda} - 1.31178}$	1.17
18000	$R_{PC} = \frac{3.26221}{\lambda + \frac{6.72772}{\lambda} - 2.89940}$	2.52
17000	$R_{PC} = \frac{3.11168}{\lambda + \frac{6.41783}{\lambda} - 3.69656}$	~7.5
16800	$R_{PC} = \frac{3.08163}{\lambda + \frac{6.35585}{\lambda} - 3.85623}$	~12

82/18 AP/HTPB 200μ AP P = 10 atm ZFRACT = 1.0

E_{OX} = 16900

E_{BINDER}	R_{PC} Expression	Max $R_{PC}^{(real)}$
28000	$R_{PC} = \frac{4.32354}{\lambda + \frac{8.91623}{\lambda} + 8.20561}$	0.33
25000	$R_{PC} = \frac{3.99156}{\lambda + \frac{8.23189}{\lambda} + 4.99056}$	0.42
22000	$R_{PC} = \frac{3.67393}{\lambda + \frac{7.57685}{\lambda} + 1.74304}$	0.60
20000	$R_{PC} = \frac{3.46872}{\lambda + \frac{7.15361}{\lambda} - 0.43942}$	0.90
18000	$R_{PC} = \frac{3.27044}{\lambda + \frac{6.74471}{\lambda} - 2.63742}$	2.09
17000	$R_{PC} = \frac{3.17319}{\lambda + \frac{6.54470}{\lambda} - 3.74268}$	-7.9
16800	$R_{PC} = \frac{3.15397}{\lambda + \frac{6.50505}{\lambda} - 3.96397}$	-18

82/18 AP/HTPB 200μ AP P = 40 atm ZFRACT = 0.0

E_{OX} = 22000

E_{BINDER}	R_{PC} Expression	Max $R_{PC}^{(real)}$
14500	$R_{PC} = \frac{3.33682}{\lambda + \frac{7.61910}{\lambda} - 2.63880}$	1.87
16900	$R_{PC} = \frac{3.40705}{\lambda + \frac{7.77856}{\lambda} - 2.23498}$	1.53
19500	$R_{PC} = \frac{3.48308}{\lambda + \frac{7.95124}{\lambda} - 1.79373}$	1.28
22000	$R_{PC} = \frac{3.55560}{\lambda + \frac{8.11729}{\lambda} - 1.36637}$	1.12
24500	$R_{PC} = \frac{3.62851}{\lambda + \frac{8.28332}{\lambda} - 0.93601}$	0.99
27000	$R_{PC} = \frac{3.70110}{\lambda + \frac{8.44932}{\lambda} - 0.50280}$	0.90

82/18 AP/HTPB 200μ AP P = 40 atm ZFRACT = 1.0

E_{OX} = 22000

E_{BINDER}	R_{PC} Expression	Max R_{PC}(real)
14500	$R_{PC} = \frac{3.48070}{\lambda + \frac{7.94763}{\lambda} - 0.58492}$	0.89
16900	$R_{PC} = \frac{3.52641}{\lambda + \frac{8.05105}{\lambda} - 0.86174}$	0.96
19500	$R_{PC} = \frac{3.59274}{\lambda + \frac{8.20157}{\lambda} - 1.16362}$	1.06
22000	$R_{PC} = \frac{3.65790}{\lambda + \frac{8.35083}{\lambda} - 1.44836}$	1.16
24500	$R_{PC} = \frac{3.73296}{\lambda + \frac{8.52175}{\lambda} - 1.73133}$	1.28
27000	$R_{PC} = \frac{3.81534}{\lambda + \frac{8.71012}{\lambda} - 2.01144}$	1.42

82/18 AP/HTPB 200μ AP P = 40 atm ZFRACT = 0.0

E_{OX} = 16900

E_{BINDER}	R_{PC} Expression	Max $R_{PC}^{(real)}$
28000	$R_{PC} = \frac{4.20167}{\lambda + \frac{9.59383}{\lambda} + 1.23747}$	0.69
26000	$R_{PC} = \frac{3.93710}{\lambda + \frac{8.98874}{\lambda} + 0.08942}$	0.81
24000	$R_{PC} = \frac{3.67207}{\lambda + \frac{8.38365}{\lambda} - 1.06803}$	1.04
22000	$R_{PC} = \frac{3.40705}{\lambda + \frac{7.77856}{\lambda} - 2.23498}$	1.53
21000	$R_{PC} = \frac{3.27439}{\lambda + \frac{7.47598}{\lambda} - 2.82181}$	2.09
20000	$R_{PC} = \frac{3.14244}{\lambda + \frac{7.17340}{\lambda} - 3.41150}$	3.46
19500	$R_{PC} = \frac{3.07668}{\lambda + \frac{7.02209}{\lambda} - 3.70688}$	5.40
19200	$R_{PC} = \frac{3.03669}{\lambda + \frac{6.93133}{\lambda} - 3.88448}$	-8.2
19000	$R_{PC} = \frac{3.01082}{\lambda + \frac{6.87078}{\lambda} - 4.00325}$	-12.5

82/18 AP/HTPB 200μ AP P = 40 atm ZFRACT = 1.0

E_{OX} = 16900

E_{BINDER}	R_{PC} Expression	Max $R_{PC}^{(real)}$
28000	$R_{PC} = \frac{4.46237}{\lambda + \frac{10.18908}{\lambda} + 4.27808}$	0.48
26000	$R_{PC} = \frac{4.14407}{\lambda + \frac{9.46128}{\lambda} + 2.57545}$	0.56
24000	$R_{PC} = \frac{3.83277}{\lambda + \frac{8.75055}{\lambda} + 0.86161}$	0.69
22000	$R_{PC} = \frac{3.52641}{\lambda + \frac{8.05105}{\lambda} - 0.86174}$	0.96
21000	$R_{PC} = \frac{3.38130}{\lambda + \frac{7.72009}{\lambda} - 1.72949}$	1.24
20000	$R_{PC} = \frac{3.23571}{\lambda + \frac{7.38630}{\lambda} - 2.59934}$	1.83
19500	$R_{PC} = \frac{3.16475}{\lambda + \frac{7.22309}{\lambda} - 3.03551}$	2.45
19200	$R_{PC} = \frac{3.11649}{\lambda + \frac{7.11349}{\lambda} - 3.29451}$	3.10
19000	$R_{PC} = \frac{3.09142}{\lambda + \frac{7.05472}{\lambda} - 3.47124}$	3.80

82/18 AP/HTPB 200μ AP P = 100 atm ZFRACT = 0.0

E_{OX} = 22000

E_{BINDER}	R_{PC} Expression	Max $R_{PC}^{(real)}$
14500	$R_{PC} = \frac{2.60821}{\lambda + \frac{7.48421}{\lambda} - 4.15148}$	-9.5
16900	$R_{PC} = \frac{2.66400}{\lambda + \frac{7.64102}{\lambda} - 3.87076}$	4.47
19500	$R_{PC} = \frac{2.72251}{\lambda + \frac{7.81076}{\lambda} - 3.56533}$	2.97
22000	$R_{PC} = \frac{2.78106}{\lambda + \frac{7.97386}{\lambda} - 3.26929}$	2.23
24500	$R_{PC} = \frac{2.83644}{\lambda + \frac{8.13692}{\lambda} - 2.97186}$	1.79
27000	$R_{PC} = \frac{2.89319}{\lambda + \frac{8.29983}{\lambda} - 2.67332}$	1.50

82/18 AP/HTPB 200μ AP P = 100 atm ZFRACT = 1.0

E_{OX} = 22000

E_{BINDER}	R_{PC} Expression	Max $R_{PC}^{(real)}$
14500	$R_{PC} = \frac{2.98627}{\lambda + \frac{8.56905}{\lambda} - 2.19964}$	1.21
16900	$R_{PC} = \frac{2.93577}{\lambda + \frac{8.42055}{\lambda} - 2.56058}$	1.42
19500	$R_{PC} = \frac{2.89202}{\lambda + \frac{8.29707}{\lambda} - 2.94572}$	1.75
22000	$R_{PC} = \frac{2.85521}{\lambda + \frac{8.18648}{\lambda} - 3.31964}$	2.29
24500	$R_{PC} = \frac{2.81901}{\lambda + \frac{8.08692}{\lambda} - 3.68660}$	3.27
27000	$R_{PC} = \frac{2.79310}{\lambda + \frac{8.01270}{\lambda} - 4.04768}$	-5.8

82/18 AP/HTPB 200μ AP P = 100 atm ZFRACT = 0.0

E_{OX} = 16900

E_{BINDER}	R_{PC} Expression	Max $R_{PC}^{(real)}$
28000	$R_{PC} = \frac{3.28368}{\lambda + \frac{9.42418}{\lambda} - 1.10756}$	0.88
26500	$R_{PC} = \frac{3.12836}{\lambda + \frac{8.97841}{\lambda} - 1.79077}$	1.06
25000	$R_{PC} = \frac{2.97257}{\lambda + \frac{8.53260}{\lambda} - 2.47838}$	1.37
23500	$R_{PC} = \frac{2.81853}{\lambda + \frac{8.08681}{\lambda} - 3.17266}$	2.05
22000	$R_{PC} = \frac{2.66399}{\lambda + \frac{7.64102}{\lambda} - 3.87077}$	4.47
21500	$R_{PC} = \frac{2.61229}{\lambda + \frac{7.49239}{\lambda} - 4.10533}$	-8.2

82/18 AP/HTPB 200μ AP P = 100 atm ZFRACT = 1.0

E_{OX} = 16900

E_{BINDER}	R_{PC} Expression	Max $R_{PC}^{(real)}$
28000	$R_{PC} = \frac{3.86873}{\lambda + \frac{11.10327}{\lambda} + 1.89025}$	0.54
26500	$R_{PC} = \frac{3.63023}{\lambda + \frac{10.41876}{\lambda} + 0.78685}$	0.62
25000	$R_{PC} = \frac{3.39111}{\lambda + \frac{9.73399}{\lambda} - 0.32583}$	0.74
23500	$R_{PC} = \frac{3.16733}{\lambda + \frac{9.08757}{\lambda} - 1.43827}$	0.95
22000	$R_{PC} = \frac{2.93577}{\lambda + \frac{8.42055}{\lambda} - 2.56058}$	1.42
21500	$R_{PC} = \frac{2.86271}{\lambda + \frac{8.21062}{\lambda} - 2.93323}$	1.74